TABLE OF CONTENTS

Page

INTRODUCTION 1

Research problematic 3

CHAPTER 1 LITERATURE REVIEW 5
1.1 Stack of materials 5
    1.1.1 Introduction to composite materials 5
    1.1.2 Carbon Fiber Reinforced Plastic (CFRP) 7
    1.1.3 Ti6Al4V alloy 8
    1.1.4 CFRP/Ti6Al4V plaque 8
1.2 Machining process operations 11
    1.2.1 Milling parameters 12
    1.2.2 Cutting tools 13
    1.2.3 Cutting forces 14
    1.2.4 Chip formation in the cutting process of CFRP 17
    1.2.5 Surface roughness 19
1.3 Thermal effects during machining 21
    1.3.1 Temperature measurement methods 22
    1.3.2 Influence of cutting temperature in the machining process 26
    1.3.3 Thermal aspects during machining CFRP 28
    1.3.4 Heat flux in CFRP plaque 33
1.4 Summary of the literature review 34
    1.4.1 Objective 34

CHAPTER 2 METHODOLOGY 37
2.1 Machine and Setup 37
2.2 Selection of cutting tool 38
2.3 Screening of experiment 41
2.4 Design of Experiments 42
2.5 Manufacturing of CFRP/Ti6Al4V plaques 46
    2.5.1 Manufacturing process of CFRP plaques 47
    2.5.2 Embedded thermocouples in CFRP 49
    2.5.3 Thermocouples on the cutting tool 56
2.6 Edge milling of [0]8/Ti6Al4V plaques 57
    2.6.1 Workpiece and cutter temperature measurement 58
    2.6.2 Cutting Forces 60
    2.6.3 Roughness on CFRP/Ti6Al4V 61
    2.6.4 Tool wear 63

CHAPTER 3 RESULTS AND DISCUSSION 65
3.1 Temperature on the workpiece and cutter 65
  3.1.1 Analysis of temperature on the Ti workpiece 65
  3.1.2 Analysis of temperature in the CFRP workpiece 71
  3.1.3 Analysis of temperature on the cutters 80
3.2 Analysis of Forces 84
  3.2.1 Feed force 84
  3.2.2 Normal force 87
  3.2.3 Axial force 89
3.3 Roughness Analysis 92
3.4 Tool wear 97

CONCLUSION 103

RECOMENDATIONS 105

BIBLIOGRAPHY 119

LIST OF TABLES

Page

Table 1-1 Advantages vs Disadvantages of CFRP/Ti6Al4V..9

Table 2-1 Machine Huron specification 37

Table 2-2 Niagara tool or Tool number 1 specifications 39

Table 2-3 Walter tool or Tool number 2 specifications 40

Table 2-4 Onsrud tool or Tool number 3 specifications 40

Table 2-5 Thermal conductivity of the different cutters 41

Table 2-6 Final DOE..42

Table 2-7 Physical properties of Ti6Al4V 48

Table 2-8 Prepeg CYCOM® 5320-1 T650-35 3K 8HS Fabric 36% physical properties..50

Table 2-9 Thermocouple workpiece statistical analysis 55

Table 2-10 Real DOE..58

Table 2-11 Mitutoyo Surftest SJ400 input parameters 63

Table 3-1 Cutter tool wear progress at different cutting parameters for the ae of 1 mm 100

Table 3-2 Cutter tools wear progress at different cutting parameters for the ae of 4.3 mm 101

LIST OF FIGURES

Page

Figure 1.1 a) Unidirectional fibers, b) woven fibers.....7

Figure 1.2 Airframe material composition on Boeing 787 Dreamliner.....10

Figure 1.3 Material composition in airplanes Airbus.....10

Figure 1.4 Edge milling operation.....11

Figure 1.5 Up milling/Down milling.....12

Figure 1.6 Cutters used for CFRP.....14

Figure 1.7 Diagram of orthogonal cutting forces.....15

Figure 1.8 Different stages in the orthogonal cutting process of CFRP/Ti at Ɵ of 0° , v of 50m/min and f of 0.20 mm/rev.....17

Figure 1.9 Cutting mechanisms in orthogonal machining of CFRP.....19

Figure 1.10 Schematic roughness representation.....20

Figure 1.11 Example of main problems in machining CFRP.....21

Figure 1.12 Thermography's examples.....23

Figure 1.13 Embedded thermocouple methods in CFRP and Ti materials.....25

Figure 1.14 An experimental investigation in milling Ti6Al4V.....27

Figure 1.15 Analysis of thermal effects on the fiber orientation.....30

Figure 1.16 Thermal analysis in CFRP milling for different fiber orientation.....31

Figure 1.17 Example of thermal damage observed by SEM.....32

Figure 2.1 Setup for CFRP/Ti.....38

Figure 2.2 Sketch of final DOE with inputs and outputs.....43

Figure 2.3 Schematic diagram of the acquisition equipment used in the experiments.....44

Figure 2.4 Forces and Temperature acquisition equipment in the final experiment 45

Figure 2.5 M320 Telemetry system 45

Figure 2.6 Sketch of thermocouple order in CFRP/Ti stack 46

Figure 2.7 Sketch of thermocouple position on Ti6Al4V plaque 47

Figure 2.8 Thermocouple welding tip view 48

Figure 2.9 Thermocouple micro-welding sample plaque 49

Figure 2.10 Thermocouples setup process 51

Figure 2.11 Flowchart of $[0]_8$/Ti6Al4V fabrication process 53

Figure 2.12 X-ray scanning example result 54

Figure 2.13 Example of thermocouple outside the titanium plaque due to the curing process 56

Figure 2.14 Embedded thermocouple process 57

Figure 2.15 PCD tool , v 50 m/min, ft 0.15 mm/tooth, ae 1 mm example 59

Figure 2.16 Methodology to know the correct position of thermocouples 60

Figure 2.17 Forces layout setup 61

Figure 2.18 Roughness setup 62

Figure 2.19 Setup to measure tool wear 64

Figure 3.1 Main effect plot for average temperature result on the Ti plaque T1 and T4 66

Figure 3.2 Pareto chart: Most significant factor on the titanium plaque and 3D graph on T4 66

Figure 3.3 Workpiece temperature on Ti plaque against thermocouple distance for a ft of 0.05 mm/tooth, v of 175 mm/tooth 68

Figure 3.4 Longitudinal cutting profile for tool #2 (a, b) and tool #3 (c,d) at ft of 0.05 mm/tooth, v of 175 m/min and an ae of 1 mm 69

Figure 3.5 Temperature through the longitudinal distance for the titanium plaque using tool #3, v of 175m/min, ft of 0.05 mm/tooth and ae of 1mm 70

Figure 3.6 Pareto Chart of the Standardized effects on T5 and T7.............................71

Figure 3.7 Pareto Chart of the Standardized effects on T6 and T8.............................72

Figure 3.8 Pareto Chart of the Standardized effects on T10 and T9...........................72

Figure 3.9 Workpiece temperature on Ti and CFRP VS thermocouple distance for ft of 0.05 mm/tooth, ae of 1 mm on (T2, T5, T7 and T9) and (T3, T6, T8 and T10)...74

Figure 3.10 Vertical cutting temperature at a cutting length of 38.1 mm (thermocouples 2-5-7-9)..75

Figure 3.11 Temperature through the thick distance T/C 2-5-7-9 for the [0]8/Ti6Al4V plaque using tool #3, v of 175m/min, ft of 0.05 mm/tooth and ae of 1mm...77

Figure 3.12 Vertical cutting temperature at a cutting length of 63.3 mm (thermocouples 3-6-8-10)..78

Figure 3.13 Temperature through the thick distance T/C 3-6-10 for the [0]8/Ti6Al4V plaque using tool #3, v of 175m/min, ft of 0.05 mm/tooth and ae of 1mm...79

Figure 3.14 Main effect plot for cutter temperature and standardized pareto chart..81

Figure 3.15 3D Graph cutter temperature (a) feed per tooth vs radial depth of cut for a v of 175m/min (b) Type of tool vs radial depth of cut for a ft of 0.05 mm/tooth...82

Figure 3.16 Scheme of applied forces on the CFRP/Ti 84

Figure 3.17 Main effect plot for average Feed force result and standardized pareto chart...85

Figure 3.18 Feed force as a function of the feed per tooth according to the different cutting parameters on each cutter 86

Figure 3.19 Normal force as a function of the feed per tooth according to the different cutting parameters on each cutter 88

Figure 3.20 Main effect plot for axial force result and standardized pareto chart 89

Figure 3.21 Axial force as a function of the feed per tooth according to the different cutting parameters on each cutter 91

Figure 3.22 Main Effect plot of Ra in function to different parameters giving by ±SEM and Ra Pareto chart of the most significant factor 93

Figure 3.23 Ra on the CFRP plaque in function of different cutting parameters *v*, *ae* and *ft* giving by ±SEM 95

Figure 3.24 Ra on the Ti6Al4V plaque in function of different cutting parameters *v*, *ae* and *ft* giving by ±SEM 96

Figure 3.25 Main effect plot for tool wear and standardized pareto chart 97

Figure 3.26 Tool wear effect on each cutting tool by using different cutting parameters 99

LIST OF ABBREVIATIONS

CFRP	Carbon Fiber Reinforced Plastic
Ti	Titanium
Al	Aluminum
G	Glass fibers
C	Carbon fibers
K	Kevlar
PMC	Polymer matrix composite
MMC	Metal matrix composite
CMC	Ceramic matrix composite
PCD	PolyCristallline Diamond
SEM	Scanning Electron Microscope, Standard Error of the mean
CNC	Computer Numerical Control
LIPPS	Laboratoire d'ingénierie des produits, procédés et systèmes
DOE	Design of Experiments
ÉTS	École de Technologie supérieure
CI	Confidence Intervals
RSM	Response-surface methodology
VB	Flank wear
BUE	Built-Up-Edge

Clicours.COM

LIST OF SYMBOLS AND UNITS OF MEASUREMENTS

E_1	Load in the fiber direction
E_2	Load in the transversal direction
T_g	Glass transition (°)
α	Coefficient of thermal expansion
β	Coefficient of moisture expansion
a_e	Radial depth of cut (mm)
V	Cutting speed (m/min)
f_r	Feed rate (mm/min)
f_t	Feed per tooth (mm/rev-tooth) or (mm/z)
f	Feed (mm/rev)
D	Cutter Diameter (m)
N	Spindles speed (rev/min)
h_c	Cut chip thickness (mm)
F_n	Normal force to shear plane (N), Force in Y (N)
F_s	Shear force (N)
F_u	Friction force (N)
F_v	Normal force to tool face
F_a	Axial force, Force in Z(N)
F_t	Tangential force (cutting force)
F_f	Feed force, thrust force, force in X (N)
α	Rake angle (°)
β	Friction angle
φ	Shear angle (°)
Fr	Radial force (N)
R	Result force (N)
β	Helix angle (°)
θ	Fiber orientation (°), cutter diameter (mm)
R_a	Arithmetic mean value

R_v	Arithmetic means to the valley height
R_z	Arithmetic ten points average height
R_t	Arithmetic maximum peak to the valley height
R_p	Arithmetic maximum peak to mean height
υ	Cutting energy, fiber volume (%)
k	Thermal conductivity
p	Density
c	Specific heat
K_m	Matrix thermal conductivity W/mK)
K_f	Fiber thermal conductivity (W/mK)
V_f	Fiber volume fraction
ΔT	Difference of temperature
q_s	Strength of the heat source
c	Specific heat capacity
α	Heat dissipation rate
y	Shortest distance from the heat source
X	Moving distance of the cutter
$\lambda_{c,\vartheta}$	Composite thermal conductivity
$\Lambda_{c,p}$	Parallel thermal conductivity to fiber orientation
$\Lambda_{c,t}$	Transversal thermal conductivity to the fiber direction
Q	Mechanical power transformed to heat
Q_t	Heat conducted by the tool
Q_w	Heat conducted by the workpiece
Q_c	Heat conducted by the chip
P_{el}	Electrical power consumed by the machine
η	Spindle efficiency
q_w	Heat flux value in the workpiece
q_t	Heat flux value in the tool
A_w	Contact area in the workpiece

A_t	Contact area in the tool
ksi	Kilopounds per square inch
Msi	Mega pounds per square inch
λc	Cut-off
λs	Evaluation length
Ls	Cutting length, filtered
N	Number of points

INTRODUCTION

With the need for decreasing fuel consumption, the aerospace industry develops new technologies with the aim of building ultra-light and resistant structures. Composite materials and titanium alloys offer a series of benefits over other materials as they are not only lightweight but also very resistant to fatigue and corrosion. Nevertheless, they are vulnerable to machining defects.

Hybrid or stacks of materials are more often used in airframes because of their outstanding mechanical properties such as high strength/weight ratio and, excellent corrosion and fatigue resistance that cannot be provided by conventional materials (Park, Beal, Kim, Kwon, & Lantrip, 2013). In addition, aircraft structures subjected to high thermo-mechanical stresses are successfully fabricated by CFRP/Ti stacks. For example, the wing-fuselage connection of the new-generation Boeing 787 Dreamliner is an engineering application for this type of material in the aeronautical industry (Xu, Mkaddem, & El Mansori, 2016). Other applications can be found in Airbus airplane models such as A380, A400M, and A350-900XWB where 15% of the structure is made of CFRP/Ti stacks of material (Hammadi, 2010). In addition, the CFRP/Ti stack offers superior mechanical and thermal load-bearing to conventional materials. This material has a yield strength of about 890 MPa, and a density of 4 g/cm3 (Park et al., 2013; Xu et al., 2016), which makes it very attractive for the thermal-load applications in the modern aerospace industry.

However, machining of Carbon Fiber-Reinforced Plastic (CFRP)/Titanium stack can be a real challenge to obtain specific geometries and dimensional tolerances in the manufacturing line. This is because each material has differences in machinability making it a difficult task. Drilling and milling are more conventional machining processes in the industry. In the case of the CFRP, it is subject to delamination, fiber pull out, fuzzing and thermal damage in the epoxy. On the other hand, titanium may have surface quality problems. Moreover, machining CFRP is very abrasive and Ti has low heat transfer and strong chemical reaction with cutting tools, provoking extreme tool wear, high-cutting forces and high tool temperatures (Khashaba, 2013; Krishnaraj, Zitoune, Collombet, & Davim, 2013).

In the military and aerospace sectors, there are several configurations for multi-layer materials based on the fiber type (Glass or Carbon) and on the type of metallic material (Aluminum or Titanium or both) (Brinksmeier, Fangmann, & Rentsch, 2011). There are different types of configurations such as CFRP/Al, CFRP/Al/CFRP, Al/CFRP/Ti, CFRP/Ti, CFRP/Ti/CFRP, Ti/CFRP/Ti, etc. (Xu et al., 2016). Therefore, this research focuses on stacks of CFRP and Ti6Al4V materials, the configuration of CFRP/Ti being the most commonly used by the aeronautic and military industries (Xu et al., 2016).

Generally, stacks of materials are assembled or built by using rivets or bolts where the CFRP and the Ti components are trimmed and drilled individually and then stacked up to enhance the required tolerances. Nevertheless, there are some special requirements in the manufacturing of light structures in aerospace where the stacks are first assembled by using adhesives and then trimmed together up to the final sizes. This is because CFRP is very sensitive to notching and shearing strengths, decreasing its mechanical properties and giving way to crack propagation when drilling operations are used. Thus, it is utmost important to find efficient machining techniques to trim both materials together. This research focuses on this aspect.

Nowadays, some publications are focusing on the trimming of CFRP (Y. G. Wang, Yan, Chen, Sun, & Liu, 2011; J. F. Chatelain & I. Zaghbani, 2012; J. Sheikh-Ahmad & Cheragui, 2012; Chatelain, Zaghbani, & Monier, 2012) and Ti (J. Sun & Guo, 2009; H. Wu & Zhang, 2015). In the case of stacks of material, researchers have been focusing on the drilling process (Brinksmeier et al., 2011; Park et al., 2013; SenthilKumar, Prabukarthi, & Krishnaraj, 2013; Xu et al., 2016). As a result, there are neither experimental nor simulation studies and much less thermal studies for the edge milling in the literature.

Research problematic

The main problem in the aerospace industry is the building of new light structures. In such a context, some applications require that the stack of material be bonded together using adhesives or resins. As a result, there is neither bolts nor rivets nor drilling process so edge milling is used to achieve the final sizes of the workpiece. The main problem of machining both materials together is that the titanium is a source of heat generation above 500 °C in dry conditions and the epoxy suffers from matrix degradation when the temperature reach the glass transition temperature (175 °C). Therefore, it is of utmost importance to study the thermal distribution and the influence of cutting parameters for the CFRP/Ti stack due to the different machinability of each material and due to the low thermal conductivity of Ti, always caring the integrity of the epoxy.

ClicCours.com

CHAPTER 1

LITERATURE REVIEW

With the aim of reducing the fuel emission, the aviation industry is developing a new generation of structures by the motivation of decreasing fuel consumption. As a result, new materials are used to build new ultra-high resistance airframes and components. Materials such as CFRP, Ti and CFRP/Ti stacks are currently used in the modern aerospace manufacturing industry that would be impossible or unimaginable some decades ago. Therefore, this chapter presents the main research related to the edge milling of CFRP, Ti, and CFRP/Ti stacks. However, before describing these works, a brief introduction to composites and machining is described in the following sections.

1.1 Stack of materials

A stack of material is an assembly of two or more layers of different types of materials. In most of the cases, the stack is attached by rivets or bolts which implies an extra cost due to the drilling process. This, in turn, adds weight because of the fixing bolts. It should be mentioned that this research focuses on stacking CFRP on the top and Ti6Al4V in the bottom, using the prepreg curing process to bond the CFRP to the Ti6Al4V, as explained in the Methodology chapter.

1.1.1 Introduction to composite materials

A composite material is the combination of two or more materials in order to build a stronger material. It is made of a matrix which can be fragile in the case of thermoset resin while on the other hand, the fibers (reinforcing material) are stiffer and stronger. The matrix acts as a bonding agent to the fibers which provides good mechanical properties to the whole composite. Additionally, fibers can also be divided in two types: 1) long (continuous) or 2) short (discontinues) (Campbell, 2010) and there are many types of fiber such as glass fibers (G),

Clicours.COM

carbon fibers (C) or kevlar (K) to name a few and the use of each one depends mainly on its application.

Another classification of composite materials is based on the matrix type:

- Polymer matrix composite (PMC)
- Metal matrix composite (MMC)
- Ceramic matrix composite (CMC)
- Carbon matrix composite

In the case of PMC matrices, it is divided into 2 categories: 1) thermoset and 2) thermoplastic. Typical thermosetting matrix are: epoxy, phenols, polyamide and polyester resin; epoxy and polyester being the most common ones for composites.

The following list shows the most important advantages of thermosets as a matrix

1. Resistance to solvents and corrosive agents
2. Resistance to heat and high temperature
3. Fatigue strength
4. Excellent adhesion
5. Excellent Polished finishing

It should be noted that thermosets cannot be melted once they are cured and have a glass transition (T_g) of about 175°C for epoxies, temperature marking the transition from the glassy to the rubbery state. It is worth mentioning that epoxy is one of the most common thermosets used in the manufacture of composites. On the other hand, thermoplastics are polymers that can be reused again and again and can be remelted and remoulded without losing their properties. Besides, the thermoplastics have two major advantages over thermoset. The first is that it has an impact resistance as high as 10 times that of thermoset resins. The second is that it can be recycled, reshaped, remoulded in order to draw complex shapes, however, probably its major disadvantage is their more complex and expensive manufacturing processes. Therefore, the material used in this project is made of continuous carbon fibers embedded in an epoxy matrix.

1.1.2 Carbon Fiber Reinforced Plastic (CFRP)

Carbon Fiber Reinforced Plastics (CFRPs) have a high strength to weight ratio, high modulus-to weight ratio, high-damping capacity, good dimensional stability to temperature changes, high rust and fatigue resistance, which is ideal for the aerospace industry. CFRPs can be found in automobiles, robotics, construction, transportation, luxury sporting goods, medical, and military applications. They are built by using unidirectional or woven fibers as shown in Figure 1.1

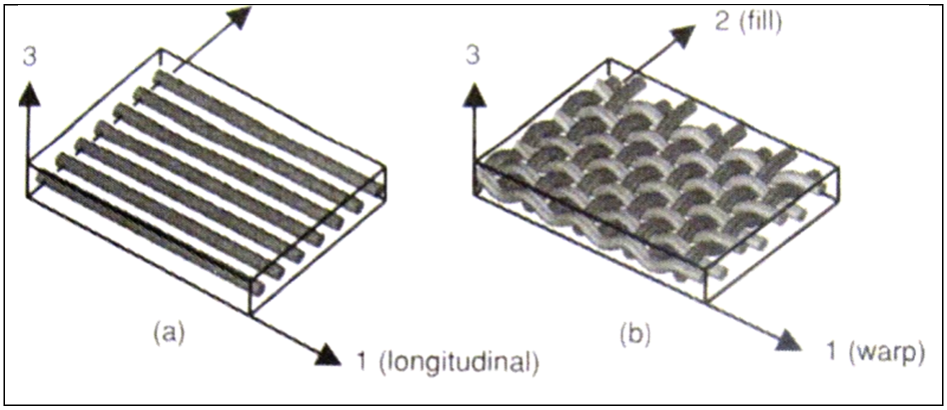

Figure 1.1a) Unidirectional fibers, b) woven fibers
(Campbell, 2010)

For the CFRP materials, the Young’s modulus in each direction is different and depends on the direction of loading. If the load is in the fiber direction (Longitudinal), it is denoted by E_1 and if it is a transversal load or in the matrix direction, it is denoted E_2. These kinds of materials are called orthotropic and their counterpart, the isotropic material like the titanium has the same Young’s modulus in all directions. The properties of CFRPs make them excellent for special applications where the load is applied only in the required direction. Another characteristic of CFRP is the coefficient of thermal expansion “α” and the coefficient of moisture expansion “β.” In the case of the thermal expansion, this is almost 0 for CFRP in the fiber direction which is an advantage for aerospace applications dealing with the large differences in temperatures that airplanes have to support in service. Nevertheless, the biggest disadvantage is that the matrix is susceptible to thermal degradation due to the thermal and moisture expansion. This last one is null for metallic materials like the titanium.

Most of the composite structures in the aerospace industry are quasi-isotropic materials where the stiffness is the same in all directions. A good design is a balanced/symmetric laminate where the tension-flexural coupling and the in-plane tension-shear coupling are null while the torsion coupling can be lowered by adjusting the ply distribution (Issac M. Daniel, 2006).

1.1.3 Ti6Al4V alloy

Titanium is highly resistant to corrosion and can be alloyed with iron, aluminum, vanadium, molybdenum, and other elements in order to produce strong, lightweight alloys for aerospace (jet engines, missiles and spacecraft), military, industrial processes (chemical and petrochemicals, desalination plants, pulp, and paper), automotive, medical and other areas (Kalpakjian & Schmid, 2014) .

In the market, there are many grades of Titanium alloys, grade 5 being the most used by the aeronautic industry, also known as Ti6Al4V or Ti 6-4. It has a composition of 6% aluminum, 4% vanadium, 0.25% (maximum) iron and 0.2% (maximum) oxygen, and the rest is titanium. This grade has an excellent combination of strength and rust resistance. Furthermore, it is used in the aerospace airframe and turbine engine components and also in a non-aerospace application such as in maritime offshore and power generation industries in particular due to its excellent corrosion resistance to seawater. Some other applications where this material can be found are in airframes, blade discs, fasteners rings, vessels, hubs and biomedical applications. Generally, it is used for high temperatures applications, e.g up to 700°C (Kalpakjian & Schmid, 2014).

1.1.4 CFRP/Ti6Al4V plaque

CFRP/Ti6Al4V is a type of stack material where the CFRP plaque is set up on top of the titanium plaque. This type of configuration takes the best of each material. Table 1-1 individually shows the advantages and disadvantages of each material. Generally, this material is joined by rivets or bolts although there are some special applications where bolts or rivets cannot be used by manufacturers' requirements.

Table 1-1 Advantages vs Disadvantages of CFRP/Ti6Al4V

CFRP	**Ti6Al4V**
Advantages	**Advantages**
Fatigue resistance	High strength/weight ratio
Rust resistance	Rust resistance
Lightweight	Fracture-resistant
High stiffness and strength	Non-toxic to humans
Disadvantages	**Disadvantages**
Vulnerable to machining defects	Difficult to machine
Orthotropic material	Low thermal conductivity
	Strong chemical affinity

CFRP/Ti6Al4V is mostly used in the aerospace industry for thermally loaded applications. A typical application of this stack is in the wing-fuselage connection in the new Boeing generation 787 Dreamliner (Xu et al., 2016). Figure 1.2 illustrates the airframe composition and its percentages.

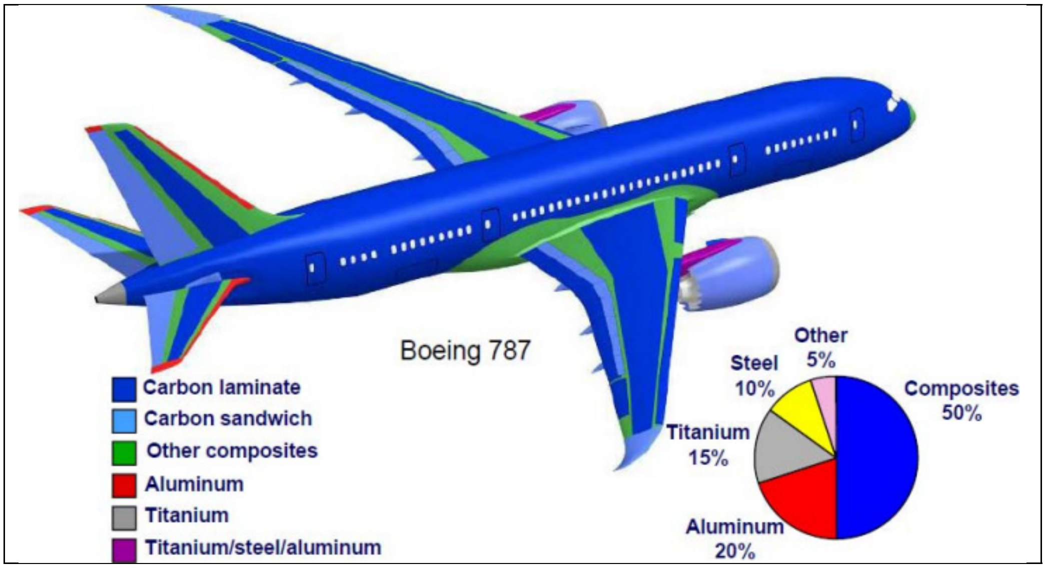
Boeing 787
Carbon laminate
Carbon sandwich
Other composites
Aluminum
Titanium
Titanium/steel/aluminum
Other 5%
Steel 10%
Composites 50%
Titanium 15%
Aluminum 20%

Figure 1.2 Airframe material composition on Boeing 787 Dreamliner
(Boeing, 2009)

Another application is found in Airbus airplane models such as A380, A400M and A350-900XWB where 15% of the structure is made of CFRP/Ti (Hammadi, 2010), see fig Figure 1.3

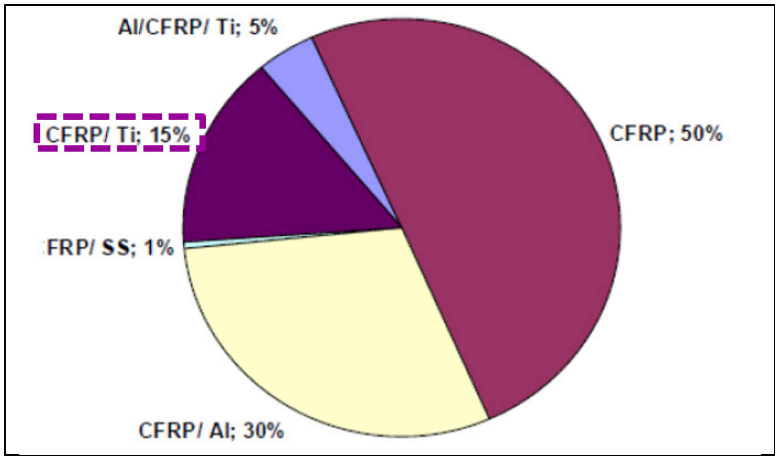

Figure 1.3 Material composition in airplanes Airbus
(A380, A400M and A350-900XWB
(Hammadi, 2010)

1.2 Machining process operations

Carbon Fiber Reinforced Plastic (CFRP) and Titanium require several machining processes to be involved in mechanical assemblies. Drilling and trimming are mostly used for CFRP plaques since they are molded to near net shape. In contrast, titanium parts are finished using drilling, milling and turning operations with the objective to enhance the surface finish, geometric shape, tolerances and so ensure a perfect assemble. For the CFRP/Ti6Al4V plaque, drilling and trimming operations are needed to assemble both plaques together. Nevertheless, our application is free of the drilling process. Thus, this operation is omitted. This is because we use a curing process to bond both pieces. As a result, our plaque does not have any rivets or bolts. Additionally, our research focuses on edge milling or profile milling where the cutter cuts the periphery or edge of a flat part, see Figure 1.4. Moreover, this type of edge milling is distinct because it has only one component related to the chip, which is a_e, the radial depth of cut. The main goal of the edge milling is to enhance final tolerances to have good surface finish in the assembly process or just give the final dimensions to the CFRP/Ti6Al4V, component.

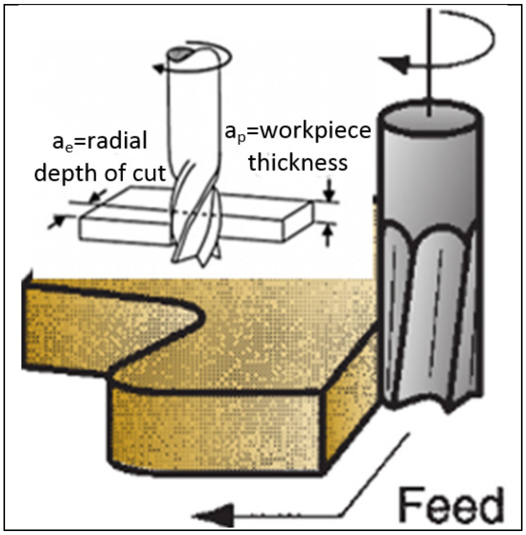

Figure 1.4 Edge milling operation
(Groover, 2013)

1.2.1 Milling parameters

Parameters are values that are selected for the cutting process in order to have a good performance of the machine, low tool wear and good surface finish. Milling operations can be performed depending on the cutter rotation and feed direction. If the cutter rotation is against the feed direction, it is called up-milling. If the cutter rotation moves in the same direction as the feed direction, it is called down milling, as shown in the right side of Figure 1.5. However, the most important characteristic of up milling is that the chip thickness starts very thin and increases during the cutting process. On the contrary, the chip thickness in down milling starts very thick and decreases during the sweeping. Moreover, down milling chips length is shorter than up milling, this means that the cutting tool engages in the workpiece for less time which helps increase the tool life.

Another feature of down milling is that the forces acting over the workpiece tend to hold the workpiece in place as opposed to up milling. In practice, down-milling performs better than up-milling and is preferred for metal machining like titanium (J. Sun & Guo, 2009; A. Li, Zhao, Dong, Wang, & Chen, 2013; Yang & Liu, 2015). In the case of CFRP, J. Y. Sheikh-Ahmad et al. (J. Y. Sheikh-Ahmad, 2009) showed that up-milling has a better surface finish than down-milling as concern delamination and roughness. Therefore, up-milling is preferred for machining CFRPs.

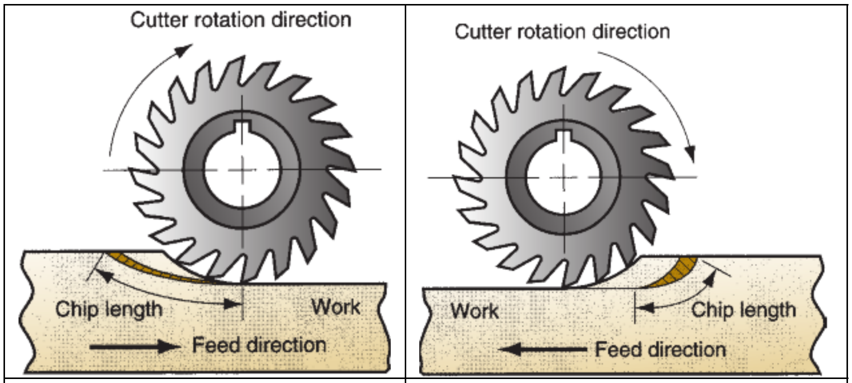

Up milling | Down milling

Figure 1.5 Up milling/Down milling
(Groover, 2013)

In addition to the sense of the cutter, it is very important to specify the moving speed with which the cutter moves or cutting speed (V) which is normally given in [m/min], see equation (1.1). The cutter feed along the workpiece is called feed rate (fr) and is given in [mm/min] by equation (1.2).

$$V = \pi . D . N \tag{1.1}$$

$$fr = ft . N . n = N . f \tag{1.2}$$

Where:

D is the tool diameter [m], N is the spindle speed [rev/min], f is feed [mm/rev], f_t is feed per tooth [mm/rev-tooth], n is the number of tooth [tooth].

1.2.2 Cutting tools

The selection of cutter material is crucial and depends on the type of material to be machined. Generally, CFRP material is machined using PolyCrystalline Diamond PCD (Lantrip, 2008; El-Hofy et al., 2011; Chatelain et al., 2012 ; H. Wang, Sun, Li, Lu, & Li, 2016; H. Wang, Sun, Zhang, Guo, & Li, 2016), while Titanium alloy is machined using uncoated or coated carbide tool due to its high-impact strength (L. Li, Chang, Wang, Zuo, & He, 2004; J. Sun & Guo, 2009; Palanisamy, Rashid, Brandt, Sun, & Dargusch, 2014; Yujing, Jie, Jianfeng, & Qingchun, 2014; Yang & Liu, 2015).

The PolyCrystalline Diamond (PCD) tools are ideal for machining abrasive materials such as CFRP due to their high wear resistance, high toughness and highest hardness of all the cutter materials. However, PCD tools are very sensitive to vibration and are not recommended for ferrous materials or hard metals because of the high solubility of the diamond at high temperatures and its brittleness. Figure 1.6 shows a compilation of the different cutter material used for machining CFRP depending on its wear resistance, cutting speed and toughness performance.

clicours.com

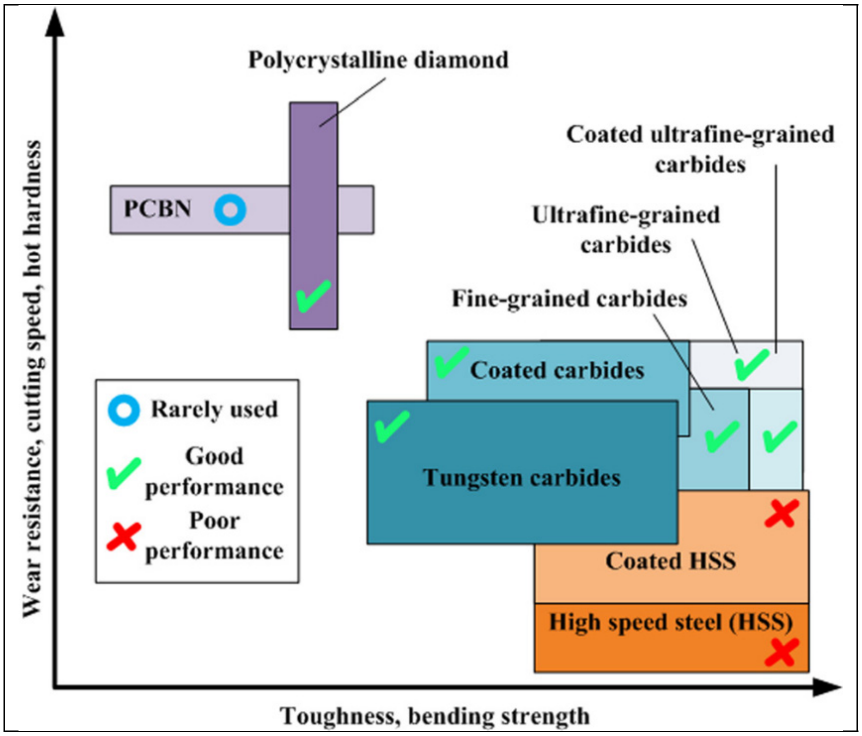
Polycrystalline diamond
PCBN
Coated ultrafine-grained carbides
Ultrafine-grained carbides
Fine-grained carbides
Coated carbides
Tungsten carbides
Coated HSS
High speed steel (HSS)
Rarely used
Good performance
Poor performance
Wear resistance, cutting speed, hot hardness
Toughness, bending strength

Figure 1.6 Cutters used for CFRP
(Che, Saxena, Han, Guo, & Ehmann, 2014; Lantrip, 2008)

1.2.3 Cutting forces

Another important factor to consider in the machining process is the cutting forces since they can help to understand the behavior of the process and its influence on the temperature, surface quality and tool wear on the cutting tool.

There exist two types of cutting processes: orthogonal and oblique cutting. Orthogonal is the least complex in the interaction between the tool and the chip on the workpiece. If the chip is straight, it is orthogonal. It is when the rake face of cutter produces an angle “rake angle” along with the contact of the cutter and the working piece. As it travels through the surface of the workpiece, a shear plane or shear angle φ is created whose total length of the workpiece is l_s. As it is moved forward, a chip thickness is created h_c, the relation between the cut chip thickness h_c, and the uncut chip thickness h is called ratio $r = h/h_c$. The forces which are involved in the interaction between the cutter and the chip are friction force F_u and the normal force to the tool face F_v, see on the top Figure 1.7

In addition to the forces applied by the tool on the chip thickness, normal force to shear plane F_n and shear force F_s are forces caused as opposition to F_u and F_v by the detachment of the chip from the workpiece. The β is the friction angle between the tool's rake face and chip and R is the resultant force or total force, see on the bottom of Figure 1.7. Its equation is given by (1.3)

$$R = \sqrt{F_t^2 + F_f^2} \tag{1.3}$$

On the other hand, if the cutter has an inclination angle I, there would be a chip flow η. Therefore, a third force is formed in the radial direction F_r component and is called oblique cutting.

R=Resultant force
F_s=Shear force
F_n=Normal force to shear plane
F_u=Friction force
F_v=Normal force to the tool face
F_t=Tangential force (**cutting force)**
F_f=Feed force or thrust force **(axial force)**
α=Rake angle
φ=Shear angle
β=Friction Angle

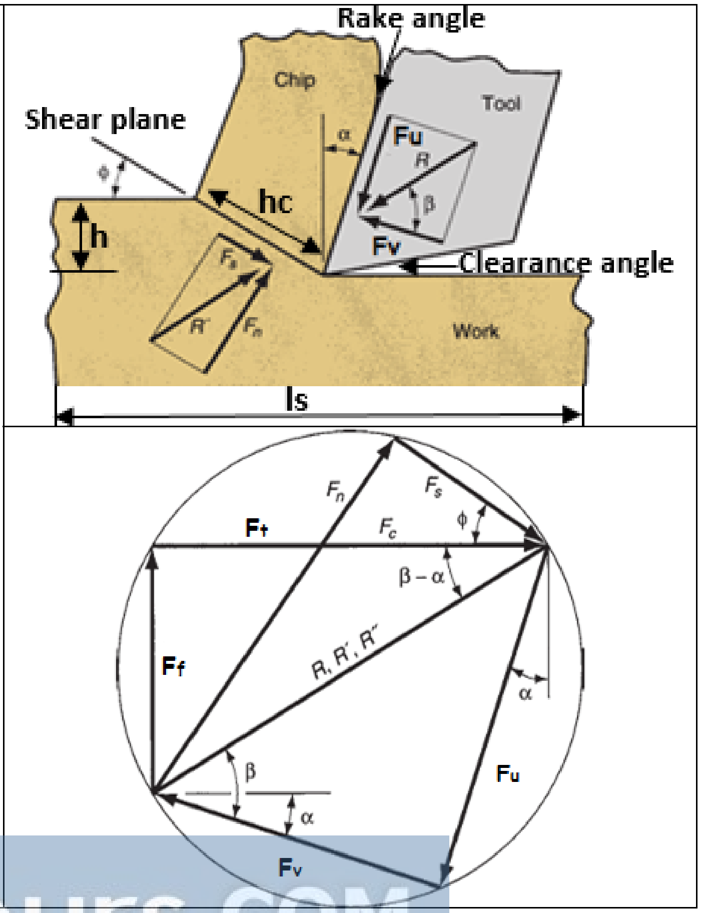
Rake angle
Chip
Tool
Shear plane
ϕ
α
Fu
R
β
hc
h
Fv
Clearance angle
Fs
R'
Fn
Work
ls
Fn
Fs
Ft
Fc
ϕ
β − α
Ff
R, R', R''
α
β
α
Fu
Fv

Figure 1.7 Diagram of orthogonal cutting forces

Clicours.COM

1.2.3.1 Cutting forces on CFRPs

There are many studies related to the cutting forces and their behavior depending on the fiber orientations and the cutting parameters (cutting speed and feed rate). Ramulu (Ramulu, 1997) studied the behavior of the thrust force in unidirectional and multi-directional graphite/epoxy during the edge trimming. The thrust force increases with the fiber orientation up to 45° and then starts to decrease with the fiber orientation up to 90°. Moreover, Ramulu and Sheikh-Ahmad (Ramulu, 1997; J. Y. Sheikh-Ahmad, 2009) studied the cutting forces in both CFRP and GFRP varying different cutting parameters. The cutting force changes depending on fibers orientation. It increases gradually up to 60° and then increases exponentially up to 90°. After 90°, the cutting force starts to decrease by increasing the fibers orientation. In the case of the thrust force, it remains almost unchanged for fiber orientation up to 90° and then has an oscillatory behavior between 90° up to 180°.

Although the fiber orientation is the most important factor in the cutting forces, the tool geometry such as the rake angle and clearance angle affects the forces as well. In fact, a positive rake angle decreases the cutting and thrust forces, whereas rake angle is not as significant as the fiber orientation (J. Y. Sheikh-Ahmad, 2009; Calzada, Kapoor, DeVor, Samuel, & Srivastava, 2012). In addition to the rake angle, Chatelain and al. (J.-f. Chatelain & I. Zaghbani, 2012) studied the effect of tool geometry on the cutting forces (helix angle β and rake angle α). Their results revealed that the lower the helix angle, the lower the cutting forces.

1.2.3.2 Cutting forces in orthogonal cutting CFRP/Ti

More recently, Jinyang et al. and El Mansori et al. (Jinyang, El Mansori, & El Mansori, 2016; Xu, El Mansori, Chen, & Ren, 2019) are the only ones who have worked in the characterization of cutting forces in the orthogonal cutting of CFRP/Ti stack. However, their stack setups are different from ours since their Ti plaque is on the right and their CFRP plaque on the left or vice-versa, see Figure 1.8. Thus, the cutting force and the thrust force are divided into five stages, depending on the position of the cutter into the workpiece material. In the first and second stages, the cutter starts cutting the CFRP and the forces are stable until the cutter reaches the third stage (joint between the CFRP and Titanium material). In the third stage, the cutting and thrust forces increase dramatically due to the change of behavior, passing from brittle fracture in CFRP to the plastic deformation in Ti. In the fourth stage, the cutter is completely within the titanium material and the forces are in the steady-state again. Finally, in the fifth stage, the cutting forces decrease after finishing the cutting process. Therefore, forces are highly influenced by the type of material, the cutting force being greater than the thrust force.

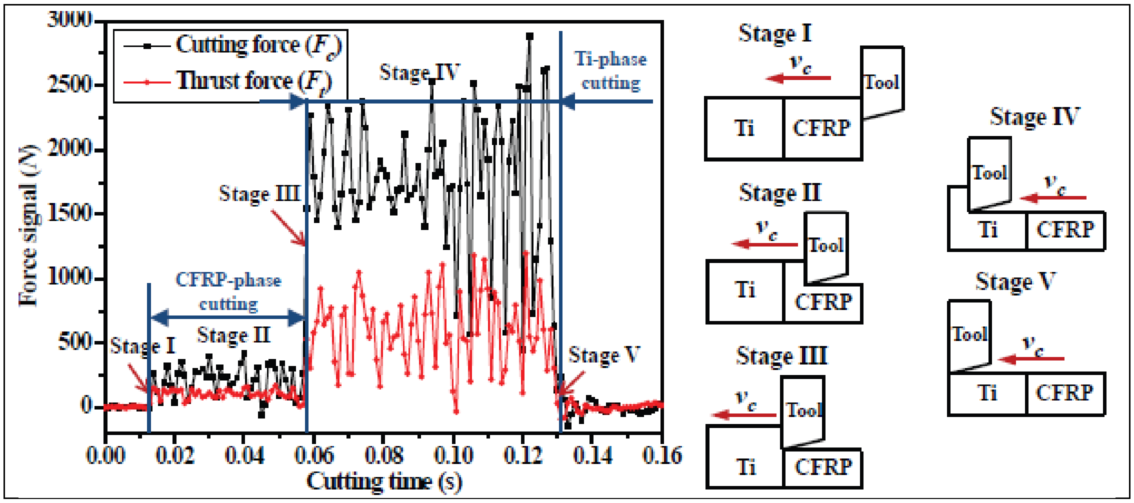

Figure 1.8 Different stages in the orthogonal cutting process of CFRP/Ti at ϴ of 0°
, v of 50m/min and f of 0.20 mm/rev
(Jinyang et al., 2016; Xu et al., 2019)

1.2.4 Chip formation in the cutting process of CFRP

The chip formation is the interaction between the cutting tool and the workpiece. In metallic materials, it is generated by continuous plastic deformations, while in the plastic materials, chip formation happens through brittle fracture, which is the case for fiber-reinforced plastic (FRP). Many authors have analyzed the chip formation following FRP machining and there are some theories in the literature although the theory of Wang's et al. (1995) is the most representative of all of them. There are five different forms of chip formation, which depends on the orientation of the fiber (*θ*) with the cutter direction and also on the sign of rake angle (positive vs negative), see. Figure 1.9. At fiber orientation of 0° and a positive rake angle, we observe that a crack begins with the contact of the workpiece and tool, and it moves along with the fiber-matrix interface. Once the cutter moves forward through the workpiece, each fiber is cut separately due to bending and compression stress or delamination, see part a) of Figure 1.9. At fiber orientation of 0° and a negative rake angle, we observe that the continuous movement of the cutter starts to compress the fiber and bends it against its origins. Thus, an in-plane shearing is created, fracturing the fiber-matrix interface. Therefore, the fiber breaks perpendicular due to “buckled” movement, see part b) of Figure 1.9. At fiber orientation of 45° and a positive rake angle, we observe that the crack is provoked by the fracture of the fiber-matrix interface, see part c). At fiber orientation of 0° and a negative rake angle, we observe that the crack is provoked by the compression of the fiber-matrix interface, see part d) of Figure 1.9. At fiber orientation of 90° and a positive rake angle, we observe that the deformation happens when the fiber is crushed and removed with the contact of the tip of the cutter, provoking the fiber fracture that is not in contact with the cutting tool, see part e) of Figure 1.9. At fiber orientation of -45° (135°). and a positive rake angle, we observe that shearing occurs when the fiber is peeled out from the workpiece due to the bending stress below the cutting tool. Additionally, it is characterized by poor surface quality, discontinuous chip, extensive delamination cracking and fiber pull-out (El-Hofy et al., 2011; Chatelain et al., 2012).

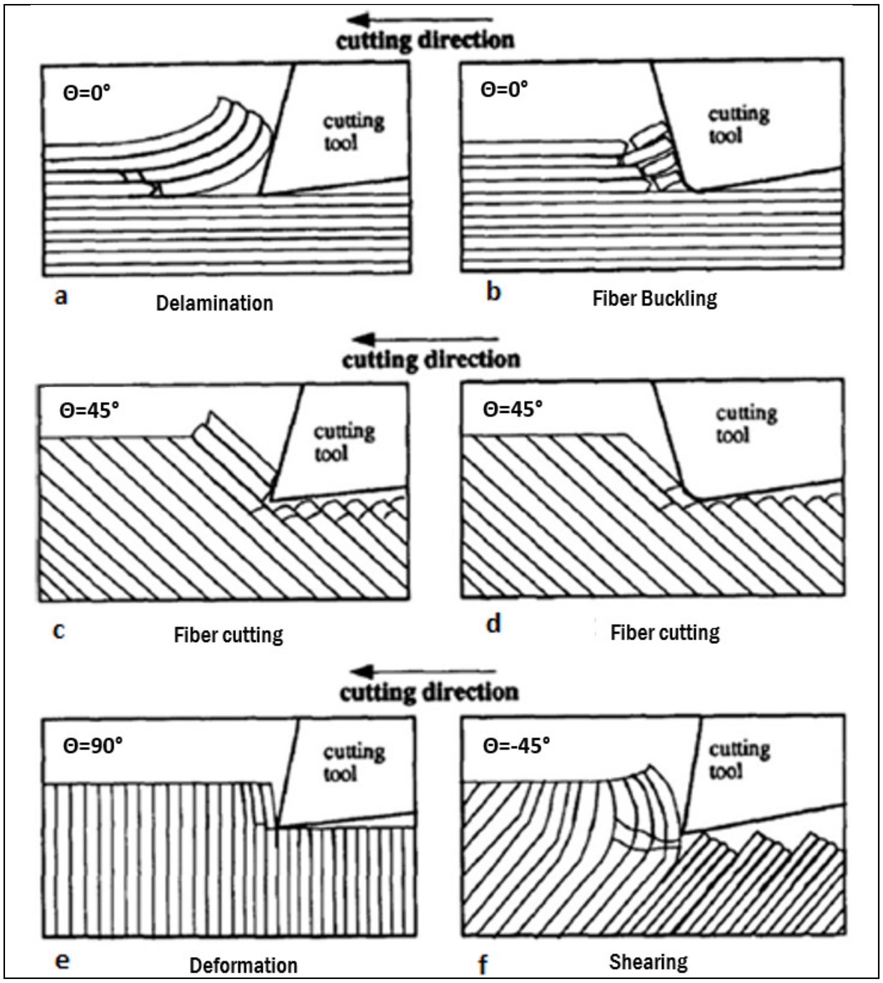
cutting direction
Θ=0°
cutting tool
Θ=0°
cutting tool
a
Delamination
b
Fiber Buckling
cutting direction
Θ=45°
cutting tool
Θ=45°
cutting tool
c
Fiber cutting
d
Fiber cutting
cutting direction
Θ=90°
cutting tool
Θ=-45°
cutting tool
e
Deformation
f
Shearing

Figure 1.9 Cutting mechanisms in orthogonal machining of CFRP
(D. H. Wang et al., 1995)

1.2.5 Surface roughness

Roughness is defined as the surface waviness in a cross-section area and depends on several factors such as the feed rate magnitude, cutting speed, flank wear, material workpiece, tool geometry, fixture stiffness, coolant, etc. The workpiece surface quality is characterized by lay, waviness and roughness. Theoretically, a lay is an imaginary line describing the contour of the ideal surface, roughness is the height of peaks and valleys of the surface and the waviness is the highest irregularity. The most frequent statistical parameters used to characterize a surface quality are: R_a (arithmetic mean value), R_v (means to the valley height), R_z (ten points average height) R_t (maximum peak to the valley height), R_p (maximum peak to mean height) (2009).

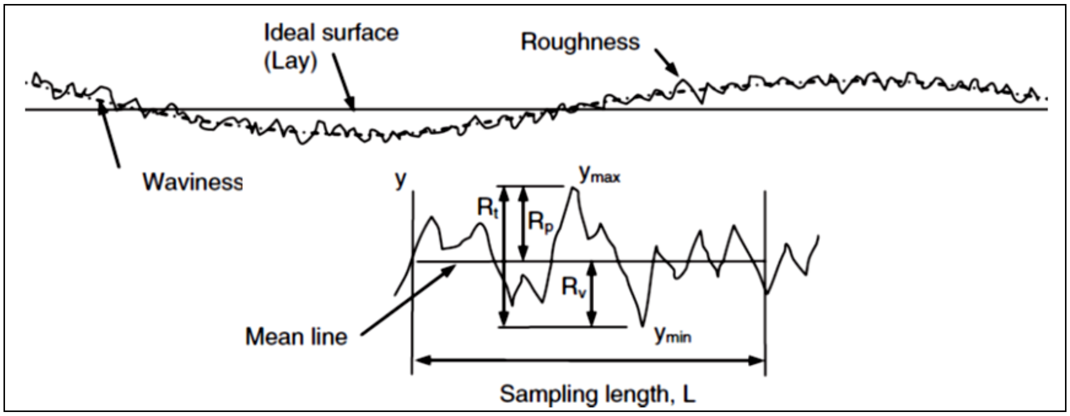

Figure 1.10 Schematic roughness representation
(J. Y. Sheikh-Ahmad, 2009)

For metals, the greater the cutting speed, the lower the surface roughness, but not for titanium alloys. Therefore, the roughness increases with the cutting speed (Nurul Amin, Ismail, & Nor Khairusshima, 2007). In a more recent study, Yang et al. (Yang & Liu, 2015) recommend a low feed per tooth and radial depth of cut and high-cutting speed to reduce the surface roughness.

In the case of CFRPs, the R_z value decreases with increasing the cutting speed and decreasing the feed rate (Davim, Reis, & António, 2004), the feed rate being the most significant effect. Therefore, the lower the feed rate, the better the surface quality whatever the cutting speed and ply orientation (Chatelain et al., 2012). Additionally, the machined surface is not only determined by the cutting parameters but also by the cutter and the fiber direction.

El-Hofy et al. (El-Hofy et al., 2011) analyzed the effects of different cutter materials and the cutting environments such as cold, dry air, concluding that neither the cutter material nor the cutting environment are significant factors. In addition to the cutter material and environment, the cutter geometry influences the roughness parameters of machined CFRPs so that 2 straight flutes or 0 helix angle (β) shows better surface quality than other cutters. Thus, the best surface roughness is at a fiber orientation of 45° and the worst is at -45° (135°) for the most typical roughness profiles (R_a, R_v, R_z) (2012; 2012).

Additionally, the CFRPs are prone to delamination, fiber pull-out, loose fiber, matrix cracking, matrix thermal degradation, etc. As a result, Figure 1.11 shows examples of problems during the machining of CFRPs.

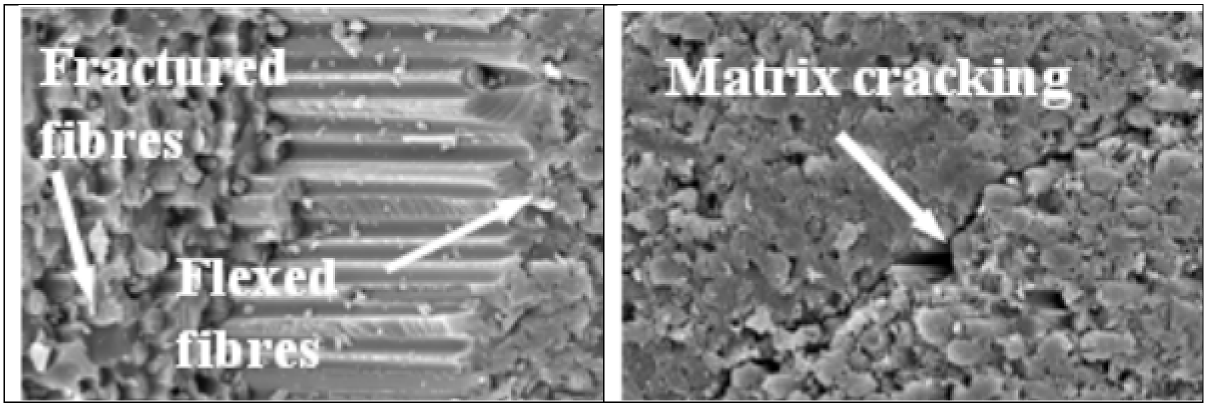

Figure 1.11 Example of main problems in machining CFRP
(El-Hofy et al., 2011)

1.3 Thermal effects during machining

As shown in the previous sections, most researchers have oriented their research in understanding the cutting parameters of CFRP and Ti plaque. However, few researchers have focused on measuring the cutting temperature during the edge milling cutting process for the CFRP and Ti plaques (Yashiro, Ogawa, & Sasahara, 2013; Lance, Chatelain, & Songmene, 2014; Santiuste, Diaz Alvarez, Soldani, & Miguelez, 2014; H. Wang, Sun, Li, et al., 2016; H. Wang, Sun, Zhang, et al., 2016; J. Sheikh-Ahmad, Almaskari, & Hafeez, 2018). The only study that is closer to the edge milling process of CFRP/Ti stack is an orthogonal study performed by Xu et al. (Xu & El Mansori, 2015, 2016), but their setup is CFRP on the right and Ti on the left or vice versa. Due to the complexity of the process, this type of model cannot fully explain the edge milling of CFRP/Ti6Al4V stack or its thermal distribution. Machining CFRP/Ti6Al4V stack is a challenge due to the different mechanical properties of each material. In the case of Ti6Al4V, it has a low thermal conductivity which can vary from 6 to 9 W/mK (H. B. Wu & Zhang, 2014; Ducobu & Rivière-Lorphèvre, 2016) and high machining temperatures of about 500°C in dry conditions. On the other hand, the CFRPs longitudinal thermal conductivity is 6 W/mK and its transversal thermal conductivity is 0.5 W/mK (Santiuste et al., 2014) adding up a glass transition of 175 °C which is the temperature at which the thermoset epoxy matrix starts to degrade. To the author’s knowledge, there is nothing related to thermal studies in CFRP/Ti.

1.3.1 Temperature measurement methods

In the case of metal machining, there are some techniques to measure the variation of temperature like heat-sensitive painting, liquids, coating, etc. In addition to heat-sensitive methods, the temperature can be measured by contact using thermometers and thermocouples or distance using pyrometers and thermal cameras. In the machining process of CFRP and Ti, thermocouples and thermal cameras are the favorites methods used due to their reliability compared to heat sensitive coating. Generally, the thermal camera is used to measure the temperature in static bodies. Pan et al. and Yashiro et al. (Yashiro et al., 2013; Pan, Kamaruddin, Ding, & Mo, 2014) used this method to measure the cutting temperature both on the tool and workpiece during the end milling surface cutting process. This method was able to measure the temperature at high-speed. However, the thermography was saturated in the case of Ti milling. Thus, it was unable to distinguish the temperature in the cutter-workpiece interface due to the high temperature on the primary shear zone, as shown in the left side of Figure 1.12. In the case of CFRP, the thermography of Yashiro et al. (Yashiro et al., 2013) was not saturated but the temperature could not be observed clearly at a specific point. This is because the area of the cutting process was always hidden by the cutter, reflecting inaccurate temperature. More recently, Sheikh-Ahmad et al. (J. Sheikh-Ahmad et al., 2018) used the black body technique which consists in heating each object to the same temperature with the aim of knowing the emissivity of each object. Therefore, the technique was able to measure the cutting temperature around the cutter, dust bloom and workpiece by the adjustment of the speed frame. The right side of Figure 1.12 shows an example of Sheikh-Ahmad's thermography camera in the edge milling of CFRP.

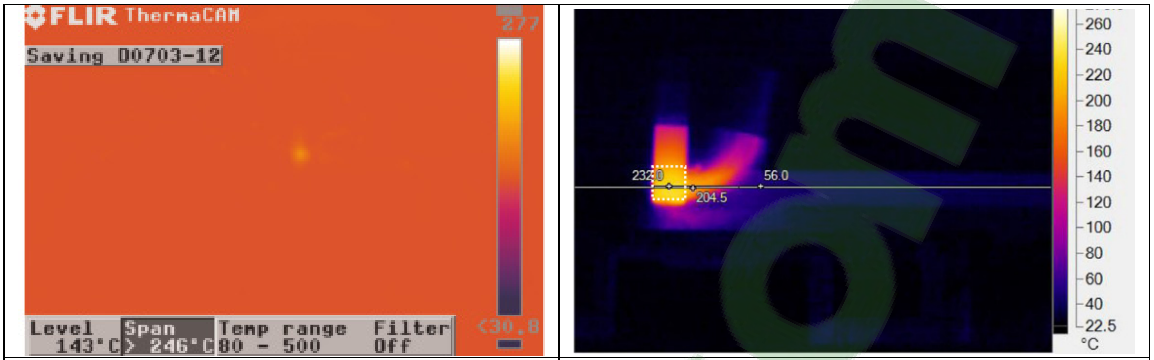

Thermography in Ti milling
(Pan, Ding, & Mo, 2014)

Thermography in CFRP
(J. Sheikh-Ahmad et al., 2018)

Figure 1.12 Thermography's examples

Many techniques applied to metal cutting are also applied to CFRP like the thermocouple method (2013). This method uses embedded type K thermocouple in both the cutter and workpiece, the type K (Chromel–Alumel) being the most common for general-purpose. For example, Li et al. (L. Li et al., 2004) measured the cutting temperature on Ti6Al4V shoulder milling, setting the thermocouples in the middle of two blocks. The thermocouple method performed well for the milling process. Nevertheless, the study showed parasite temperature measurements due to the low stiffness and high vibration of the setup.

Yashiro et al. (2013) measured the temperature by embedding thermocouples during the lay-up process of the CFRP, see image 1) of Figure 1.13. On the other hand, Lance et al. (Lance et al., 2014) and J. Sheihk-Ahmad et al. (2018) used the drilled method to embed the thermocouples into the CFRP. Their method consists of drilling and filling the holes with thermal conducting paste with the aim of measuring the temperature on the workpiece. Thus, they inserted the thermocouples as closely as possible from the cutting edge. Image 2) of Figure 1.13 shows an example of the drilling method used by J. Sheihk-Ahmad et al. In the case of Lance et al. (Lance et al., 2014), their thermocouples were not placed at the same distance because of the low stiffness of the micro-drill used in the process, combined with the orthotropic properties of CFRP. Therefore, Lance et al.(2014) registered differences in the temperature of the thermocouples due to the positioning errors during the drilling process of CFRP/Ti6Al4V. Haijin et al., H. Wang et al., and Yujing et al. (Yujing et al., 2014; H. Wang, Sun, Li, et al., 2016; H. Wang, Sun, Zhang, et al., 2016) used a semi-artificial thermocouple to

clicours.com

measure the temperature both in Titanium and in CFRP in separate works. The semi-artificial thermocouple is a handmade thermocouple similar to a metal sheet, calibrated by correlating the voltage to temperature. Even though there is no physical device, the semi-artificial thermocouple is able to measure the cutter temperature, see image 3) of Figure 1.13. Researchers are also interested in measuring the temperature of the cutter. Brinksmeier et al. (2011) stuck thermocouple on the tip of the cutter and Yashiro et al. (2013) correlated the temperature through the differences of voltage between the CFRP and the cutter material. Both methods used wires from the experimental setup to the acquisition data. Thus, it is susceptible to break/unplug during the edge milling cutting process. Although the wired connection has positive results, it needs a special preparation setup to prevent wrong measurements (Brinksmeier et al., 2011; Yashiro et al., 2013). Another method, thanks to technological evolution, to measure the temperature on the cutter tool is through a telemetry system. It transmits the signal from the tool holder to a transducer via a wireless system. As a result, this method uses embedded thermocouple near the cutting point which is connected to the tool holder and is able to measure the temperature in real-time (Kerrigan, Thil, Hewison, & O'Donnell, 2012; Lance et al., 2014; Ghafarizadeh, Lebrun, & Chatelain, 2016; Kerrigan, O’Donnell, & O’Donnell, 2016; Delahaigue, Chatelain, & Lebrun, 2017). Nevertheless, the disadvantage of both methods is that the thermocouple is prone to detach from the cutter. This is a result of the dynamic forces and the friction between pieces during the cutting process.

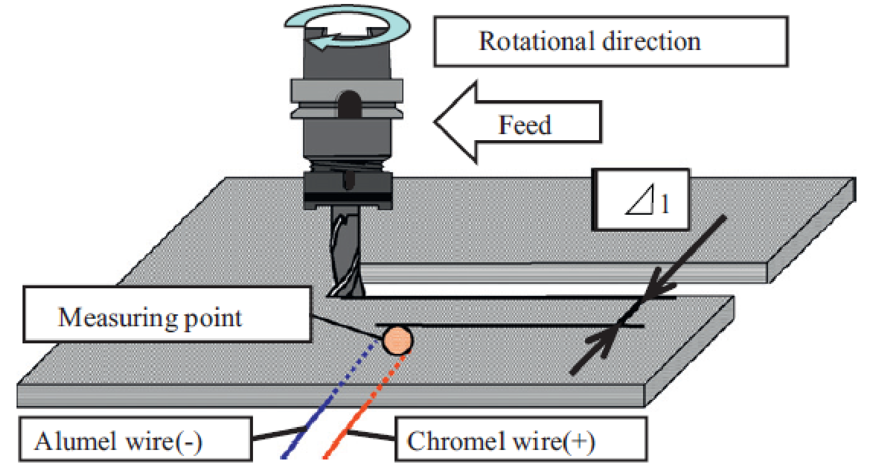
Rotational direction
Feed
⊿1
Measuring point
Alumel wire(-)
Chromel wire(+)

1). Layout method (Yashiro et al., 2013)

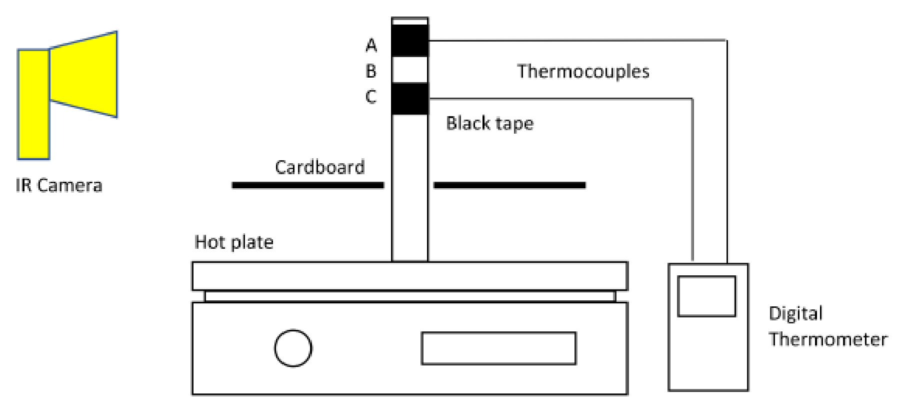
A
B
C
Thermocouples
Black tape
Cardboard
IR Camera
Hot plate
Digital Thermometer

2). Drilling method (J. Sheikh-Ahmad et al., 2018)

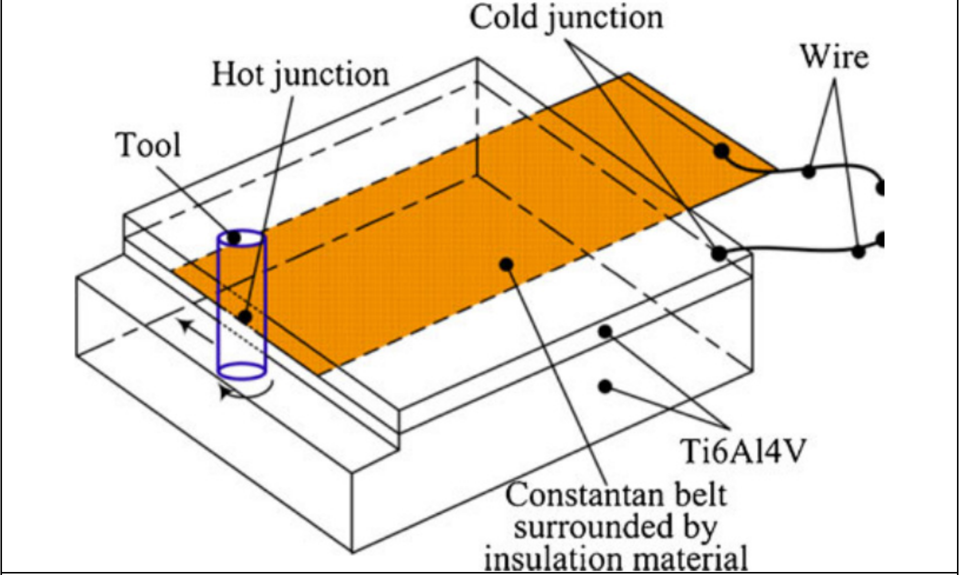
Cold junction
Wire
Hot junction
Tool
Ti6Al4V
Constantan belt surrounded by insulation material

3). Semi-artificial method (Yujing et al., 2014)

Figure 1.13 Embedded thermocouple methods in CFRP and Ti materials

Clicours.COM

1.3.2 Influence of cutting temperature in the machining process

The machining process of metallic materials is produced by the plastic deformation, which is converted into heat. The main source of heat is located on the primary shear zone (shear force and normal force to shear plane in Figure 1.7) and the tool-chip interface. High temperatures in the cutting process can be verified by the dark-bluish color of the chips caused by the metal oxidation. In most metals, 90% of the heat is taken away by the chip while 80% of all the heat is concentrated on the cutter edge during the machining of titanium alloy. This is because of its low thermal conductivity (Nouari & Ginting, 2006). For reference purposes only, the thermal conductivity of the Ti6Al4V can vary from 6 to 9 W/mK (H. B. Wu & Zhang, 2014; Ducobu & Rivière-Lorphèvre, 2016). While for steels, it is 50 W/m °K (Nurul Amin et al., 2007). Generally, the machining temperature (T_m) can be represented by the equation (1.4)

$$T_m = u\sqrt{\frac{vf}{kpc}} \tag{1.4}$$

Where v is the cutting speed, f is the feed, u is the specific cutting energy, k is the thermal conductivity, p is the density and c is the specific heat of the workpiece (Shaw, 2004; Pramanik & Littlefair, 2015). It is clear that the temperature is influenced by the cutting parameters and material properties. This means the harder the workpiece material, the higher the cutting temperature. Therefore, it needs higher specific cutting energy and consequently increases the cutting temperature in the case of metals.

1.3.2.1 Influence of cutting parameters on the temperature of Ti

Pan et al. (Pan, Ding, et al., 2014; Pan, Kamaruddin, et al., 2014) studied the effects of the cutting speed, feed rate and axial depth of cut on the cutting forces in end milling. The study shows the forces increase with the cutting speed. However, the feed rate was more statistically significant than the cutting speed and axial depth of cut.

In the literature, most works are focused on understanding the effects of the cutting parameters in the forces. Yujing et al. (Yujing et al., 2014) studied the cutting parameters over the interface workpiece-tool temperature with a semi-artificial thermocouple according to the cutter exit/enter, see the right part of Figure 1.14. The study showed that the cutting speed is the main factor and is more statistically significant than the feed rate, followed by the radial feed and lastly the axial feed, following that order, see the right part of Figure 1.14.

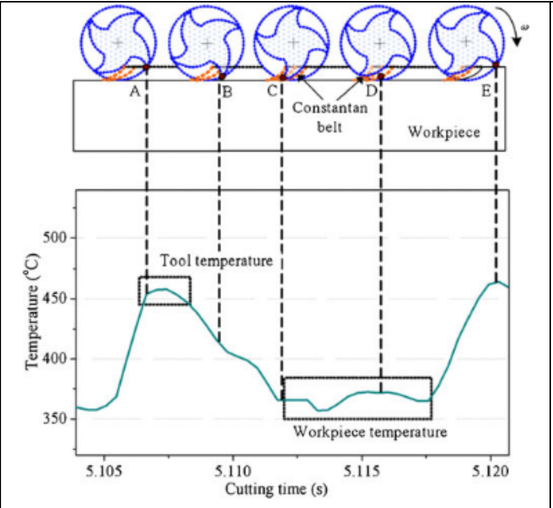

Thermocouple recording method

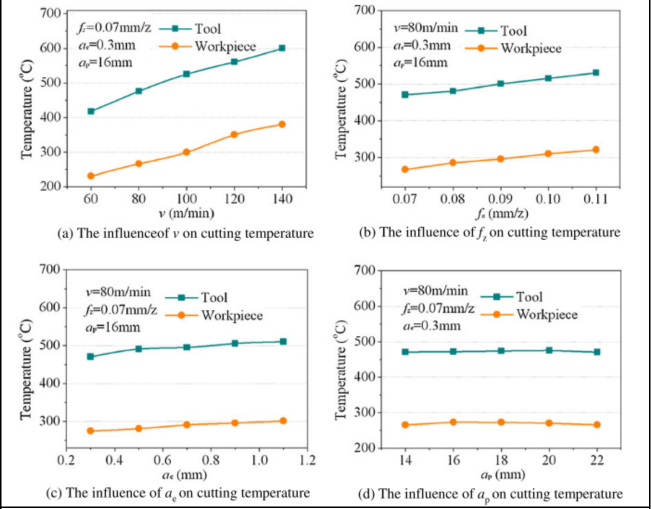

(a) The influenceof v on cutting temperature

(b) The influence of f_z on cutting temperature

(c) The influence of a_e on cutting temperature

(d) The influence of a_p on cutting temperature

Cutting parameters influence

Figure 1.14 An experimental investigation in milling Ti6Al4V
(Yujing et al., 2014)

1.3.2.2 Influence of cutting parameters on the temperature of CFRP

As it was mentioned at the beginning of this chapter, a few researchers focused on understanding the thermal effects on CFRP. Yashiro et al. (2013) studied the influence of the cutting parameters over the temperature, keeping the feed per tooth as a constant through the development of the experiments. Their study revealed that the lower cutter speed, the higher the temperature in the workpiece. As a result, they suggested a high-cutting speed of up to 300 m/min to decrease the workpiece temperature. This is because using these cutting speed values, the CFRP plaque did not show matrix thermal damage looking through the Scanning Electron Microscope (SEM). Therefore, the temperature was below 180°C which is the glass transition temperature for thermoset matrix resin. However, it should be mentioned that type K thermocouple was very sensitive to the distance and it was registered a temperature difference of about 54°C between the distance of the cutting edge and thermocouple tip (Δl) equal 0.6 and Δl equal 0.3 mm from the cutter edge, keeping the same cutting conditions.

Haijin et al. (H. Wang, Sun, Li, et al., 2016) studied the effects of cutting parameters on the force and temperature. The study found that the greater the cutting speed, the lower the forces. However, this is opposite to the temperature since the growth of temperature is notably higher with the increase in the cutting speed. In addition to the cutting speed, the analysis also focused on the effects of the feed rate and the radial depth of cut and their effects on the forces and the temperature. By increasing the magnitude of the feed rate, there is a significant growth in the forces. However, this effect is much less significant in the temperature increase. For the radial depth of cut, neither force nor temperature is influenced by this parameter. Therefore, in order to keep a low temperature on the workpiece and machine efficiency, it is recommended setting up a low cutting speed, low feed rate, and high radial depth of cut. Thus, the cutting speed is the factor which influences the temperature and feed rate is the factor which influences the cutting forces. In the case of the radial depth of cut, this has little influence both on temperature and forces.

Kerrigan et al. (Kerrigan et al., 2016) measured the cutter temperature using an embedded K thermocouple, through a Wireless Tool Holder module system and infrared camera for the workpiece. Their results showed that feed rate is the main factor effect, followed by the axial depth of cut and finally the workpiece location on the cutter axis for the cutting forces. On the other hand, the temperature on the cutting tool showed a different behavior from forces. The axial depth of cut is the most significant factor, followed by the central workpiece location on the cutter axis while the feed rate is the least significant factor. It should be mentioned that although the study used a thermal camera to measure the temperature of the workpiece, there is no information about their results.

1.3.3 Thermal aspects during machining CFRP

Machining CFRPs materials can provoke different cutting defects both in the fibers and matrix. The most common defects in CFRP are fiber pull out, delamination, matrix cracking and thermal damage. In the case of thermal damage, it occurs when the temperature inside the CFRP exceeds the thermoset glass transition temperature (T_g). This temperature is about 175 °C ±10 °C for the epoxy matrices. Additionally, the thermoset matrix has very poor thermal conductivity and is about 0.21 W/mK (Khashaba, 2013) to 0.35 W/mK (Nomura & Haji-Sheikh, 2018). The thermal conductivity of the composite (fiber + matrix) can be calculated by using the rule of mixture, equation (1.5).

$$K_c = K_f V_f + K_m(1 - V_f) \tag{1.5}$$

Where K_m and K_f are the thermal conductivity of the matrix and fiber and V_f is the fiber volume fraction. Therefore, the CFRP's longitudinal thermal conductivity is 6 W/mK and its transversal thermal conductivity is 0.5 W/mK (Santiuste et al., 2014), which are very low compared to steel at 50 W/mK.

H. Wang et al. (2016) studied fiber orientation on thermal effects during the milling process by using a semi-artificial thermocouple. The study found that the cutting forces start to rise and then to decrease with the increase of the cutting speed at fiber orientation θ of 0°, 45°, 90° and 135°, see the left side of Figure 1.15. This is because the heat generated by the cutter in the cutting zone softens the epoxy matrix. As a result, the amount of energy transferred into the CFRP workpiece increase too. Similar results were found by Yashiro et al. (2013). The right part of Figure 1.15 shows that cutting temperature in the 45° fiber orientation is always the lowest while the 135° fiber orientation is always the highest no matter how fast the cutting speed is.

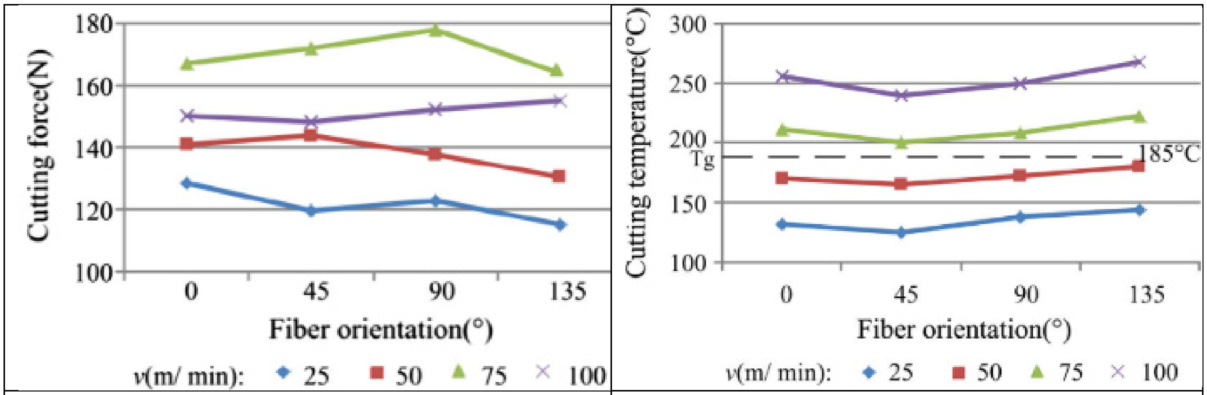

Effects of cutting forces vs θ

Effects of temperature vs θ

Figure 1.15 Analysis of thermal effects on the fiber orientation
(H. Wang, Sun, Zhang, et al., 2016)

This can be explained by using the heat transfer equation:

$$\Delta T = \frac{q_s}{\rho c(4\pi a v X)^{1/2}} . exp\left(-\frac{vy}{4aX}^{2}\right) \tag{1.6}$$

Where ΔT is the temperature increase, q_s is the heat source; c is the specific heat capacity, ρ is the heat medium density; λ is the thermal conductivity, $\alpha = \lambda/\rho c$ is the heat dissipation rate, v is the cutting speed; y is the shortest distance from the heat source to the reference point and X is the moving distance of the cutter, $X=vt$. By solving equation (1.6) in terms of partial derivative ($\delta\Delta T/\delta\alpha$), the temperature can decrease by increasing the heat dissipation rate $2\alpha t>y$. This means that the thermal build-up and the rise in temperature are due to the low thermal conductivity of the material when the monitoring position is very near to the surface of the cut. Thus, the thermal conductivity for each fiber orientation is different because the heat dissipation rate α changes according to ϑ, as shown in Figure 1.16. As a result, the temperature rises from point A to B.

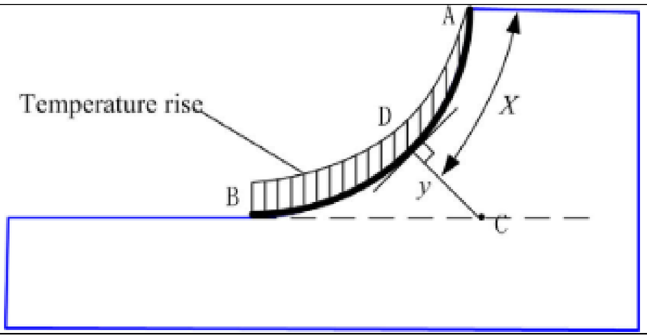
A
Temperature rise
D
X
B
y
C

Thermal analysis of milling

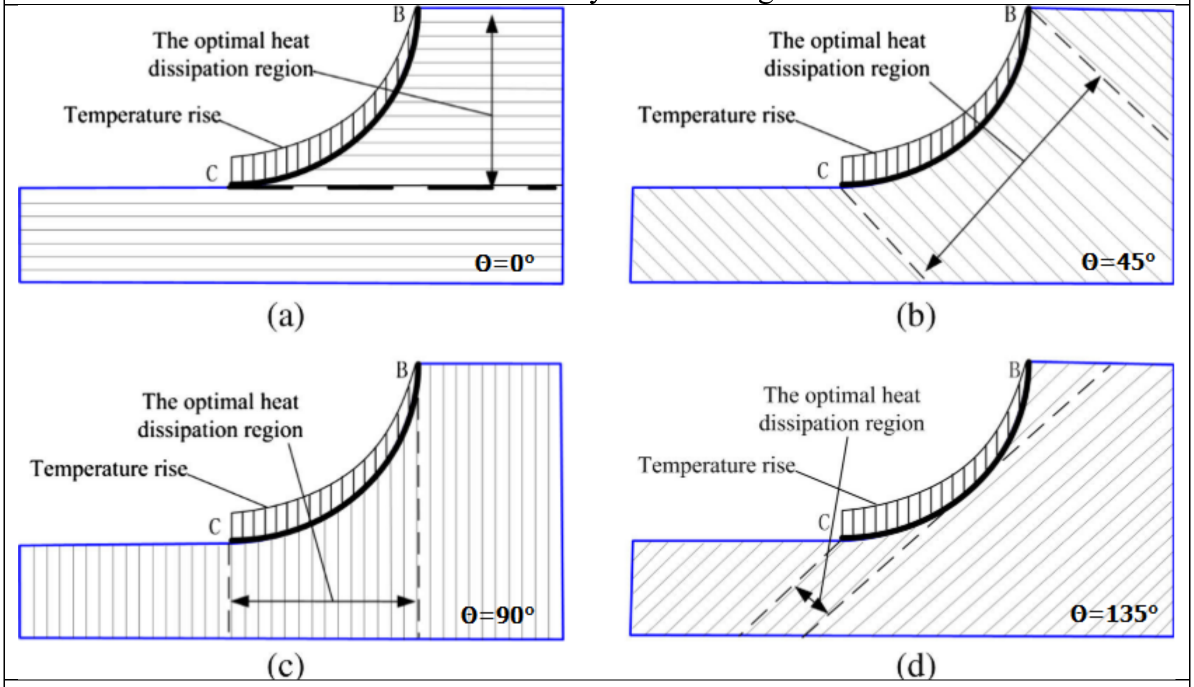
The optimal heat dissipation region
B
Temperature rise
C
θ=0°
(a)
The optimal heat dissipation region
B
Temperature rise
C
θ=45°
(b)
The optimal heat dissipation region
B
Temperature rise
C
θ=90°
(c)
The optimal heat dissipation region
B
Temperature rise
C
θ=135°
(d)

Thermal effect on the fiber orientation

Figure 1.16 Thermal analysis in CFRP milling for different fiber orientation
(H. Wang, Sun, Zhang, et al., 2016)

In the case of unidirectional CFRP, the thermal conductivity λ is described by equation (1.7):

$$\lambda_{c,\theta} = \lambda_{c,\rho} \cos^2 \theta + \lambda_{c,t} \sin^2 \theta \tag{1.7}$$

Where θ is the fiber orientation with respect to cutter movement, $\lambda_{c,\theta}$ is composite thermal conductivity, $\lambda_{c,\rho}$ is the thermal conductivity in a parallel orientation with the fiber, $\lambda_{c,t}$ is the thermal conductivity in a transverse orientation direction with the fiber. It should be noted that $\lambda_{c,\rho}$ are 10 times greater than $\lambda_{c,t}$. The highest heat dissipation is along the 45° fiber orientation.

This is because the heat dissipation region is the same for all angles and it is fixed by the tool radius. Thus, heat dissipates more in the 45° direction since its thermal conductivity is higher in the fiber direction than in the transverse direction following the cutter path from B to C as compared to 0° and 90°, as shown in the right side of Figure 1.16. In the case of 0° and 90°, the heat dissipation is the same for both of them. Nevertheless, the fiber breakage due to machining at 0° is different than for the 90° fiber orientation. Thus, the surface finishing is much better in the case of 0° which is totally covered with epoxy. However, in the case of 90°, the fiber is exposed by the cutting fracture. Finally, the worst case of heat flow is given by 135° because the heat flows almost perpendicular to fibers for all the cutter path (from B to C). It also has the worst surface finish and roughness of all the fiber orientations. In addition, Figure 1.17 (region 1 to 3) shows the carbon fibers and mini-grooves due to thermal damage. This is as a result of the heat concentration in the workpiece, resulting in both mechanical and matrix thermal damage when the *Tg* is exceeded.

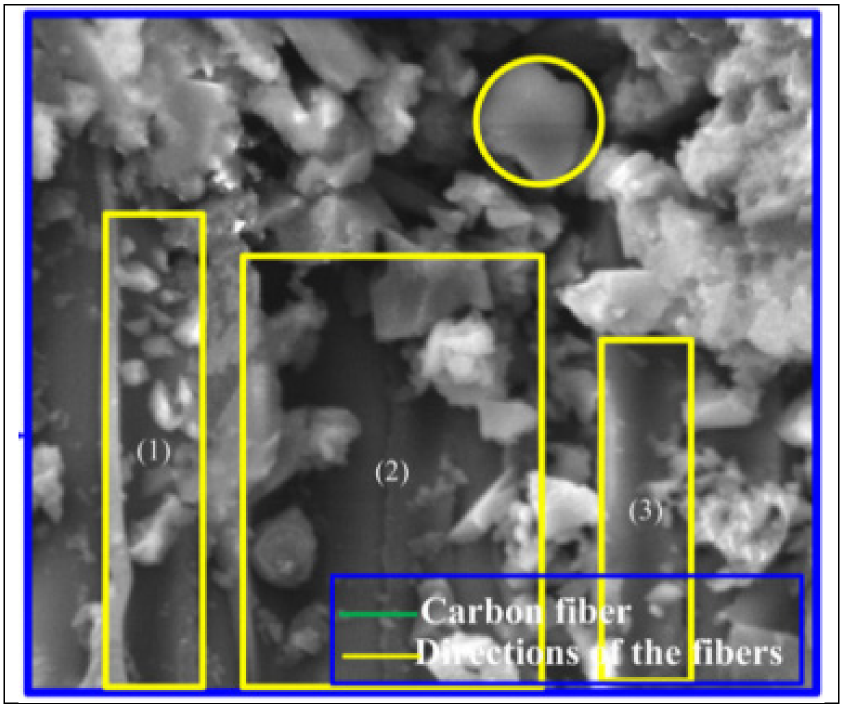

Figure 1.17 Example of thermal damage observed by SEM
(H. Wang et al., 2016)

1.3.4 Heat flux in CFRP plaque

Sheikh-Ahmad et al. (2018) studied the heat flux surrounding the workpiece, chip and tool by using thermographs. The temperature was measured every 3 seconds on the cutter and chip, combining an experimental and numerical study. Additionally, they tested different tool materials and geometries during the edge trimming of CFRP plaque. In order to avoid saturated images, the black body technique was used with the aim of knowing the emissivity of each object. The study showed that the hottest cutting zone was located in the cutter registering temperatures from 220 to 250°C. Then it is followed by the chip temperature from 160 to 220°C and lastly, the workpiece registered the coldest temperature of about 60°C due to the heat dissipation through the chip. The study also shows that the helix angle has an effect on the temperature. Therefore, the smaller the helix flux of the cutter tool, the higher the temperature on the cutter since the chip cannot be easily evacuated, blocking all the heat flow. Statistically speaking, neither the cutting speed nor the feed rate was statistically significant in the heat exchange on the cutter. On the other hand, the feed is statistically significant on the workpiece temperature. Thus, the higher the feed rate, the lower the temperature on the workpiece. This result is contradictory to other works (Yashiro et al., 2013; H. Wang, Sun, Li, et al., 2016) in which the main factor is the cutting speed. Analytically, the heat flux in the machining process can be calculated by using an equation of energy balance (1.8):

$$\dot{Q} = \dot{Q}_t + \dot{Q}_w + \dot{Q}_c \tag{1.8}$$

Where $\dot{Q}$ is the mechanical power transformed to heat, $\dot{Q}_t$ is heat conducted by the tool, $\dot{Q}_w$ is heat conducted by the workpiece, $\dot{Q}_c$ is heat conducted by the chip. Hence, equation (1.8) can also be represented by equation (1.9):

$$\begin{gathered} \dot{Q} = P_{el}\eta \\ \dot{Q}_w = \dot{q}_w . A_w \\ \dot{Q}_t = \dot{q}_t . A_t \end{gathered} \tag{1.9}$$

clicours.com

Where P_{el} is electrical power consumed by the machine, η is the spindle efficiency, $\dot{q}_w$ is the heat flux value in the workpiece, $\dot{q}_t$ is heat flux value in the tool, A_w is contact area in the workpiece and finally, A_t is the contact area in the tool. The study showed that 5% of the heat is transferred to the workpiece, 30% to the cutter and lastly 65% was carried away by the chip. The PCD tool is the one that received the least heat portion. Therefore, the greater the chip thickness, the higher the heat transferred to the chip thickness.

1.4 Summary of the literature review

After the literature review, we found that there are no experimental study regarding the thermal distribution within the material due to the edge milling of CFRP/Ti6Al4V stack. The only two studies that consider both materials are orthogonal studies (Jinyang et al., 2016; 2019) which characterize the cutting forces at each stage of the cutter within the workpiece material. However, there are some separate works that study the thermal effects using different method measurements for both Titanium (Lin et al., 2013; Yujing et al., 2014) and CFRP (Yashiro et al., 2013; Santiuste et al., 2014; Kerrigan et al., 2016; H. Wang, Sun, Li, et al., 2016; H. Wang, Sun, Zhang, et al., 2016; J. Sheikh-Ahmad et al., 2018). Thus, these methods were reviewed on the basis of their findings, the tool-workpiece thermocouple method (Yashiro et al., 2013; J. Sheikh-Ahmad et al., 2018) being the one with the best results. This is because the workpiece and cutter temperature were measured independently avoiding saturated image in the case of thermal cameras (Pan, Kamaruddin, et al., 2014) or mixed-up measurements in the case of the semi-artificial method (Yujing et al., 2014; H. Wang, Sun, Li, et al., 2016; H. Wang, Sun, Zhang, et al., 2016). Finally, it was also reviewed how the temperature within the workpiece changes depending on the cutting parameters for both CFRP and Ti materials, the cutting speed being the most relevant factor in both cases.

1.4.1 Objective

The main goal of this thesis is to study the thermal effects in the edge milling of CFRP/Ti6Al4V hybrid material using three types of cutters in machining process, varying the cutting speed *v*, feed per tooth *ft* and radial depth of cut a_e and their influences on the cutting temperature for both the workpiece and the cutter.

In addition to the workpiece and cutter temperature, this research addresses three sub-objectives with the aim of knowing the influence of the different cutter materials and cutter parameters (*v*, *ft* and *ae*) over the cutting forces, roughness and tool wear in order give final recommendations regarding the manufacturing of edge milling of CFRP/Ti6Al4V plaques.

This thesis is divided in three chapters and ends with a conclusion and recommendations. The first chapter is subdivided into 4 sections. The first and second sections describe the fundamentals of CFRP/Ti6Al4V stacks and the CFRP and Ti6Al4V machining process. The third section presents the most relevant publications regarding thermal effects in CFRP and Ti6Al4V materials due to machining. The second chapter presents the methodology utilized in this research such as cutter selection, screening, manufacturing process of specimens and interpretation of the output variables. Chapter 3 describes the result and discussion concerning the machining experiments of our specimen of CFRP/Ti6Al4V stacks of materials.

Clicours.COM

CHAPTER 2

METHODOLOGY

As described in the previous chapter, the main goal of this thesis is to study the thermal effects on CFRP/Ti6Al4V in the process of edge milling. In particular, we study the tool-workpiece thermocouple method in this research by using commercial thermocouples. Additionally, we study the effects of the forces, roughness, tool wear for different types of cutters while varying cutting speed v, feed per tooth ft and radial depth of cut a_e. Therefore, this chapter describes in a detailed and precise manner the steps followed in this research.

2.1 Machine and Setup

The edge milling operation was performed with the HURON K2X10 Computer Numerical Control (CNC) machine tool. The CNC is located in the Laboratoire d'Ingénierie des Produits, Procédés et Systèmes (LIPPS). This is a 3-axis machine which uses the Siemens 840D controller having a maximum rotating speed of 28,000 RPM. Moreover, the machine is equipped with a vacuum system for dust removal during the machining of CFRP materials. The specifications of the machine are presented in Table 2-1.

Table 2-1 Machine Huron specification

Huron K2X10	**Description**	UGV-3 axis CNC
	Manufacturer	Huron K2X10
	Driver	Siemens 840D
	Tool pocket	20
	Races	1000x800x500 mm
	Spindle Speed	28,000 RPM
	Cutting feed rate	30000 mm/min

Machining hard materials like Ti6Al4V is a difficult task due to the strong impact forces when the teeth engage in the workpiece. The most commons defects are bad surface finish, dimensional accuracy, premature wear, failure of the cutting tool. This is due to the high fluctuation of the forces. Thus, choosing a stiff work-holding setup is extremely important to keep the integrity of the workpieces and cutters involved in the cutting process. The LIPPS setup offers these characteristics eliminating the vibration of the cutting forces which disrupt temperature measurements. The setup is built in 2 parts: the upper part has the shape of an “L” and the bottom part has the shape similar to the greek letter “Omega” (Ω), as shown in Figure 2.1. This setup works for plaques with a max length of 101.6 mm (4 in), max width of 50.8 mm (2 in) and adjustable grip. Therefore, both workpiece and cutter are protected by the setup stiffness.

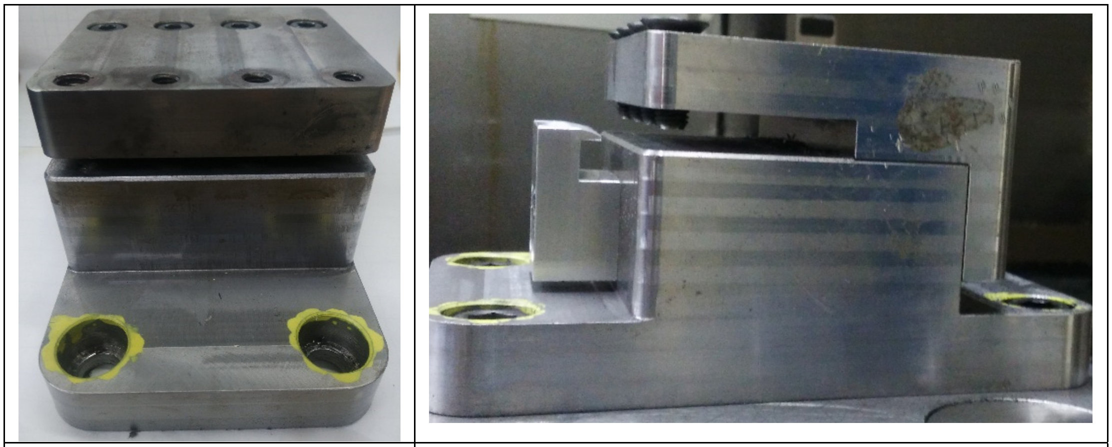

Set up front view

Set up right view

Figure 2.1 Setup for CFRP/Ti

2.2 Selection of cutting tool

The correct selection of cutting tools is among the most important factors for machining operations and their selection depends on what is going to be machined. This is because there is no special tool for edge milling of CFRP/Ti stack. Our selection is based on the literature review. In the case of CFRP material, PCD cutters are ideal for machining abrasive material such as CFRP due to their high wear resistance (Bérubé et al., 2012; Chatelain et al., 2012 ; H. Wang, Sun, Li, et al., 2016; J. Sheikh-Ahmad et al., 2018). This choice has been made even though PCD cutters are not recommended to machine ferrous materials. In the case of

Ti6Al4V, this material is generally machined using uncoated or coated carbide tools because of its high-impact strength (J. Sun & Guo, 2009; Yujing et al., 2014; Yang & Liu, 2015). Therefore, the experiments will use three different cutters of 12.7 mm (1/2”) of diameter: 1 for machining Titanium alloys, 1 for machining CFRP and 1 for a general purpose. This is with the aim of measuring the influence of the different types of cutters over the cutting temperature, forces and surface finish.

1. Tool number 1 is a Niagara multipurpose uncoated cutter. This tool can be used for machining titanium alloys even though it is susceptible to tool wear. Moreover, this tool is the cheapest of the three. The specifications of Tool number 1 are presented in Table 2-2.

Table 2-2 Niagara tool or Tool number 1 specifications

	Company	Niagara General purpose C430
	Tool part number	N85534
	Coating	Uncoated Solid carbide
	Diameter	12.7 mm (1/2”)
	Shank Diameter	12.7 mm (1/2”)
	Cutting length	25.4 mm (1”)
	# of flutes [N]	4
	Helix angle [β] °	30°
Niagara or Tool or tool # 1	**Rake angle**	0°

2. Tool number 2 is a Walter TAA (TiAlN+ TiAlN) coated cutter and is specially designed for machining Ti alloys. Montoya et al. (Montoya & Chatelain, 2013) used this type of coating to perform CFRP/Ti6Al4V elliptical drilling. In addition, its cost is 10 to 6 times cheaper than PCD cutters and 3 or 4 times more expensive than tool 1. The specifications of Tool number 2 are presented in Table 2-3.

Table 2-3 Walter tool or Tool number 2 specifications

	Company	Walter Proto. Max. Inox
	Tool part number	AH2034217-1/2
	Coating	TAA
	Diameter	12.7 mm (1/2”)
	Shank Diameter	12.7 mm (1/2”)
	Depth of cut	25.4 mm (1”)
	# of flutes [N]	4
	Helix angle [β] °	35/38°
Walter Proto or tool # 2	**Rake angle °**	2°

3. Tool number 3 is an Onsrud PCD cutter with 2 straight flutes and is specially designed for machining CFRP materials. This tool geometry was used by Bérubé et al. (Bérubé et al., 2012; Chatelain et al., 2012) showing great surface quality over other cutters geometries. However, it is the most expensive cutter of all three. The specifications of Tool number 3 are presented in Table 2-4.

Table 2-4 Onsrud tool or Tool number 3 specifications

	Company	ONSRUD
	Tool part number	68-020
	Coating	PCD
	Diameter	12.7 mm (1/2”)
	Shank Diameter	12.7 mm (1/2”)
	Depth of cut	19.05 mm (¾”)
	# of flutes [N]	2
	Helix angle [β] °	0°
ONSRUD or tool #3	**Rake angle °**	20°

In addition, Table 2-5 shows the thermal conductivity of each material according to the literature.

Table 2-5 Thermal conductivity of the different cutters

Type of tool	**K (W/mK)**	**Reference**
WC-Co	80	(J. Y. Sheikh-Ahmad, 2009)
Coated TiAlN	4.63	(Samani, Chen, Ding, & Zeng, 2010)
PCD	543	(J. Y. Sheikh-Ahmad, 2009)

2.3 Screening of experiment

In order to find a cutting operation range (cutting speed, feed per tooth and radial depth of cut) for the different cutters, a series of tests were developed with the aim of developing a final Design of Experiments (DOE). In the case of tool number 2, we found a lot of information about the cutting parameters since it is designed for cutting Titanium's alloys. For example, the manufacturer (Walter GPS) recommends cutting speed of about 61.5 m/min and feed per tooth of about 0.115 mm/rev-tooth under lubrication conditions. However, we found greater cutting parameters values in the literature. Yujing et al. (Yujing et al., 2014) carried out experiments using a maximum cutting speed of 140 m/min, feed per tooth of 0.11 mm/rev-toot, radial depth of cut of 1.2 mm under dry conditions. It is worth mentioning that the set of experiments was performed using down milling. On the other hand, the manufacturer for tool number 3 forbids the use of this tool on ferrous materials though there are some experimental studies in machining Titanium alloys using it. However, these studies are only limited to PCD inserts (Pan, Kamaruddin, et al., 2014). Due to the unknown information related to the PCD tool of machining titanium alloys, there was a need to build a homogenous DOE for all the cutters. Thus, the scope of the screening was to find the maximum operating range without creating tool damage but more particularly in the case of the PCD tool. This is due to the fact that it has been developed to cut composite instead of titanium.

We developed a series of tests doing small increments of cutting speed, feed per tooth and radial depth of cut for each cutter on Ti6Al4V plaques. This is with the aim of opening as wide as possible the cutting parameters range even though tool number 2 is studied in the literature on titanium cutting. The tests were carried out under dry conditions and down milling. Our study concluded that we can go far beyond what is proposed by Walter GPS or what is found in the literature for tool number 2. Thus, this tool was able to reach up to a cutting speed of 300 m/min, feed per tooth up to 0.3 mm/rev-tooth and radial depth of cut up to 40% (5.08 mm) of the tool diameter (12.7 mm). In the case of tool number 3 (PCD tool), the tool supplier designed it for values below the radial cutting depth of 1.5 mm and when we tested it for a radial depth of cut of 2 mm, the tool was chipped. Therefore, the PCD tool cannot be used for values above 1.5 mm. As a result of the preliminary tests, the DOE has 3 levels of cutting speed and feed per tooth and 2 levels for the radial depth of cut for the Walter tool, (Table 2-6). On the other hand, the PCD tool has the same number of cutting speed and feed per tooth levels, but with the difference that it has only one radial depth of cut level. This is because it could not sustain 5 mm of radial depth of cut. Lastly, Niagara tool was later added in order to see how its uncoated property affects the cutting temperature.

In addition, the screening test helped us to check that there would be no anomalies in the setup like excess of vibration and any other abnormality with the temperature equipment. This is due to the large amount number of thermocouples on each titanium plaque.

Table 2-6 Final DOE

Level	**Cutting Speed** ***v (m/min)***	**Feed per tooth** f_t ***(mm/tooth)***	**Radial depth of cut** a_e ***(mm)***
1	50	0.05	1.5
2	175	0.15	5
3	300	0.25	

2.4 Design of Experiments

Once the cutting range is known, we can proceed to build the DOE. Additionally, it will help us to plan the number of CFRP/Ti6Al4V plaques that need to be manufactured and the necessary equipment used to measure the different parameters. DOE is a statistical method which helps collect data from an experiment and allows to know which factor contributes most to the process responses. The cutting speed *v*, feed per tooth f_t and radial depth of cut a_e are the factors to be controlled during the edge milling cutting process and each factor is divided by levels. Thus, the higher the number of levels for each factor, the greater the number of experiments to perform in the DOE. There are many types of DOE (Factorial design, Central Composite Design, Box-Behnken design, Taguchi design, etc.) in the literature but the full factorial and Taguchi are the most used by the researchers. As a result, the full factorial design will be used in this research since it allows us to completely study the linearity of the different cutting parameters. Thus, our DOE is made of 45 tests in the full factorial plan of experiments; 18 tests for the Niagara tool (Tool # 1), 18 tests for the Walter tool (Tool #2) and 9 tests for the Onsrud tool (tool # 3). In addition, the parameters like temperature, forces, roughness and tool wear are measured in the experiments see (Figure 2.2).

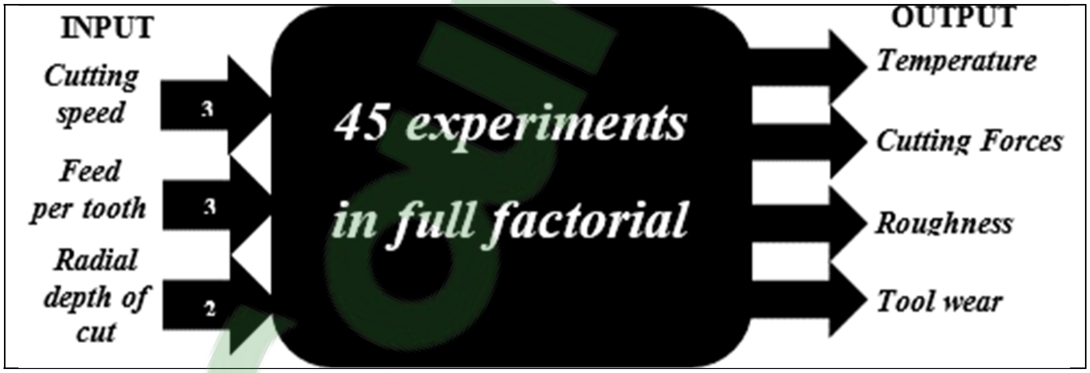

Figure 2.2 Sketch of final DOE with inputs and outputs

1. The temperature was measured both on the tool and workpiece using the tool work-piece thermocouple method (Yashiro et al., 2013; Lance et al., 2014). The CFRP/Ti6Al4V plaque and cutting tool were embedded with thermocouples. In the case of the workpiece, the signal was recorded by a NI 9213 thermocouple input module from Texas Instrument. On the other hand, the cutting tool temperature was recorded by a Michigan Scientific Corp. M320 which is a wireless telemetry system.
2. Fx, Fy and Fz cutting forces were measured using a three-axis dynamometer table Kistler 9255B.

Clicours.com

3. Ra roughness on CFRP/Ti6Al4V stack was measured using a Mitutoyo SJ400 profilometer.
4. Cutters tool wear was measured using the Keyence VHC-500F optical microscope.

The Figure 2.3 shows a diagram of the equipment used to measure the temperature using the tool-workpiece thermocouple method and the Kistler dynamometer table is utilized for recording the cutting forces Fx, Fy and Fz.

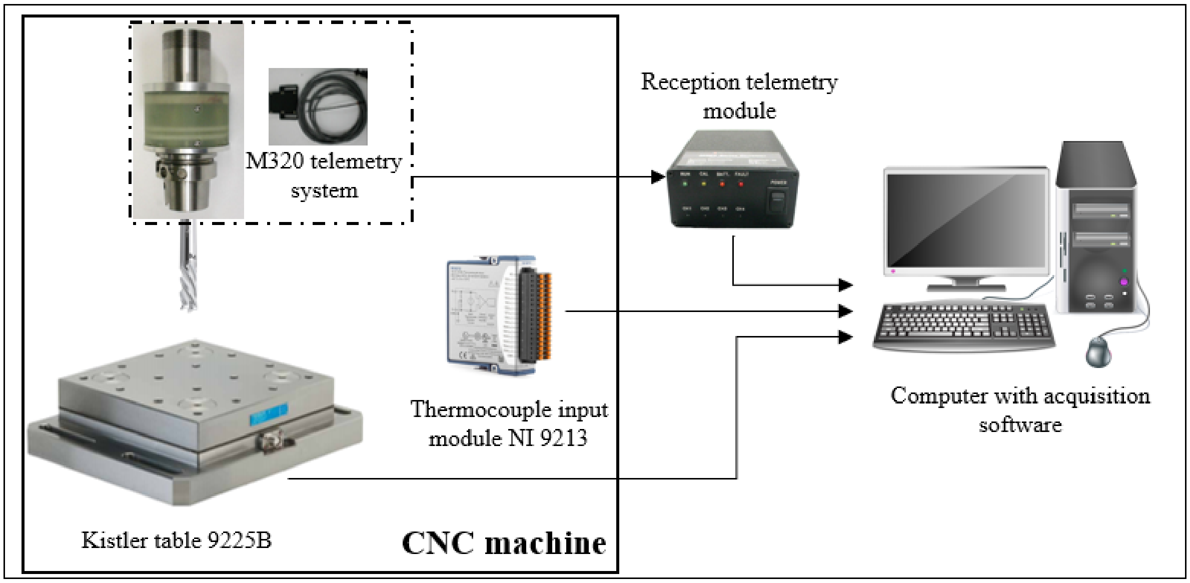
Reception telemetry module
M320 telemetry system
Thermocouple input module NI 9213
Computer with acquisition software
Kistler table 9225B
CNC machine

Figure 2.3 Schematic diagram of the acquisition equipment used in the experiments

Figure 2.4 and Figure 2.5 show the real components used for the forces and temperature recordings. In addition, Figure 2.5 shows the thermocouple input module NI-9213.

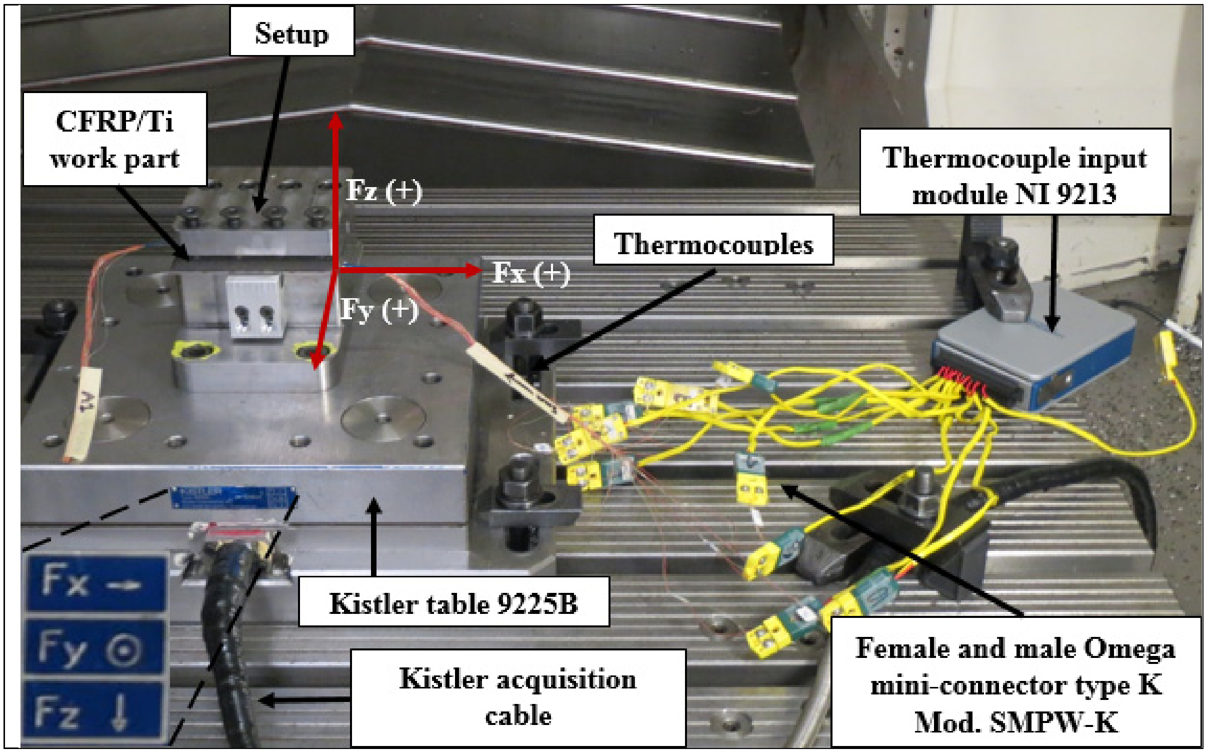
Setup
CFRP/Ti work part
Fz (+)
Fx (+)
Fy (+)
Thermocouple input module NI 9213
Thermocouples
Kistler table 9225B
Kistler acquisition cable
Female and male Omega mini-connector type K Mod. SMPW-K
Fx →
Fy ⊙
Fz ↓

Figure 2.4 Forces and Temperature acquisition equipment in the final experiment

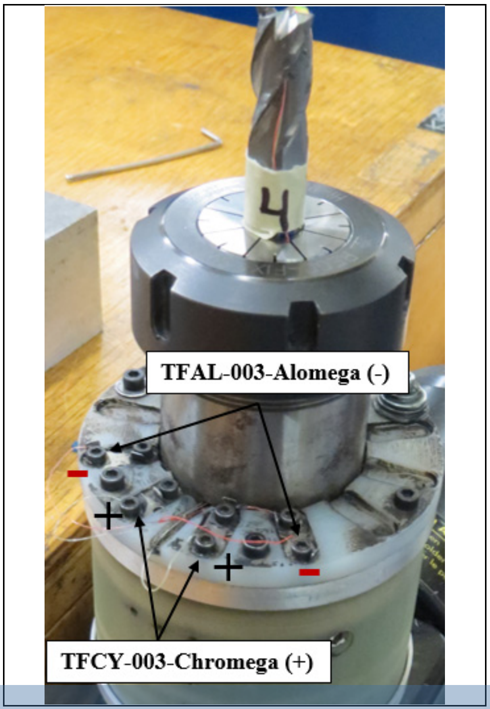
4
TFAL-003-Alomega (-)
−
+
+
−
TFCY-003-Chromega (+)

Figure 2.5 M320 Telemetry system

Clicours.COM

2.5 Manufacturing of CFRP/Ti6Al4V plaques

The setup works for plaques with a maximum length of 101.6 mm (4 in), a maximum width of 50.8 mm (2 in) and an adjustable clamp without losing the setup stiffness. Thus, the CFRP/Ti plaque has a cutting length of 101.6 (4 in) and a width of 50.8 mm (2 in). For the material thicknesses, the Ti6Al4V plaque is 3.175 mm (1/8 in) thick while the CFRP plaque is 2.825 mm (~ 7/64 in) thick, which correspond to the thicknesses used in the assembly process of CFRP/Ti6Al4V plaque in the aeronautical industry (Montoya & Chatelain, 2013; Lance et al., 2014; Luo, Li, Zhang, Cheng, & Liu, 2015).

Regarding the CFRP/Ti6Al4V plaque temperature acquisition, the literature review helped to find a configuration of thermocouple position which allows collecting the maximum of data per cutting pass. Therefore, 10 thermocouples were used on each side of the plaque. Four were welded on the titanium plaque 25.4 mm (1”) apart of each other with the first one located at 12.7 mm from the edge of the plaque, such a distance corresponding to the cutter diameter. Moreover, six thermocouples were embedded between the first three CFRP layers in two symmetrical columns and close to the titanium plaque, expecting the heat to flow through the CFRP layers. Figure 2.6 shows the thermocouples exact distribution.

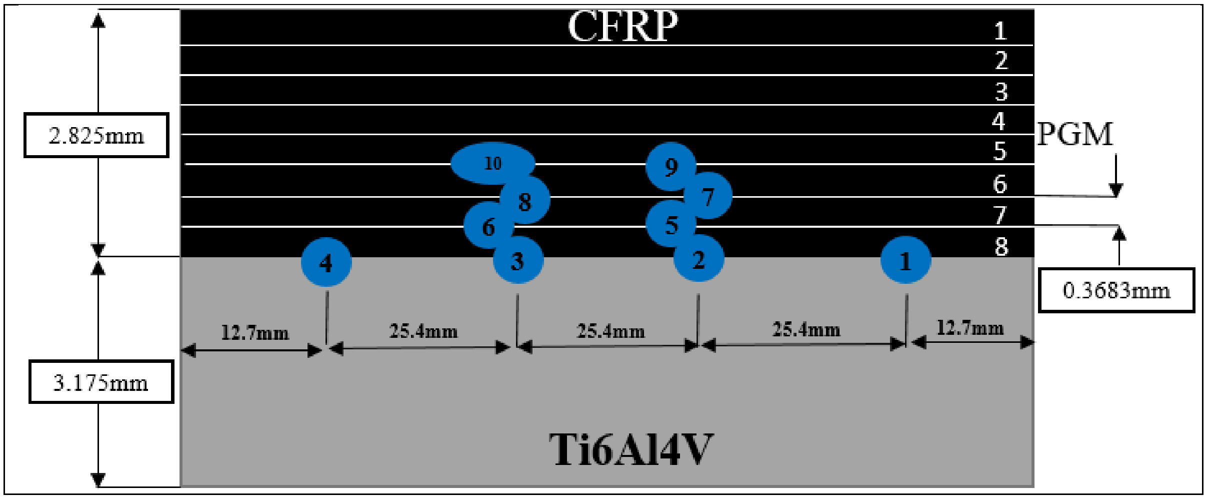

Figure 2.6 Sketch of thermocouple order in CFRP/Ti stack

In order to reduce the number, time, and cost of the plaques, both sides of the titanium plaque were used, one side for a cutting radial depth of cut 1.5 mm and the other of 5 mm considering the cutting direction at the mounting time. A total of 450 thermocouples were used only to measure the temperature on the workpiece, (Figure 2.7).

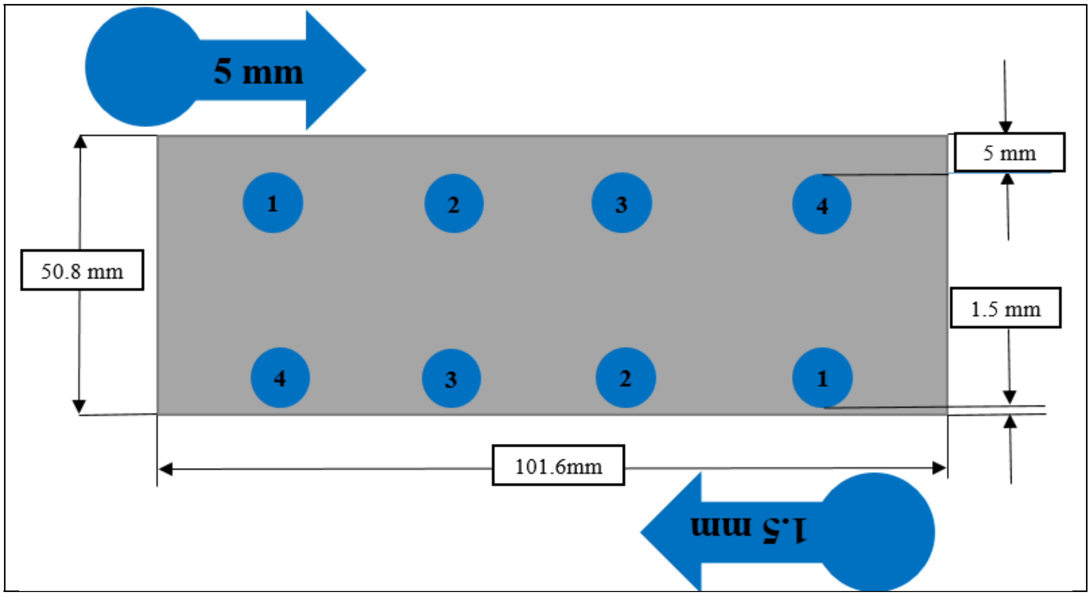

Figure 2.7 Sketch of thermocouple position on Ti6Al4V plaque

2.5.1 Manufacturing process of CFRP plaques

As mentioned in the previous section, more than 450 thermocouples were manufactured only to measure the temperature in the workpiece and more than 90 thermocouples to measure the temperature on the cutters. The type K thermocouple was selected because it is the most widely used on the market for general purposes. It is manufactured by OMEGA® and each wire has a diameter of 0.08 mm (0.003”). TFCY-003- Chromega® has a positive polarity and yellow color and is made in chrome, while TFAL-003- Alomega® has a negative polarity and red color and is made in aluminum. The Chromega- Alomega® has a response time of about 0.025s and accuracy of ±2.2°C. It should be mentioned that the smaller the thermocouple diameter, the faster the response time. Therefore, a small diameter is perfect to measure temperature in high-speed applications and does not bulge between CFRP layers. In order to join both wires, the Omega TL weld machine® was used to weld the tips of both materials. Additionally, three methods were used in order to test the quality of the junction such as the conductivity, welding shape tip, and strength. The Figure 2.8 shows an example of a thermocouple welding tip view. Thus, more than 10% were rejected due to welding defects.

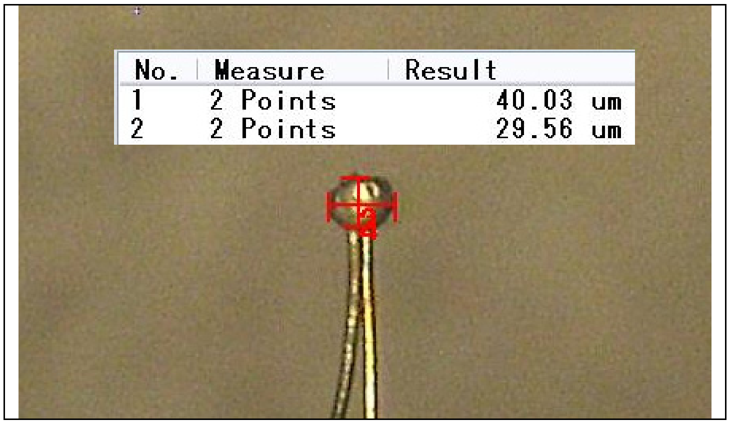

No.	Measure	Result
1	2 Points	40.03 um
2	2 Points	29.56 um

Figure 2.8 Thermocouple welding tip view

As shown in Figure 2.7 and Figure 2.9, eight thermocouples were welded on each titanium plaque. Four on each side depending on the radial depth of cut. Therefore, in order to know the welding position of each thermocouple, we drew lines of 1.5 mm and 5 mm from the cutting edge on each titanium plaque using the Mitutoyo 192-655 height gage. Then the thermocouples were welded by using the micro-welding machine Vishay model 700 portable strain gage welding and soldering unit®. Nevertheless. this was a delicate process. This is because excess power could break the thermocouples if the welding power is not correctly adjusted. Thus, we would have to start all over again. Table 2-7 shows the Ti6Al4V plaque physical properties:

Table 2-7 Physical properties of Ti6Al4V

Grade	**Tensile strength (MPa)**	**Elastic modulus (GPa)**	**Melting point (°C)**	**Density (g/cm^3)**	**Thermal conductivity W/mK**
5	895	113	1650	4.5	7.5

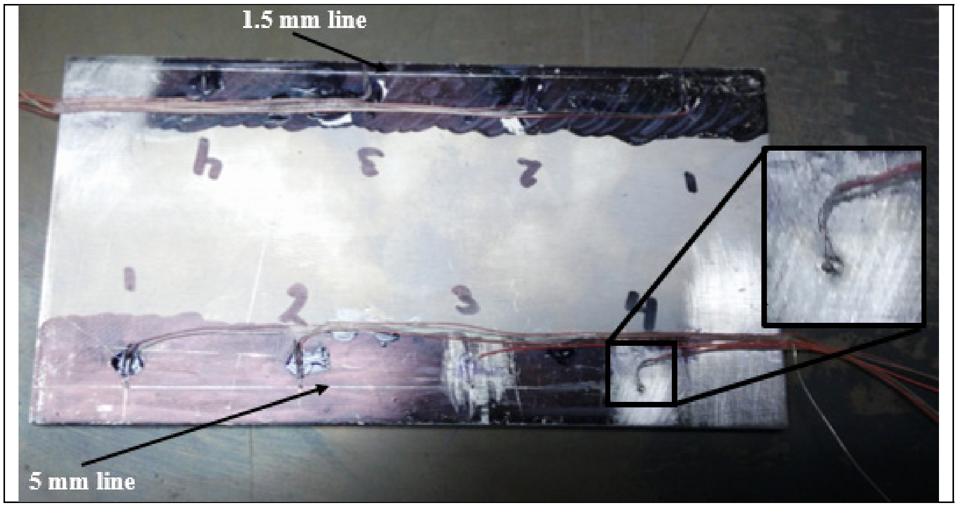

Figure 2.9 Thermocouple micro-welding sample plaque

2.5.2 Embedded thermocouples in CFRP

After finishing the welding process, we looked for a suitable method for embedding the thermocouples between the CFRP layers. This is due to a large number of thermocouples inside each CFRP/Ti6Al4V stack. We tested both Vacuum Assisted Resin Transfer Molding (VARTM) and prepreg manufacturing process. The process that was best suited without breaking the thermocouples in the demolding step was the prepregs. The composite used to manufacture the CFRP plaques was the woven fabric CYCOM® 5320-1 T650-35 3K 8HS Fabric 36%. This last percentage corresponds to the resin content by weight of the uncured prepreg and this CFRP was donated by Bombardier to the École de Technologie Supérieure (ÉTS). Therefore, in order to reach a CFRP thickness of 2.825 mm, we needed 8 layers of fabric with a thickness of 0.0145 in (0.3683 mm) each in the warp/weft direction or $[0]_8$. It should be noted that according to the manufacturer, the fabric is balanced (same thread count in the warp and weft directions) and it has a tolerance of 24.0 +/- 1.0 picks/inch. Table 2-8 shows more information about the mechanical properties of the CFRP prepreg.

Table 2-8 Prepeg CYCOM® 5320-1 T650-35 3K 8HS Fabric 36% physical properties

Specifications:		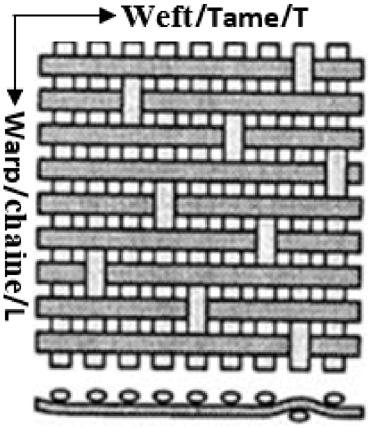
Fiber	Cytec T650/35 3K	
Resin	CYCOM® 5320-1	
Tg(dry)[1]	374°F (190°C)	
Fiber volume	56.7%	
Thickness after curing	0.0145 in (0.3683 mm)	
Number of warp and weft tolerance	24.0 +/- 1.0 picks/inch	
0° Tensile ASTM D3039 **Strength (ksi)** **Modulus (Msi)** **Poisson's Ratio**	131.3 ksi (905.25 MPa) 10.02 (69.08 GPa) 0.048	75°F (23.88°C) Dry
90° Tensile ASTM D3039 **Strength (ksi)** **Modulus (Msi)**	129.9 (895.62 MPa) 9.9 (68.25 GPa)	75°F (23.88°C) Dry

One of the most important challenges in the manufacturing of CFRP/Ti6Al4V was to position the thermocouples on the prepreg plies. This is because the waviness of the CFRP fabric does not allow us to precisely position the thermocouples. As a result, we could not accurately measure the location of the thermocouples as if we measured it on the titanium plaque. Thus, we built a Plexiglas® fixture to set up the thermocouples. Then the prepreg plies were cut to near net shape and put on the fixture in order to mark the radial depth of cut and thermocouple position. Each thermocouple was glued to the ply with epoxy glue, (see the top of Figure 2.10). Afterwards, the prepreg ply was stacked on the top of each other using the titanium as support. This also increases the stiffness of the mold and will bond the Ti6Al4V to the CFRP during the curing process. Finally, the thermocouples were wrapped in parchment and aluminum paper in order to prevent them from breakage during the demolding process (see the bottom of Figure 2.10).

---

[1] Tg Mehod: DMA (ASTM D7028, 35mm dual cantilever)

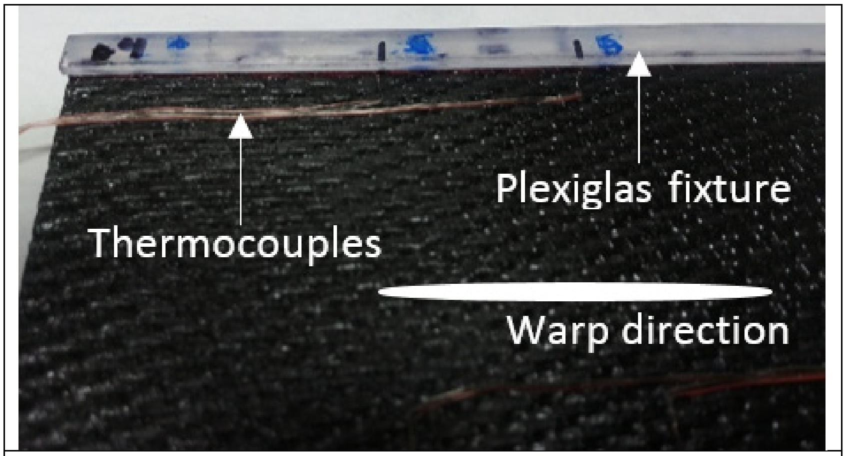
Plexiglas fixture
Thermocouples
Warp direction

Plexiglas fixture

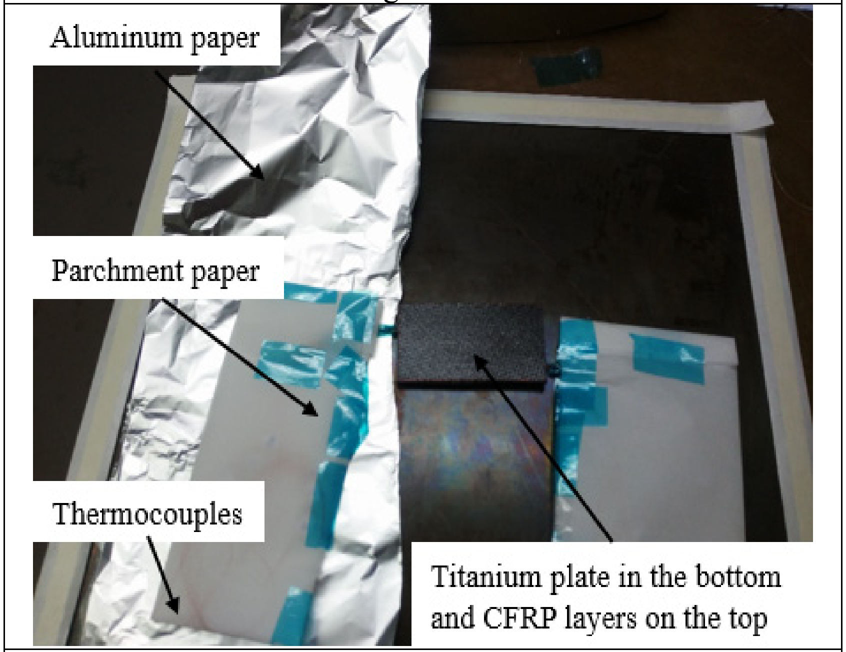
Aluminum paper
Parchment paper
Thermocouples
Titanium plate in the bottom and CFRP layers on the top

Wrapping thermocouple process

Figure 2.10 Thermocouples setup process

Moreover, the prepregs curing process helped to bond the CFRP plies to Ti6Al4V plaque. As a result, the CFRP/ Ti6Al4V is free of bolts or rivets. Finally, the oven Despatch TAD2-52-1E was programmed following the CYCOM®'s curing cycle and its curing process is the following.

- Heat to 140±5° F for 120±10 minutes; Ramp at 2±1° F per minute to 250±10° F; Hold at 250±10° F for 120±10 minutes; Cool at <10 °F below 140° F.

Figure 2.11 shows an overview of the process flow for the preparation of embedded thermocouple within $[0]_8$/Ti6Al4V plaques in which all the steps are summarized from the thermocouple process to the final workpiece.

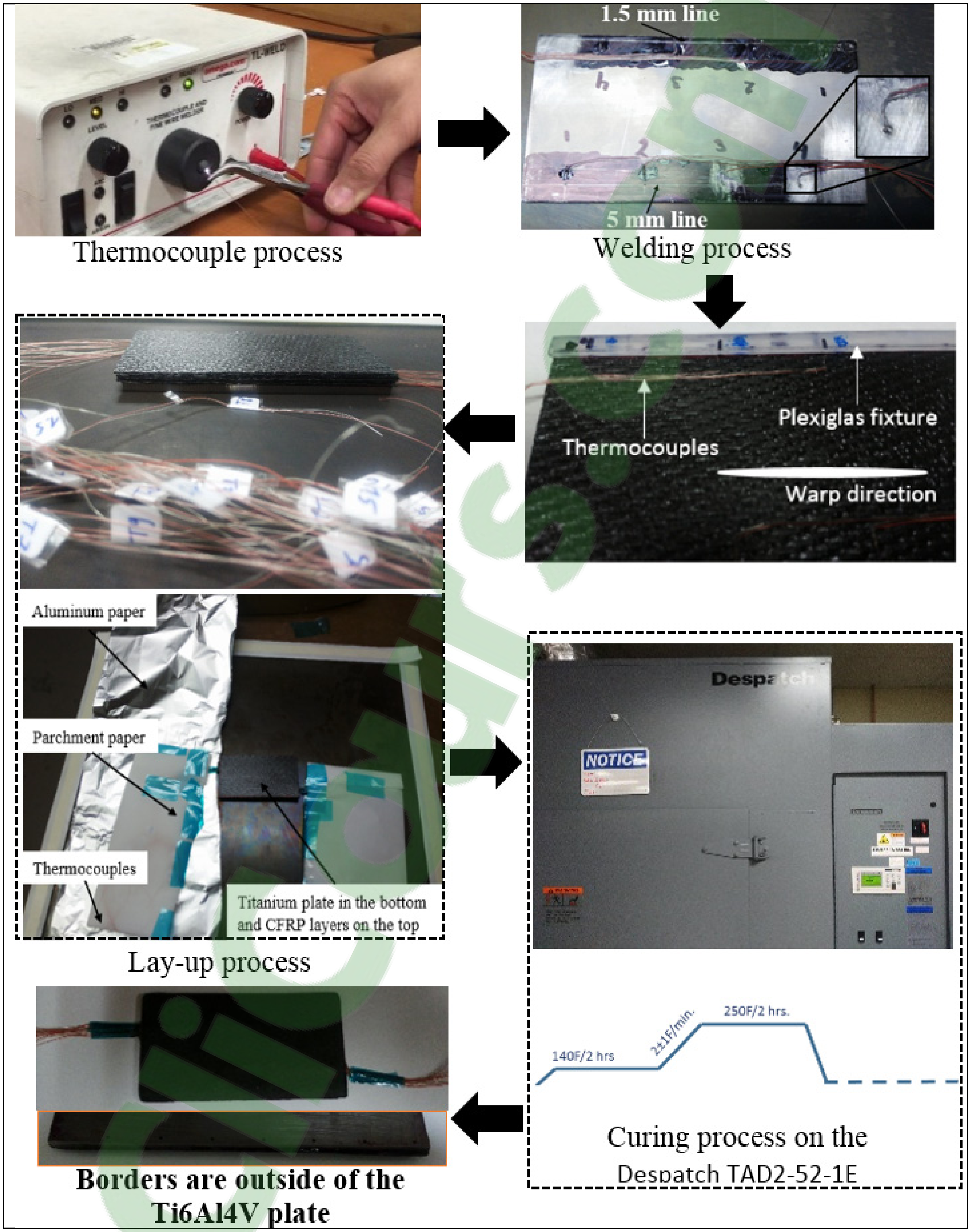
1.5 mm line
5 mm line
Thermocouple process
Welding process
Plexiglas fixture
Thermocouples
Warp direction
Aluminum paper
Parchment paper
Thermocouples
Titanium plate in the bottom and CFRP layers on the top
Lay-up process
Despatch
NOTICE
140F/2 hrs
2±1F/min.
250F/2 hrs.
Curing process on the Despatch TAD2-52-1E
Borders are outside of the Ti6Al4V plate

Figure 2.11 Flowchart of $[0]_8$/Ti6Al4V fabrication process

2.5.2.1 Measurement of the position of the thermocouples within the workpiece

Due to the curing cycle of prepreg layers, the thermocouples between the layers were displaced. As a result, we looked for several scanning methods such as ultrasound scanning and X-ray to know the exact position of the thermocouples within the CFRP/Ti6Al4V plaque. The method that had the best results was the X-rays based on its image clarity. The X-ray was done by Mistras Group located in Terrebonne, Montreal and the position of each thermocouple was measured using a digital Vernier. The measurement was repeated three times in order to reduce the measurement error. However, one of the major drawbacks of this method was that the X-ray films were taken in an old-fashioned way so we digitalized them using a digital camera, 10,000 lux light and Adobe Lightroom CC software to have publication imaging, see Figure 2.12. The X-ray was separated in three batches, see ANNEX I in order to find the digitalized X-ray images:

- Batch A for cutter number 1 or Niagara tool
- Batch B for cutter number 2 or Walter tool
- Batch C for cutter number 3 or Onsrud tool

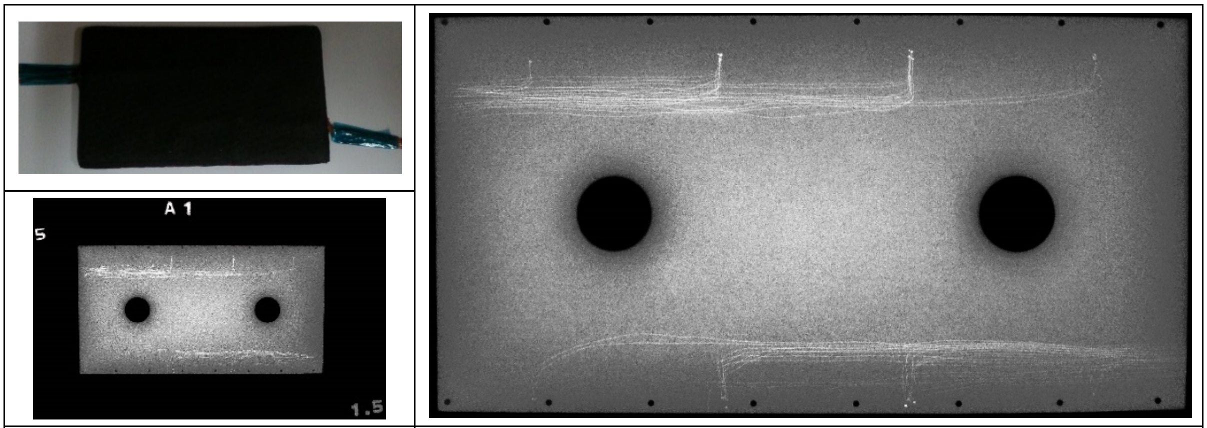

Example A1 plaque

Zoom for example A1

Figure 2.12 X-ray scanning example result

The statistics program Minitab® was used to determine the skewness of each embedded CFRP/Ti plaque and so obtain the optimum radial depth of cut for both 5 mm and 1.5 mm.

Assuming, the closer the thermocouple tip of the cutter, the higher the temperature recorded by the adquisition system(Yashiro et al., 2013). Therefore, the statistical analysis looked for a balance between temperature measurement and the number of lost thermocouples due to unprecise positioning or movement of thermocouples during cure of the resin.

Table 2-9 shows the statistical analysis for finding the optimal radial depth of cut. As can be seen, both cutting depths have a negative skewness, meaning the nominal average is a bit backwards. Therefore, we must adjust the radial depth of cut, starting from the particular case of each CFRP/Ti plaque to the general case of the number of thermocouples loss in the full experiment. By reviewing the X-Ray films, 20 thermocouples were outside the edge of the titanium plaque. As a result, they were not considered in the statistical analysis. Figure 2.13 shows an example of how a thermocouple can be out of the titanium plaque. We found that the optimal radial depth of cut was 1 mm instead of 1.5 mm with a loss of 14.81%. For a cutting depth of 5 mm, the optimal cut was 4.3 mm instead of 5 mm with a loss of 16.47%. To see the complete analysis showing the relationship between the radial depth of cut, the temperature and the number of lost thermocouple, please refer to ANNEX I.

Table 2-9 Thermocouple workpiece statistical analysis

Statistical analysis	**1.5 mm**	**5 mm**
Skewness	*-0.625*	*-0.91*
Kurtosis	1.2829	0.9518
Mode	1.51	4.975
Mean	*1.45*	*4.82*
Total of thermocouples in Stat. analysis	270	170
Total of thermocouples on the workpiece	280	180
Optimal Proposal value	***1***	***4.3***
# of loss of thermocouples in the Stat. Analysis	**40**	**28**
% of loss of thermocouples	**14.815**	**16.471**

Clicours.COM

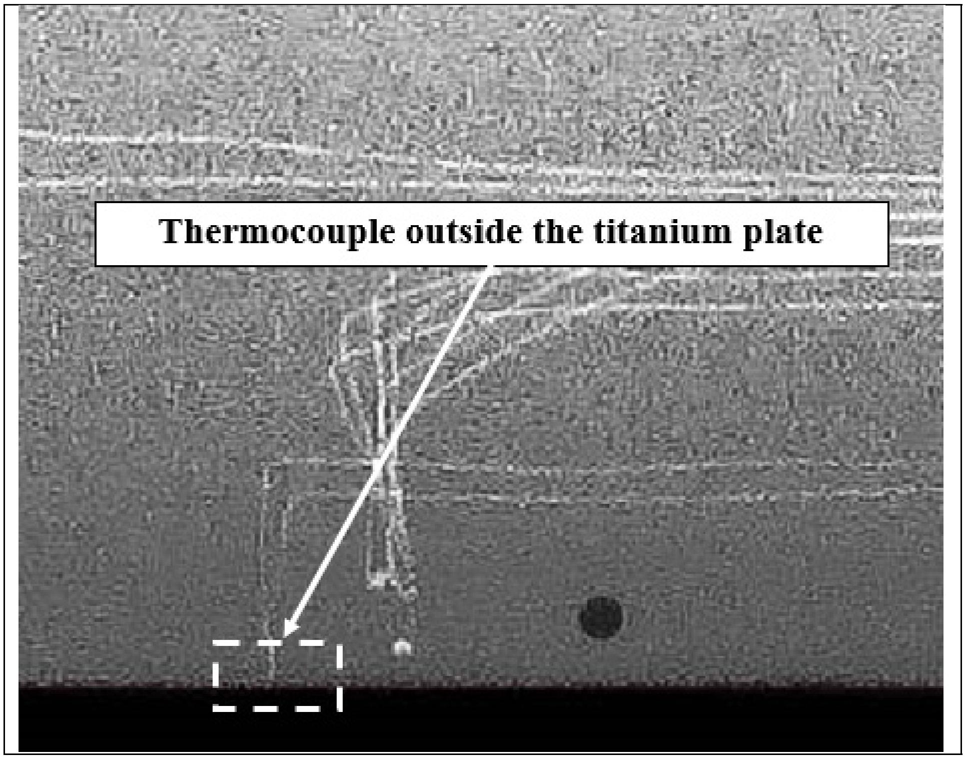

Figure 2.13 Example of thermocouple outside the titanium plaque due to the curing process

2.5.3 Thermocouples on the cutting tool

Once finished embeddeding thermocouples on the workpiece, the cutter was mounted with thermocouples in order to measure the temperature in each test. More than 90 thermocouples were used for this purpose, with each tool divided by sections and each section located 7 mm apart, see the left side of Figure 2.14. Thus, the thermocouple is inserted about 1 mm above the thickness of the CFRP/Ti6Al4V plaque which is 6 mm of thickness, see right side of Figure 2.14. In the case of tool number 1 and 2, they were divided into 3 sections while for tool number 3, it was divided into 2 sections. This is because the cutting length on tool number 3 is shorter than the tools 1 and 2. In addition, each section was mounted with two thermocouples, one on each side.

To have a better adhesion of the thermal paste and the epoxy to the tool surface, the helix angle surface was scratched with an old PCD tool to create a rugged surface. Then, the scratched surface was cleaned with acetone $(CH_3)_2CO$ and we measured the correct position of the thermocouple with a digital Vernier. Subsequently, the thermocouple was stuck using the OMEGABOND 400 thermal paste, curing it for 24hrs. Finally, we covered the thermal paste with J-B Marine Weld Epoxy Adhesive® and curing for another 24hrs. The right side of Figure 2.14 shows the cutter result

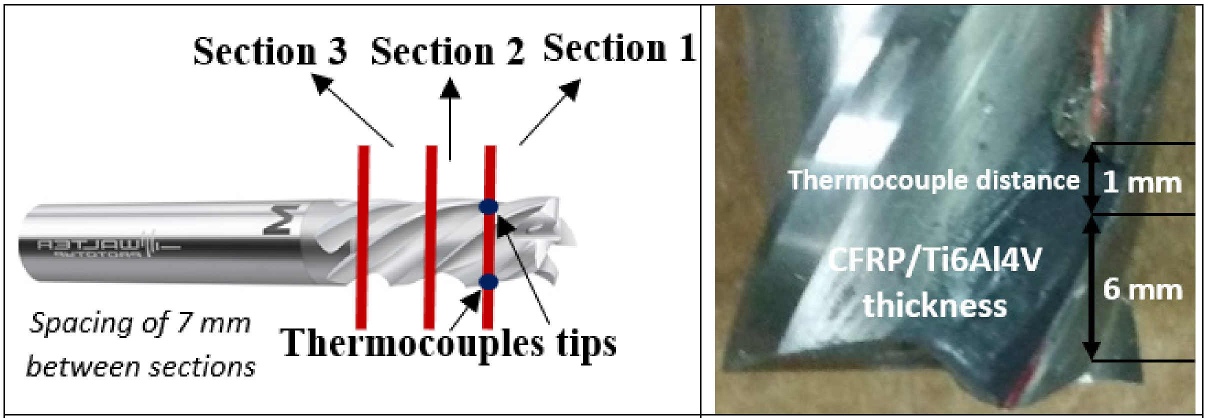
Section 3
Section 2
Section 1
Spacing of 7 mm
between sections
Thermocouples tips
Thermocouple distance
1 mm
CFRP/Ti6Al4V
thickness
6 mm

Tool layout

Epoxy

Figure 2.14 Embedded thermocouple process

2.6 Edge milling of [0]8/Ti6Al4V plaques

After preparation of the workpiece and tool, the final test was performed using the Huron K2X10 CNC machine. As mentioned previously, 45 tests were made; 18 for the Niagara tool (Tool #1), 18 for the Walter tool (Tool #2) and 9 for the Onsrud tool (Tool #3). All tests were performed under dry condition, down milling and a test per section as described above. Figure 2.4 and Figure 2.5 show the components used for the forces and temperature recordings and Table 2-10 shows the DOE with the new values of radial depth of cut as obtained in this chapter by X-ray and statically analysis.

Table 2-10 Real DOE

Level	**Cutting Speed** *v (m/min)*	**Feed per tooth** f_t *(mm/tooth)*	**Radial depth of cut** a_e *(mm)*
1	50	0.05	1
2	175	0.15	4.3
3	300	0.25	

2.6.1 Workpiece and cutter temperature measurement

Workpiece temperature was measured with 10 embedded type K thermocouples (TFCY-003-Chromega(+)®-TFAL-003-Alomega(-)®). The signal is transferred by the thermocouple to the input module National Instrument NI-9213 at a sampling frequency of 6000 Hz. Additionally, the NI-9213 has the following technical specs: 16 TC, 24 Bits, high-resolution mode <0.02°C and high-speed mode <0.25°C for thermocouples type K. Figure 2.5 shows the thermocouple input module NI-9213. For the cutter, the temperature was recorded using an M320 Thermocouple Measurement System connected to two thermocouples type K with the same characteristic than the workpiece, see Figure 2.15. The M320 is a telemetry system designed to measure the temperature on the cutting tool via wireless and has the following specs: input ranges type K from 0 to 1100°C, speed range from 0 to 12000 RPM, accuracy:+/-1% of Full Scale and data bandwidth of 1000 Hz (High) and 100 Hz (Low). The signal is transmitted from the tool holder to a telemetry receiver device, which converts the RF signal to an analog signal corresponding to the temperature. Both NI 9213 and M320 are connected to the acquisition system and in turn, to the computer which uses LABVIEW. The raw data are transformed using the Matlab software for later processing. Figure 2.15 shows an example of Matlab data recovery of the workpiece and cutter temperature on a PCD tool during cutting at a cutting speed of 50 m/min, a feed per tooth of 0.15 mm/tooth and radial depth of cut of 1 mm. For the workpiece temperature (left part of Figure 2.15), ten temperatures are shown (T1 to T10), with T1 (red line) in contact with the tool. For the cutter temperature, both thermocouples are represented by T1 and T2, (right side of Figure 2.15). Additionally, Figure

2.15 shows that the cutting process is transient for both the cutter and workpiece, with higher temperatures for the cutter.

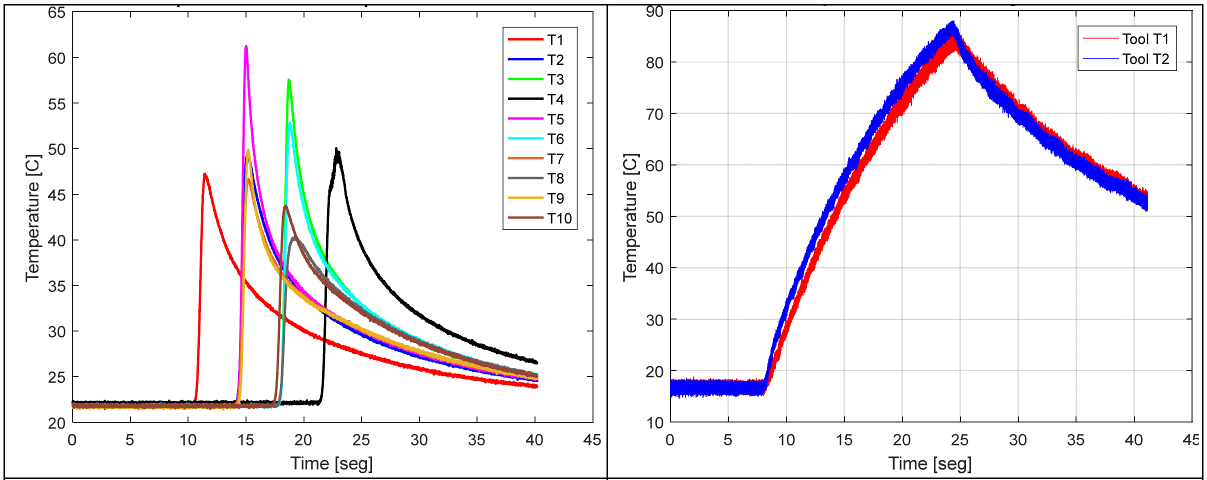

C1-B-Workpiece temperature example

C1-B-Cutter temperature example

Figure 2.15 PCD tool , v 50 m/min, ft 0.15 mm/tooth, ae 1 mm example

To know the correct position of thermocouples, Matlab graphs were correlated against X-ray films for each test to distinguish the exact position of each thermocouple. As an example, in the right side Figure 2.16, T3 is the lightest point because it corresponds to a welding point. A similar patron was seen for T1 and T4 where there is a single thermocouple. Additionally, by using the Yashiro's assumption (2013), the closer the thermocouple tip to the cutter, the higher the measured temperature within the CFRP workpiece. As a result, we discarded T3 (welded thermocouple on Ti plaque) on the left side of Figure 2.15 and the right side of Figure 2.16. Then, the closest point to the edge is T6 on the right side of Figure 2.16 and this corresponds to the highest temperature T6 within the $[0]_8$ plaque on the left side of Figure 2.15.

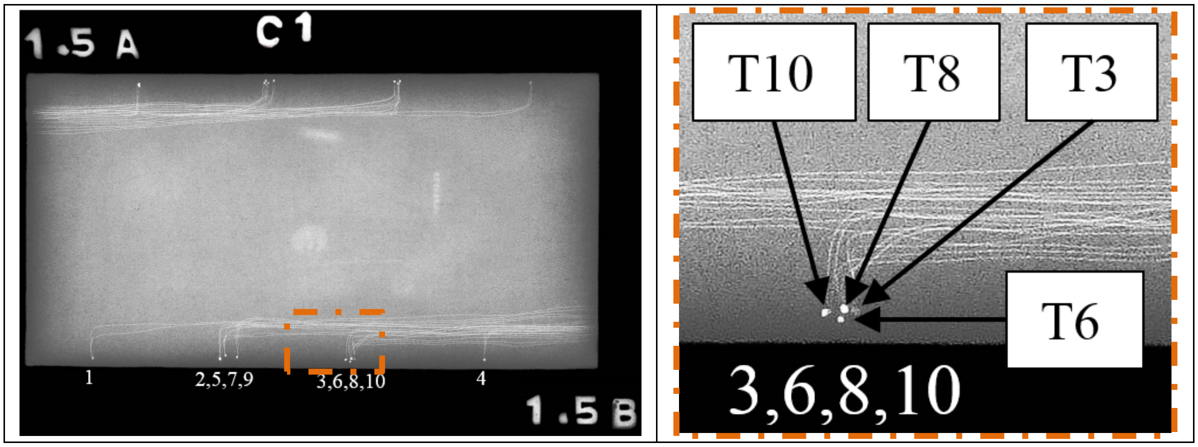

Figure 2.16 Methodology to know the correct position of thermocouples

After correlating the position and temperature of each thermocouple, we developed a Matlab code to extract the maximum point of each thermocouple. For the cutter temperature, we extract the maximum point and then make an average of both thermocouples.

2.6.2 Cutting Forces

The 3-axis dynamometer Kistler 9255B table was used to measure the forces Fx, Fy and Fz (from -20KN to 20KN in the X, Y directions and -10KN to 40KN in the Z direction). The left side of Figure 2.17 shows a layout of the forces on the workpiece. These forces are known to be:

- $F_x = F_f$ (Feed force), it is the force which opposes due to the cutting tool and the material.
- $F_y = F_n$ (Normal force), it is the force normal to F_f and composes the direct trihedron (F_f, F_a, F_n).
- $F_z = F_a$ (Axial force), it is the force on the cutting length direction of cutting tool or –Z.

The data was received in raw form and treated using MATLAB. The matlab program processes the data as the following steps:

1. Transform LABVIEW file (.tdms) to MATLAB file (.mat),
2. Correct and filter the signal to delete the noise,
3. Limit and cut the forces to 30 cycles, see the right part of Figure 2.17,
4. Calculate the mean over 30 cycles for *Fx*, *Fy* and *Fz*.

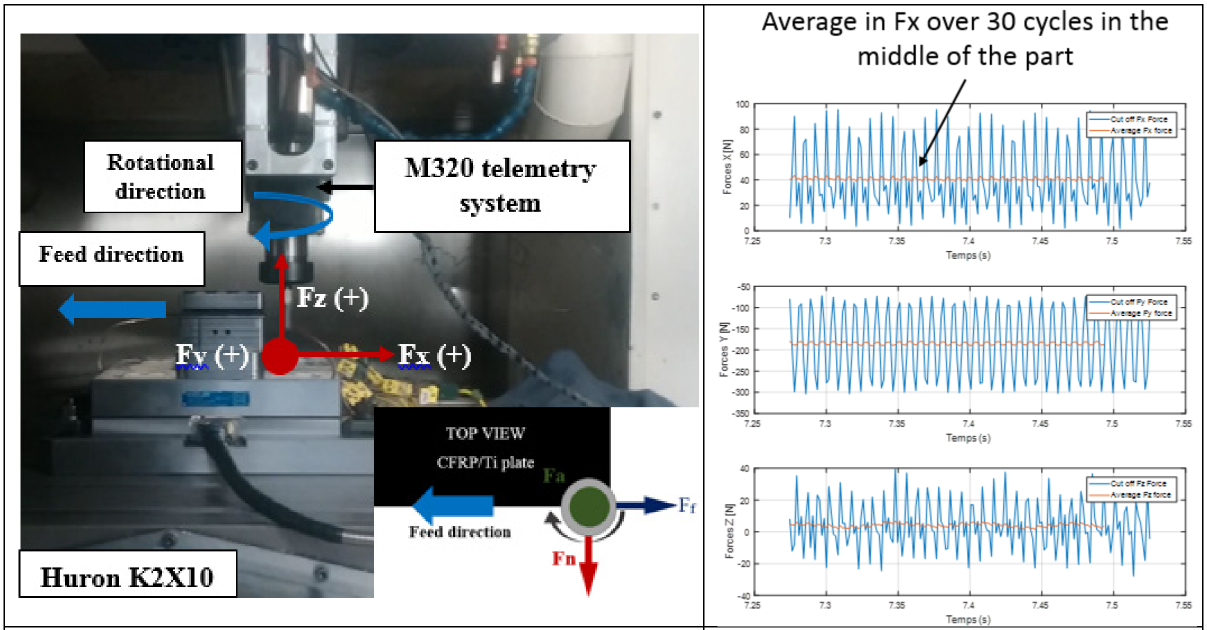

Forces setup

Matlab graph

Figure 2.17 Forces layout setup

2.6.3 Roughness on CFRP/Ti6Al4V

After finishing the machining operation, the surface roughness is studied to know the surface quality due to the different cutting parameters and cutters. The SJ400 Mitutoyo Surftest profilometer was used to measure the surface roughness in both CFRP and Ti materials. The profilometer is equipped with a spherical pointer diamond of 2 µm radius on a tip of 90°. In addition, it has a resolution of 0.125 nm and is controlled by the SURFPAK-SJ acquisition software that allows data processing.

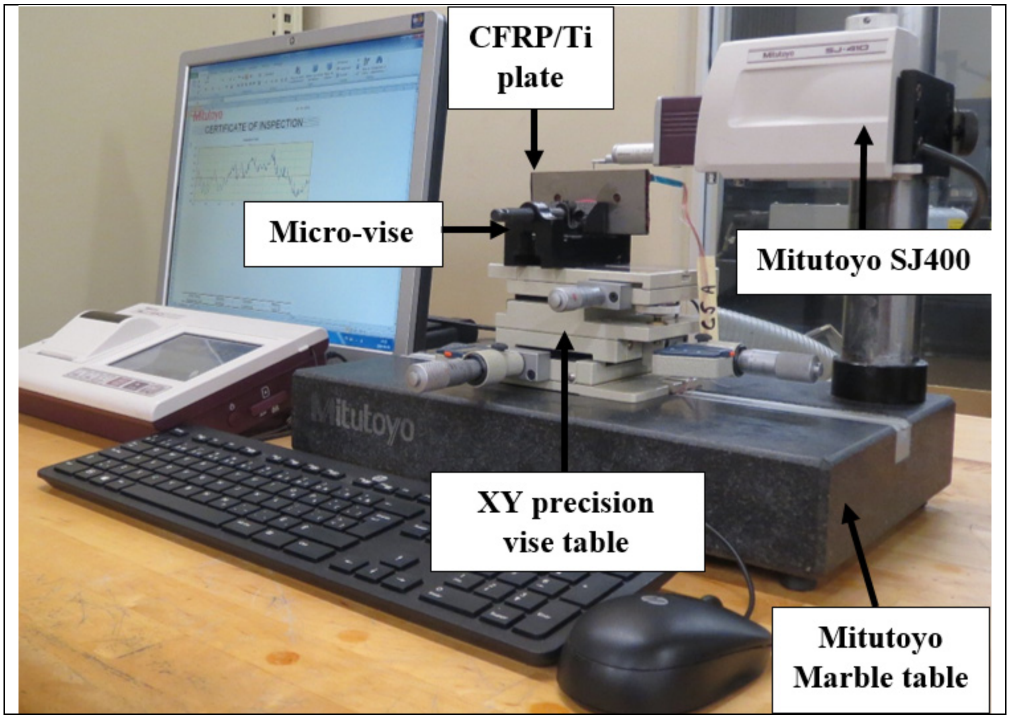

Figure 2.18 Roughness setup

Before starting the measurements, the test plaques were cleaned with compressed air to remove the CFRP powder or chips that may skew the results. Figure 2.18 shows a general setup used by Mitutoyo profilometer which is equipped with a micro-vise used to hold the CFRP/Ti plaque. An XY precision vise table is used to align the sample with the profilometer. Moreover, the tests were performed following the ISO 4287-1997 standard. Table 2-11 shows the input parameters set up in the SURFPAK-SJ software of the profilometer. The surface roughness was measured once on the Ti6Al4V due to its isotropic properties and twice in two different sections for the CFRP due to its orthotropic properties. Then, each file was joined into a single file using an Excel Macro processing the primary profile P to roughness profile R. The parameters used are a cut-off λc of 0.8mm ($0.1 < Ra \leq 2$) in 4 sets of 4 mm each of them in order to have a total evaluation length of 16 mm.

Table 2-11 Mitutoyo Surftest SJ400 input parameters

Standard Norm	ISO 1997
Profile type	P
Filter type	GAUSS
Sampling length	0.8
Filtered *Ls*	2.5
Number of points *N*	20
Evaluation length λs	16 mm
Cut-off λc	0.8 mm

2.6.4 Tool wear

The tool wear was measured using the Keyence VHC-500F digital microscope, which has a resolution of 2 million pixels; 1600 (H) x 1200 (V). The cutter was divided by sections and each section corresponds to a new test as it was described in section 2.5.3. In order to know the effects of the cutting parameters on the cutters, the tool wear on each flute was measured using the measuring toolbox included in the Keyence software. The recommended flank wear (*VB*) is 300 µm (0.3 mm) following the ISO8688. Figure 2.19 shows an example of the tool wear setup where we used a stand and playdough to hold cutter. It is worth mentioning that the cutter was cleaned with acetone for removing the excess of epoxy on the cutter tools surface.

clicours.com

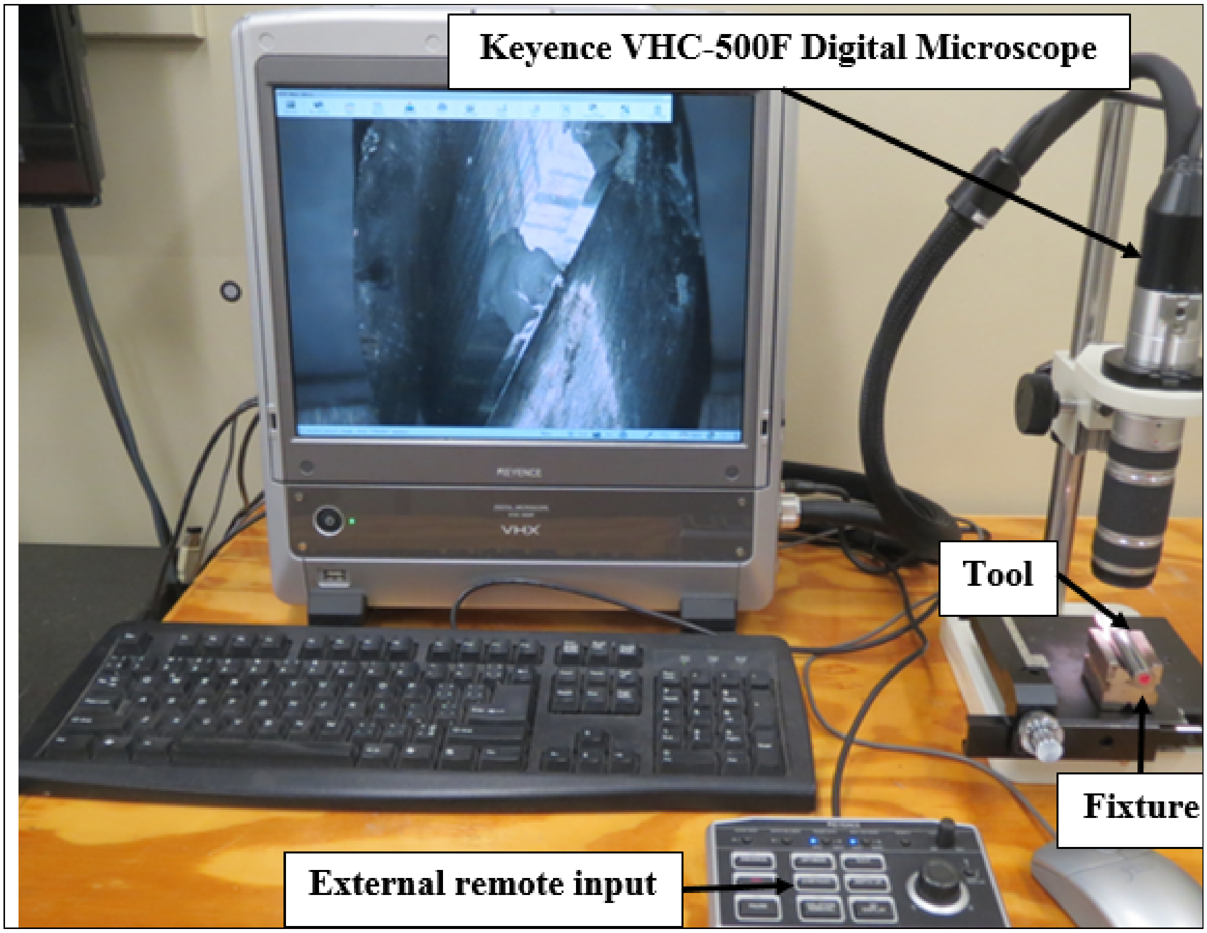
Keyence VHC-500F Digital Microscope
Tool
Fixture
External remote input

Figure 2.19 Setup to measure tool wear

CHAPTER 3

RESULTS AND DISCUSSION

In order to analyze the results, different statistical programs were used throughout this chapter such as Minitab, JMP, Excel and Matlab. Moreover, the Response-Surface Methodology (RSM) is used through this chapter to study the relationship between the cutting parameters and the output responses and to find the best optimal cutting parameters.

3.1 Temperature on the workpiece and cutter

3.1.1 Analysis of temperature on the Ti workpiece

Recapitulating the position of the thermocouples within each CFRP/Ti6Al4V plaque, Figure 2.6 shows a drawing of the thermocouple distribution inside the CFRP/Ti6Al4V plaque embedded with 10 thermocouples. Thus, thermocouple T1-2-3-4 are welded on the titanium plaque, T1 being the first thermocouple in contact with the cutter and T4 the last one. For T2 and T3, columns of thermocouples are located in the CFRP laminate between plies. Figure 2.6 shows a sketch of the thermocouple distribution inside the CFRP/Ti6Al4V. From the statistical analysis (using Minitab® software), Figure 3.1 shows that the type of tool and feed per tooth are the most important factors within the temperature of the titanium plate due to the different cutting parameters. In the case of cutters, Tool #1 is the tool that caused the lowest workpiece temperature while tool #2 and Tool #3 showed similar temperature behavior and a higher temperature. Furthermore, the *ft* has an influence on the titanium plaque temperature so the higher the *ft*, the lower the temperature on the workpiece. On the contrary, the *ae* and the *v* have no influence on the temperature and there is a little increment between T1 and T4. This might be due to the increase in temperature during the transition period.

The standard effects pareto table (Left side of Figure 3.2) shows that the feed per tooth is the most significant factor followed by the combination of tool type-feed per tooth using the Response-Surface Methodology (RSM). Moreover, a 3D graph (right side of Figure 3.2) shows that a low feed per tooth has a great influence on the temperature on the titanium plaque when

Clicours.COM

the Walter tool and the Onsrud tools are used in the edge milling as opposed to the Niagara tool. Note that thermocouples T1, T2, and T3 show a similar behavior than T4.

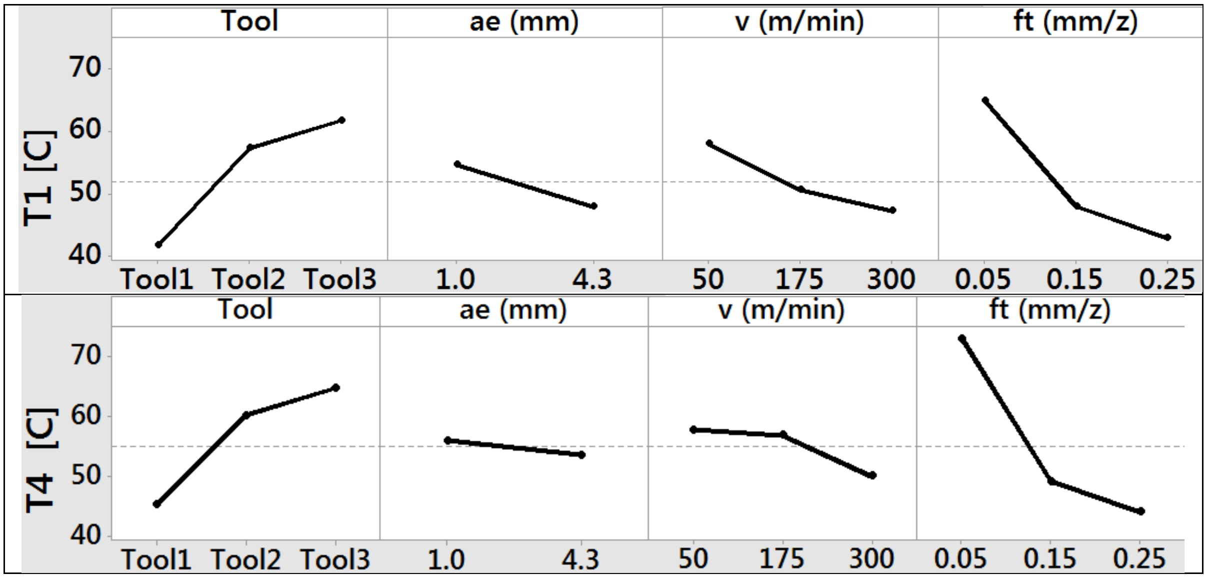

Figure 3.1 Main effect plot for average temperature result on the Ti plaque T1 and T4

The right part of Figure 3.2 (data in ANNEX II) shows that the feed per tooth of 0.05 mm/tooth has a strong influence on the workpiece temperature. Therefore, it is important to know how the distances of the thermocouples influence on the titanium plaque.

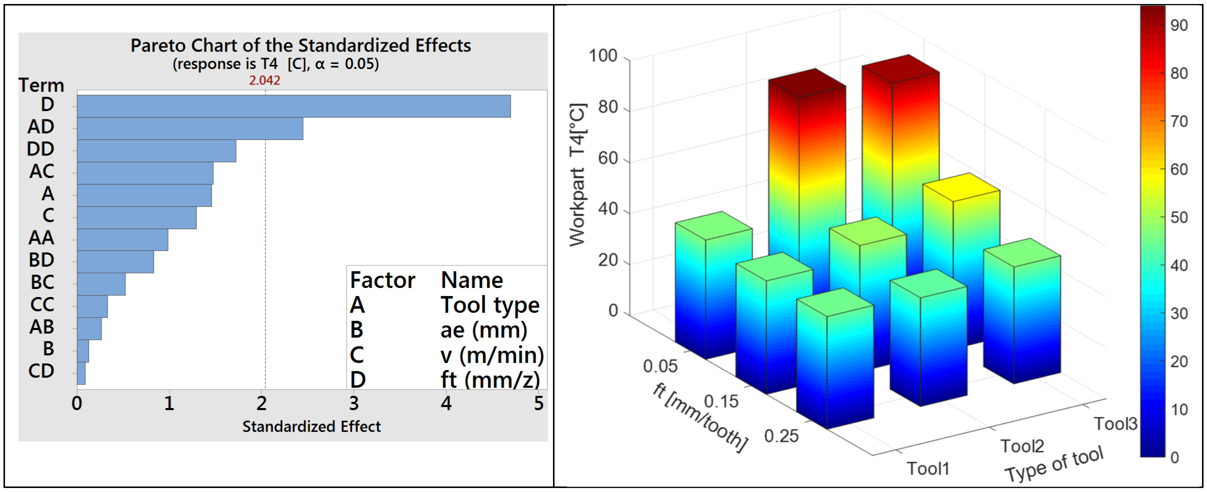

Figure 3.2 Pareto chart: Most significant factor on the titanium plaque and 3D graph on T4

For this low feed per tooth, Figure 3.3 a) and c) show the titanium temperature (thermocouples 1 to 4) for the three tools used (tool #1 to tool #3) and the two radial depth of cut (1 and 4.3 mm). The initial location of each thermocouple with respect to the plate edge is also shown in Figure 3.3 b) and d) for comparison with temperatures. It is observed that much higher temperature was recorded for tools #2 and #3, and this behavior is not really influenced by the radial depth of cut and initial thermocouple location. In addition, the highest peak temperature is shown on tool #3-T3 because T3 is the closest thermocouple to the cutting edge as shown in Figure 3.3 a) and b). Its temperature is represented on a jet colormap, while the thermocouple distance is represented as opposed to the jet colormap. In other words, the closer the thermocouple distance from the cutting edge, the higher the thermocouple temperature with a reddish tone in the top as shown in Figure 3.3 a). Thus, tool #3 has the highest peak temperature T3 and corresponds to the lighter blue color in thermocouple distance T3 as shown in Figure 3.3 b). This is because T3 is the closest to the radial depth of cut of 1 mm. On the contrary, thermocouple T3 for tool #2 shows the lowest temperature of all thermocouples as shown in Figure 3.3 c). This is because their thermocouples are further from the cutting edge. As a result, it is showing an intense dark blue tone so the relation workpiece temperature-thermocouple distance is very sensitive to the radial depth of cut as shown in Figure 3.3 d). Thus, even a few tenths of millimeters can increase the temperature on the workpiece. More specifically for the tool #2, 0.13 mm of difference can affect the temperature by 23.74 °C on Titanium plaque from T3 to T4 using an *ae* of 4.3 mm, *ft* of 0.05 mm/tooth. Furthermore, we can observe that the cutting temperature increases through the cutting length. This is because the titanium is a source of heating. As a result, the heating within the workpiece rises during the cutting length as shown in tool #2-T4 in Figure 3.3 c) and d) or in tool #2-T1 and T1 in Figure 3.3 a) and b). Data from Figure 3.3 can be found in ANNEX II.

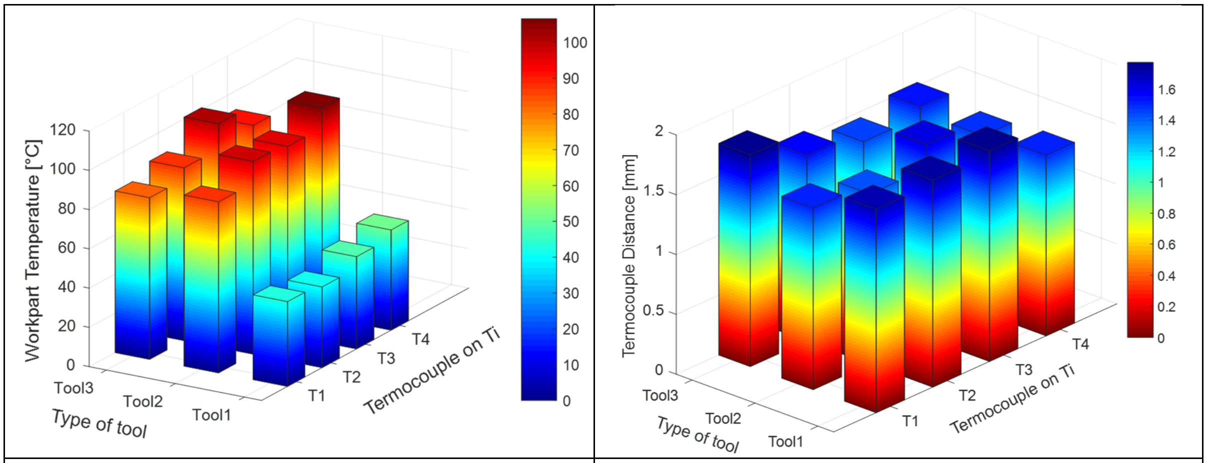

(**a**) T1-2-3-4 temperature for ae 1mm (**b**) T1-2-3-4 position for ae 1 mm

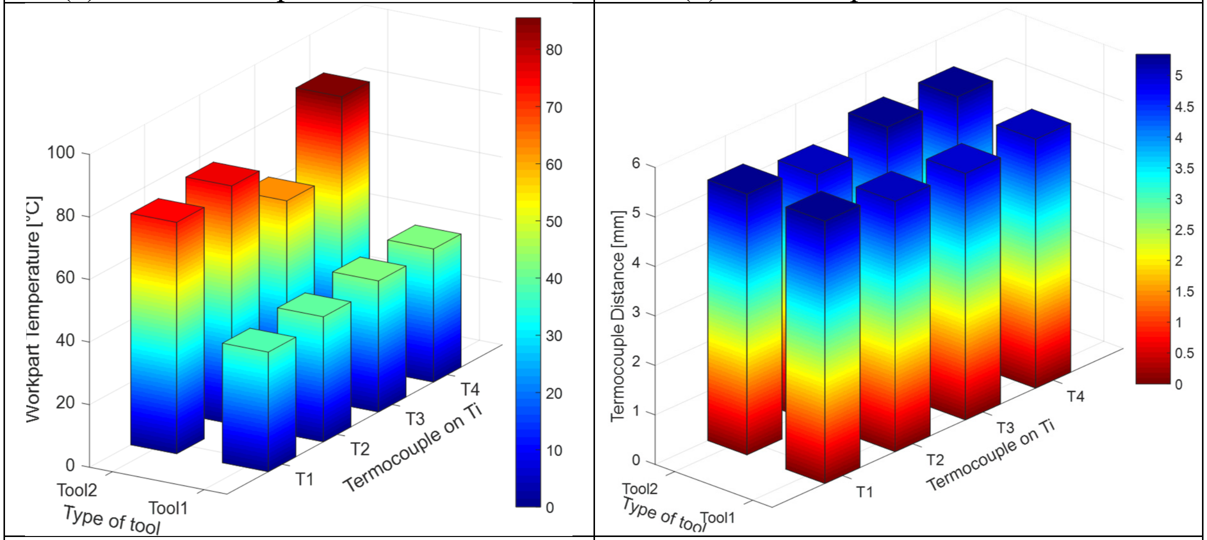

(**c**) T1-2-3-4 temperature for ae 4.3 mm (**d**) T1-2-3-4 position for ae 4.3 mm

Figure 3.3 Workpiece temperature on Ti plaque against thermocouple distance for a ft of .05 mm/tooth, v of 175 mm/tooth

Figure 3.4 shows the temperature variation on the Ti6Al4V plaque through the longitudinal cut caused by the tool #2 and tool #3. Figure 3.4 a) and b) shows the temperature within the Ti6Al4V plaque using tool #2 and Figure 3.4 c) and d) for the tool #3. Figure 3.4 a) shows a linear trend of the temperature and Figure 3.4 b) shows the temperature profile within the Ti6Al4V plaque through the cutting length. It shows that temperature increases linearly with the cutting length. Additionally, the highest temperature section within the plaque is at the end of the cutting length. In the case of tool #3, Figure 3.4 c) shows that the heat is conducted less rapidly within the Ti6Al4V plaque than the tool #2. This is because the slop is less pronounced.

Although, Figure 3.4 d) shows that the temperature at the beginning of the cutting length is higher than Figure 3.4 c).

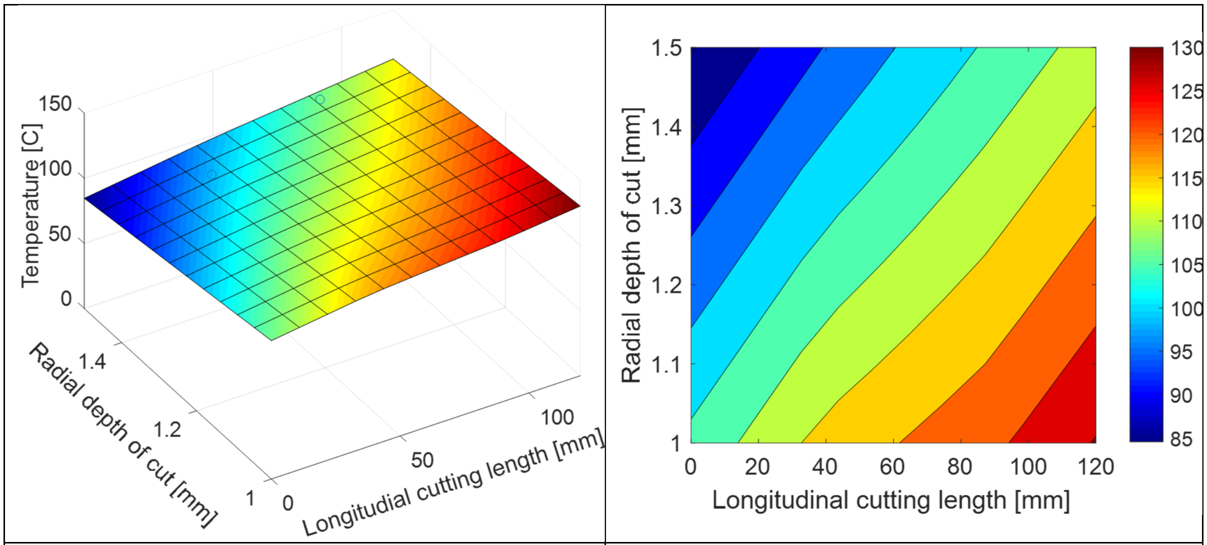

(**a**) 3D Ti plaque temperature for tool 2

(**b**) 2D Ti plaque temperature for tool 2

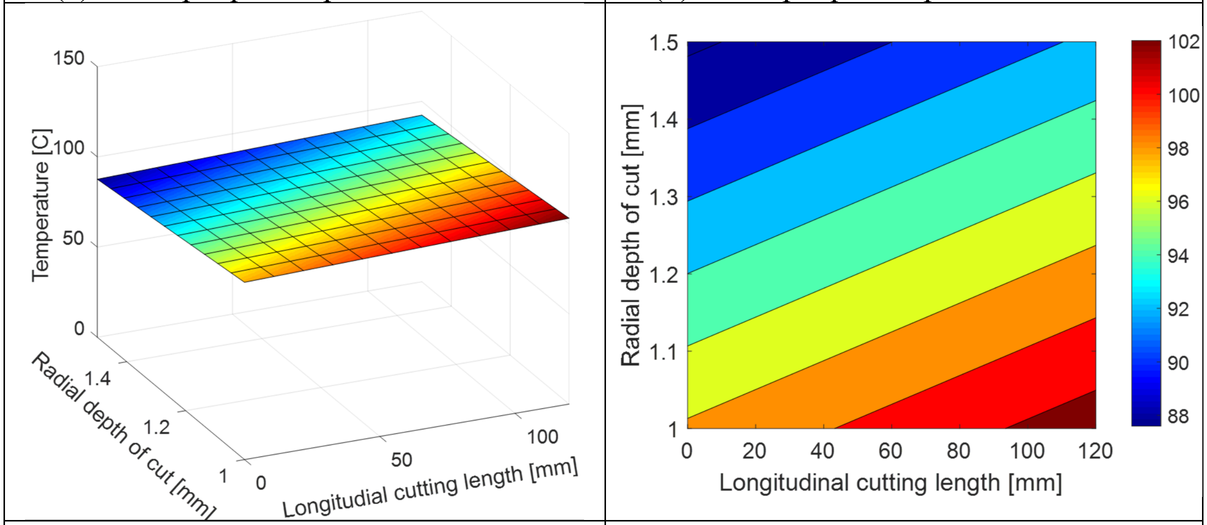

(**c**) 3D Ti plaque temperature for tool 3

(**d**) 2D Ti plaque temperature for tool 3

Figure 3.4 Longitudinal cutting profile for tool #2 (a, b) and tool #3 (c,d) at ft of 0.05 mm/tooth, v of 175 m/min and an ae of 1 mm

In order to see the events of the cutting process through the longitudinal distance for the thermocouples T1-2-3-4 within the Ti6Al4V plaque, the schematic diagram shows theses events as shown in Figure 3.5. The cutting parameters used were the worst with which the highest temperature is obtained (*ft* of 0.05 mm/tooth, *v* of 175 m/min) for tool #3. The solid orange line represents the through-longitudinal temperature profile just before the cutter reaches the thermocouple location along the cutting length while the solid blue line represents the heat dissipation after the cutter reaches the thermocouple and the solid red line represents the maximum temperature when the cutter is on the thermocouple. Both the yellow line (before cutting) and blue line (after cutting) were plotted with a separation time of 0.00327 second. This is with the aim of seeing how quickly the temperature changes in the same period of time. This means as the temperature increases through the cutting length, the gradient between both curves increases from 5.07 °C to 23 °C in 0.00653 seconds, keeping a constant change temperature and independently of the radial depth distance. In the case of both red lines, the solid red line shows the maximum temperature on each thermocouple using the real data while the slashed line shows the interpolation temperature in a fix radial depth of cut.

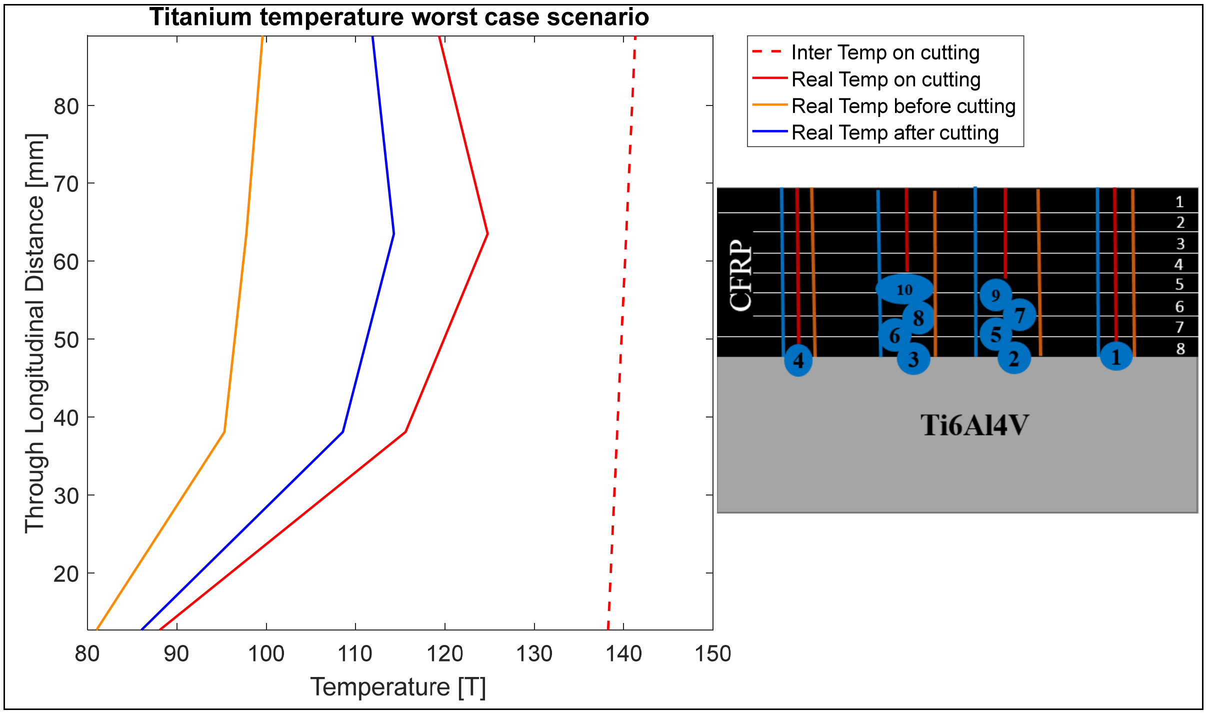

Figure 3.5 Temperature through the longitudinal distance for the titanium plaque using tool #3, v of 175m/min, ft of 0.05 mm/tooth and ae of 1mm

Based on the results, the experiment found that the feed per tooth and the tool type are the factors that have more influence on the titanium temperature. This is opposed to Y. Sun et al. and Yujing et al. (2014; 2017) research where their studies found that the most relevant factor is the cutting speed, followed by the feed per tooth. This is due to the method used to measure the temperature within the cutter and workpiece. In addition, their method does not show how the semi-artificial thermocouple is able to measure the temperature in both the workpiece or cutter temperature or if their measure belongs to the cutter or workpiece or both of them.

In addition, we found that the tool #3 transferred the heat less rapidly to the workpiece than tool #2. It is worth noting that both Yujing et al. (2014), and our work were performed under dry conditions and down milling. Therefore, these cutting conditions can be dismissed from the discussion.

3.1.2 Analysis of temperature in the CFRP workpiece

In the case of the embedded thermocouples within the plies of the CFRP section, Figure 3.6 shows the pareto chart of standardized effects on the maximum temperature measured inside the CFRP plate for the thermocouples T5 and T7 at the same cutting length as T2 on the Titanium plaque. The thermocouple distribution is shown in Figure 2.6.

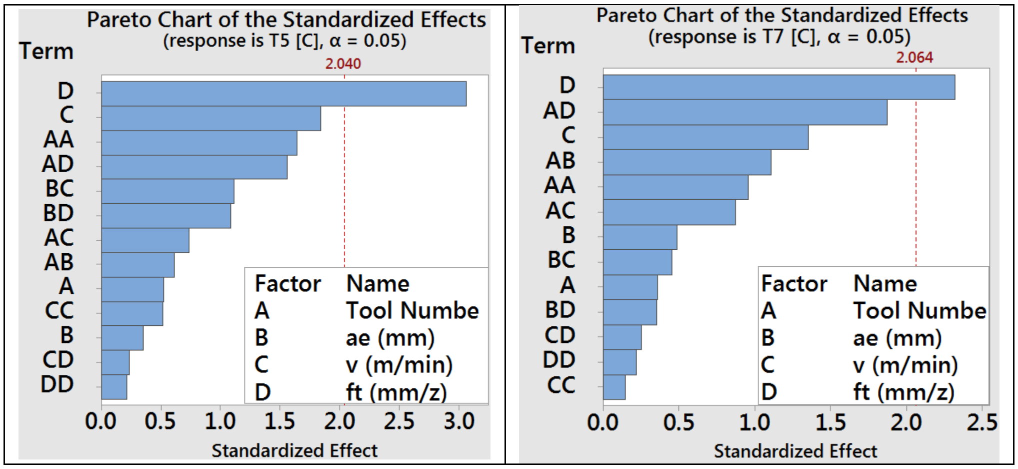

Figure 3.6 Pareto Chart of the Standardized effects on T5 and T7

The RSM shows that the feed per tooth is over the reference line of significant effects (Lenth's Pseudo-Standard Error) for both thermocouples; however, the cutting speed is for thermocouple T9 (see the right side of Figure 3.8). This difference could be due to the fact that nearly 35.56% of the thermocouples were lost due to the cutting depth optimization, please refer to ANNEX I for details.

In the case of T6 and T8 in the same cutting length as T3 on the Titanium plaque, they have a similar behavior than T5 and T7 which the most significant factor is the feed per tooth, as shown in Figure 3.7.

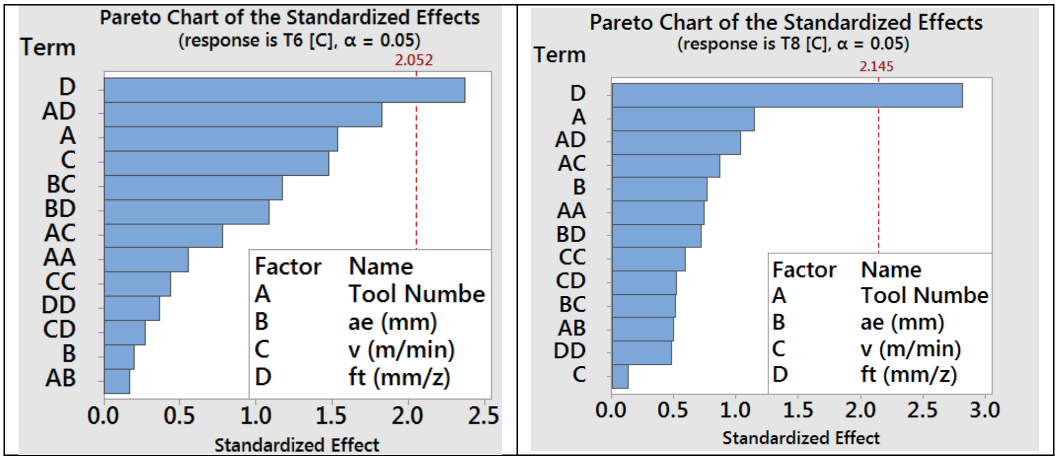

Figure 3.7 Pareto Chart of the Standardized effects on T6 and T8

Similarly, the most significant factor is the feed per tooth followed by the radial depth of cut although it does not exceed the line of statistically significant for the T10, (left side of Figure 3.8). This difference could be due to the fact of displacement of thermocouples during the curing process.

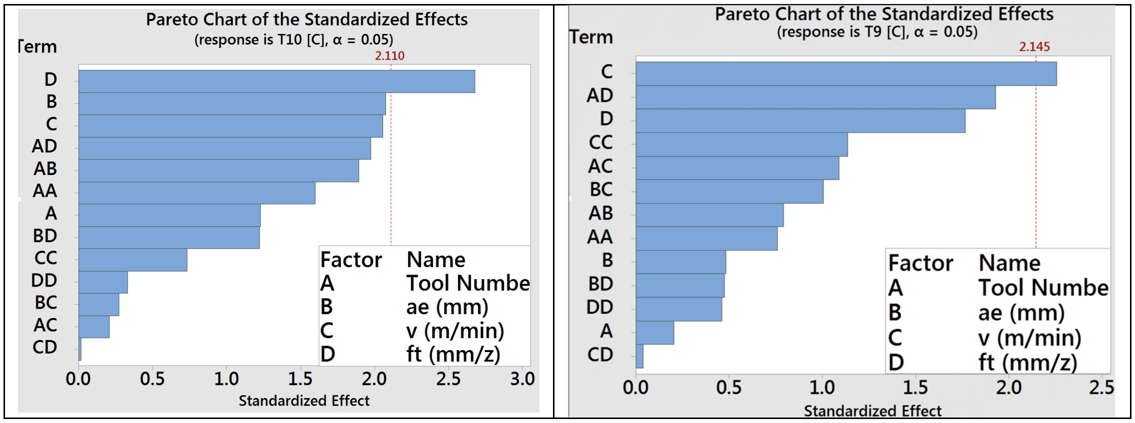

Figure 3.8 Pareto Chart of the Standardized effects on T10 and T9

Figure 3.9 (data in ANNEX II) analyses of the interaction between the feed per tooth against the type of tool and the change of temperature between the CFRP/Ti6Al4V plaque interface for an ae 1 mm and ft of 0.05 mm/tooth. This is because the feed factor is the most significant factor in both workpiece materials.

is, Figure 3.9 shows the temperature and distance for both columns of embedded thermocouples 2-5-7-9 and 3-6-8-10. The Figure 3.9 a) shows the first column to be in contact with the cutter thermocouples 2-5-7-9 while the Figure 3.9 c) is the second column of thermocouples 3-6-8-10. The temperature within workpiece caused by each cutter is shown in Figure 3.9 a) and c), while their thermocouples position within the CFRP/Ti6Al4V plaque is shown in Figure 3.9 b) and d). As shown in Figure 3.9 a) and c), tool #2 and tool #3 have a higher temperature than tool #1 for both radial depths of cut. For example, in the case of tool #2, the average thermocouple distance of T5 is 0.93 mm, which is even less than the optimal radial depth of cut of 1 mm. As a result, in this particular case, the temperature on thermocouple T5 is 125.39 °C for a feed per tooth *(ft)* of 0.05 mm/tooth, which is even lower than the transition glass temperature T_g of 190°C for the Prepeg CYCOM® 5320-1 T650-35 3K 8HS Fabric 36%, according to the datasheet in section 2.5. Moreover, the temperature on thermocouple T2 is lower than T5 with the same cutting length because T2 is further from the cutting edge than T5 by around 0.5 mm.

For thermocouples 3-6-8-10 in the second thermocouple column, the temperature on the titanium plaque, represented by thermocouple T3, is greater than the temperature within plies in the CFRP of about 16°C with respect to T6 for the tool #3, as shown in Figure 3.9 c). In the case of the thermocouples position within the CFRP plies, T6 and T10 have the same temperature while T8 temperature is higher due to its thermocouple position, which is closer to the cutter edge, as shown in Figure 3.9 d). Thus, a difference of 0.28 mm between thermocouples can vary the temperature within the CFRP plies by about 36.84°C under the same cutting conditions. As a result, small thermocouples distance variation can have an enormous influence on the thermocouple temperature. In the case of interaction analysis for a radial depth of 4.3 mm, see ANNEX II. This is because the radial depth of cut is not statistically significant.

Clicours.com

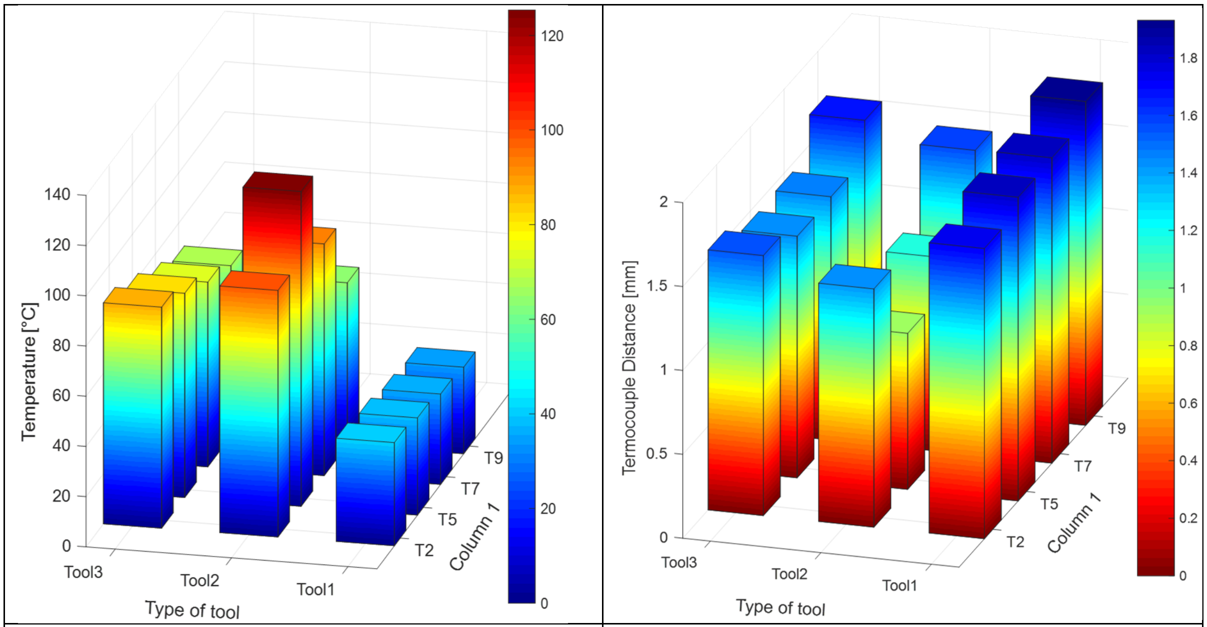

(**a**) Thermocouple T2-5-7-9 temperature (**b**) Thermocouple T2-5-7-9 position

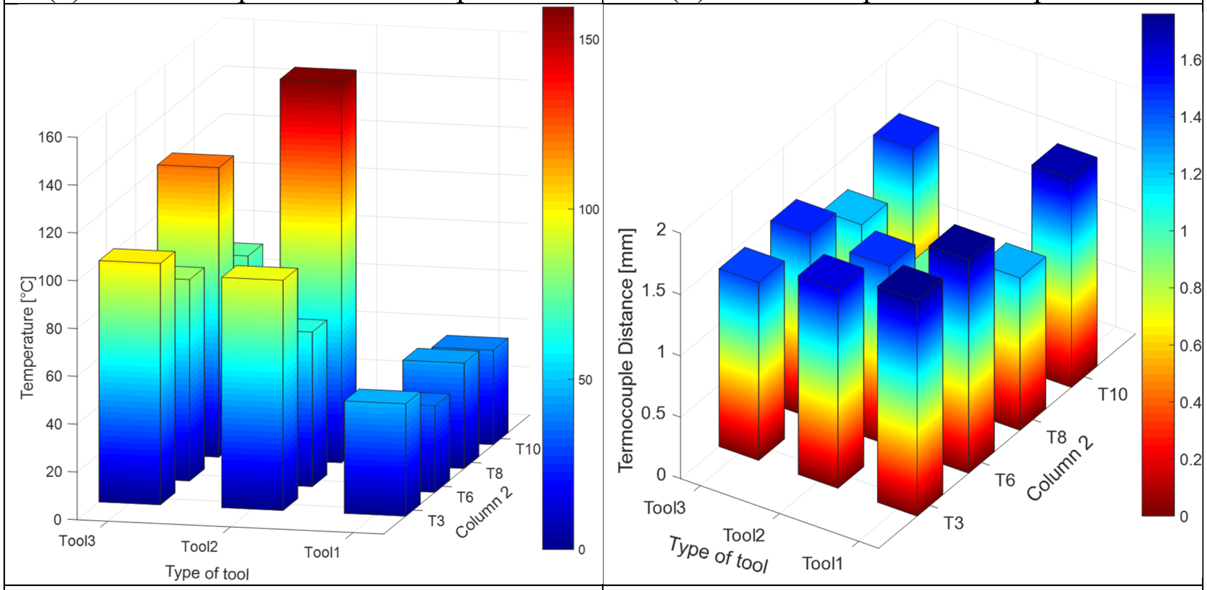

(**c**) Thermocouple T3-6-8-10 temperature (**d**) Thermocouple T3-6-8-10 position

Figure 3.9 Workpiece temperature on Ti and CFRP VS thermocouple distance for ft of 0.05 mm/tooth, ae of 1 mm on (T2, T5, T7 and T9) and (T3, T6, T8 and T10)

Moreover, Figure 3.10 shows the gradient vertical cutting temperature at a cutting length of 38.1 mm for thermocouples 2-5-7-9. Figure 3.10 a) and b) show the change of temperature in the thickness of the stack for the tool #2. Thus, it shows that the maximum cutting temperature is located at the Ti6Al4V plaque and decreases between the CFRP layers in waveform. Figure 3.10 c) and d) show the temperature using tool #3. In this case, the highest temperature is also located in the section of the Ti6Al4V plaque near to the cutting edge and changes after the second CFRP layer and continues between the layers. Both Figure 3.10 b) and Figure 3.10 d) keep the maximum temperature in the interface of the Ti6Al4V/CFRP stack and decreases with the thickness.

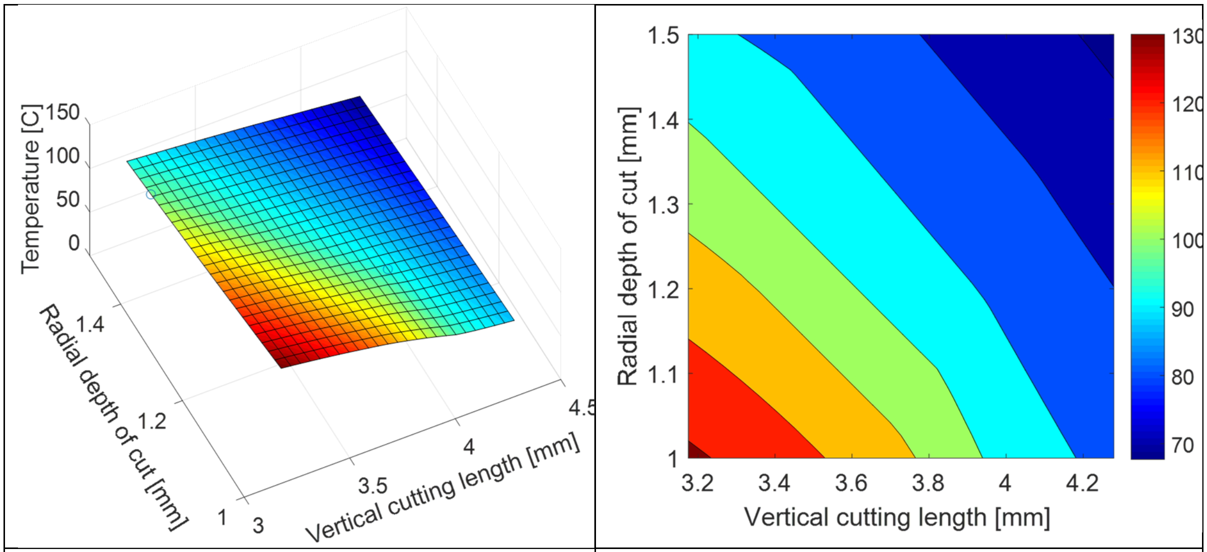

(**a**) 3D temperature for tool #2 | (**b**) 2D temperature for tool #2

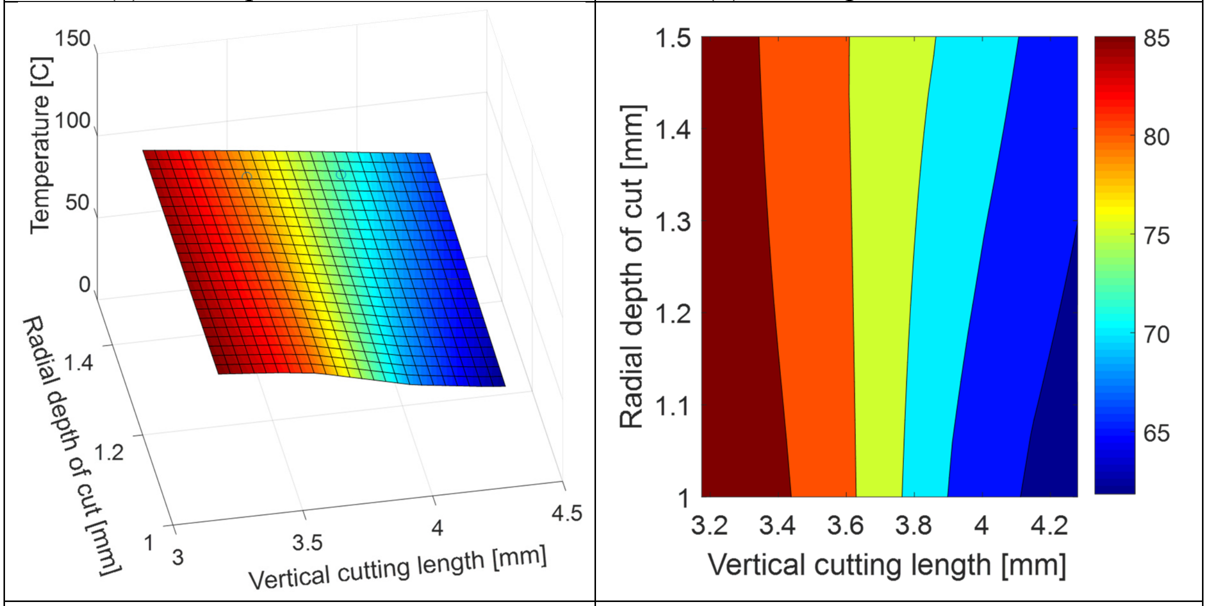

(**c**) 3D temperature for tool #3 | (**d**) 2D temperature for tool #3

Figure 3.10 Vertical cutting temperature at a cutting length of 38.1 mm (thermocouples 2-5-7-9)

Clicours.COM

In order to see the events of the cutting process through the thick distance for the thermocouples T2-5-7-9 within the $[0]_8$/Ti6Al4V plaque, the schematic diagram shows theses events as shown in Figure 3.11. The cutting parameters used were the worst with which the highest temperature is obtained (ft of 0.05 mm/tooth, v of 175 m/min) for tool #3. The solid orange line represents the heat transfer temperature to the thermocouple position before the cutter touches the thermocouple while the solid blue line represents the heat dissipation after the cutter reaches the thermocouple and the solid red line represents the maximum temperature when the cutter is on the thermocouple. Both the curve before and after cutting were symmetrically plotted with a separation time of 0.00327 seconds from the maximum curve in order to compare the heating and dissipation gradient for T/Cs T2-5-7-9. This is with the fact of maintaining both gradients in the same condition. After analyzing both curves (before and after cutting), the heat within the Ti6Al4V plaque stays longer than the heat within $[0]_8$ plaque with a rate of 4.5. In the case of both red lines, the solid red line shows the maximum temperature on each thermocouple using the real data while the slashed line shows the interpolation temperature near to the cutter. Thus, the interpolated model shows a higher temperature than real data. This is because the model is plotted using a radial depth of 1 mm. The value with which the experiments were carried out. In fact, the peak value belongs to T/C T7 in the solid red line is at 0.98 mm from the cutting edge and corresponds to the interpolation value. On the other hand, thermocouple T5 is at 1.68 mm from the cutting edge and it is the lowest value.

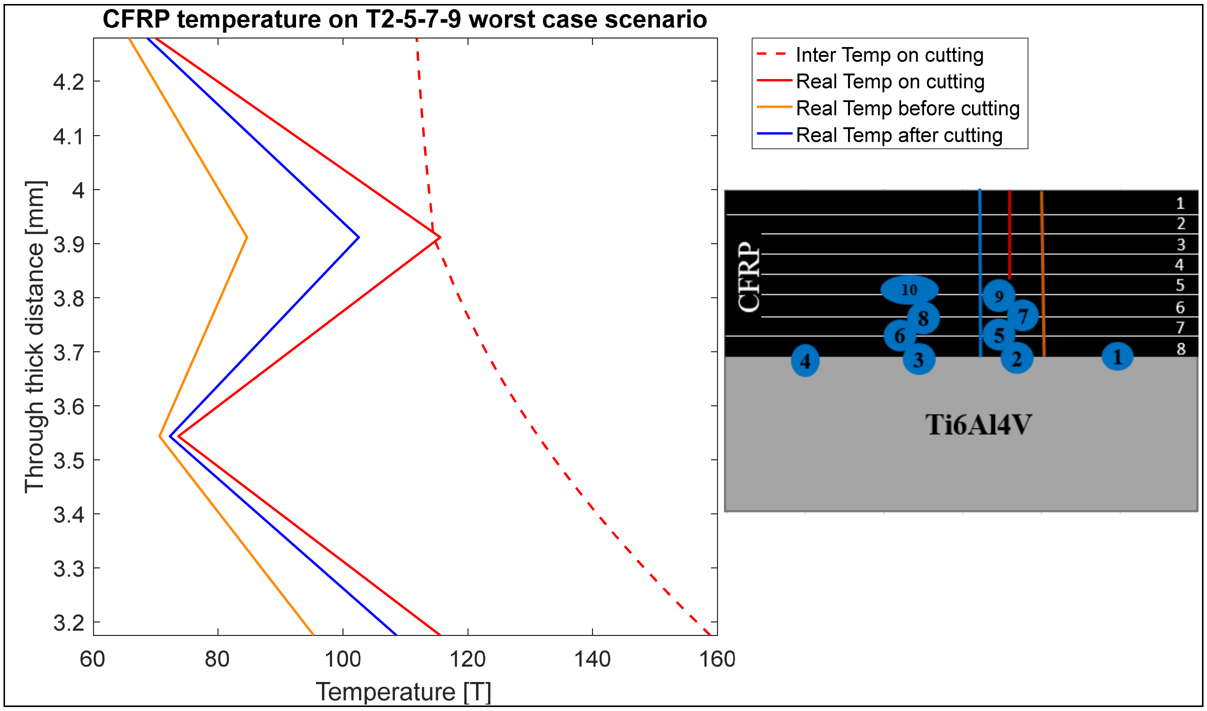

Figure 3.11 Temperature through the thick distance T/C 2-5-7-9 for the [0]8/Ti6Al4V plaque using tool #3, v of 175m/min, ft of 0.05 mm/tooth and ae of 1mm

Figure 3.12 shows the vertical cutting temperature at a cutting length of 63.5 mm for thermocouples 3-6-8-10. Figure 3.12 a) and b) show the temperature for the tool #2 and Figure 3.12 c) and d) for the tool #3. Figure 3.12 a) and b) show that the temperature within the Ti6Al4V plaque decreases faster through the CFRP layers and the temperature is higher than Figure 3.10 b). This is due to the temperature increases with the longitudinal cutting length, as shown in Figure 3.4 b). Thus, the heat transfer between layers from the Ti6Al4Vplaque to the CFRP layers is higher. Figure 3.12 c) shows that the temperature conducted within the CFRP/Ti6Al4V stack is more between layers than Figure 3.12 a). This is due to the tool #3 which transfers more heat to the workpiece as shown in Figure 3.12 d).

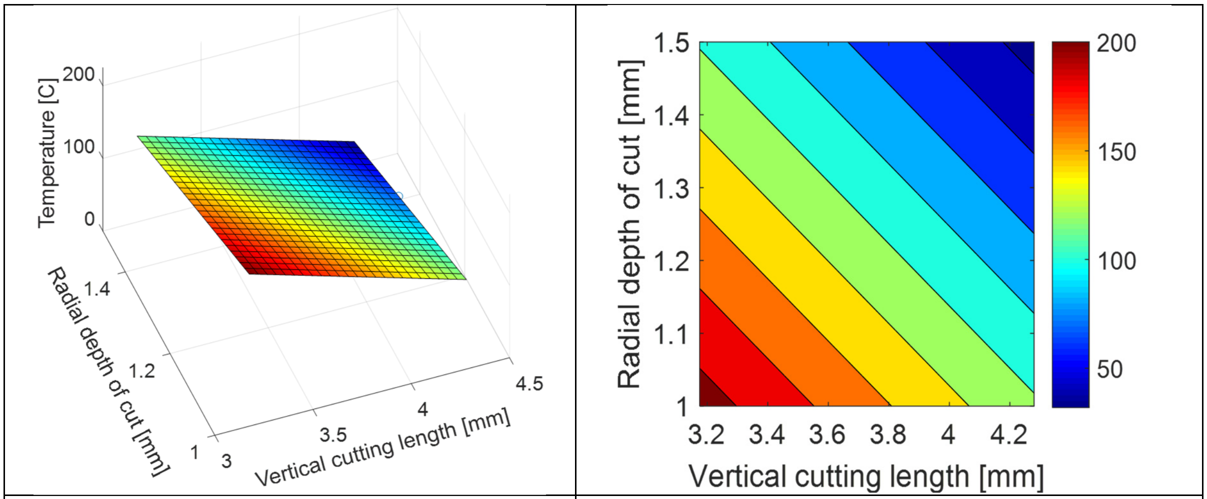

(**a**) 3D temperature for tool #2 | (**b**) 2D temperature for tool #2

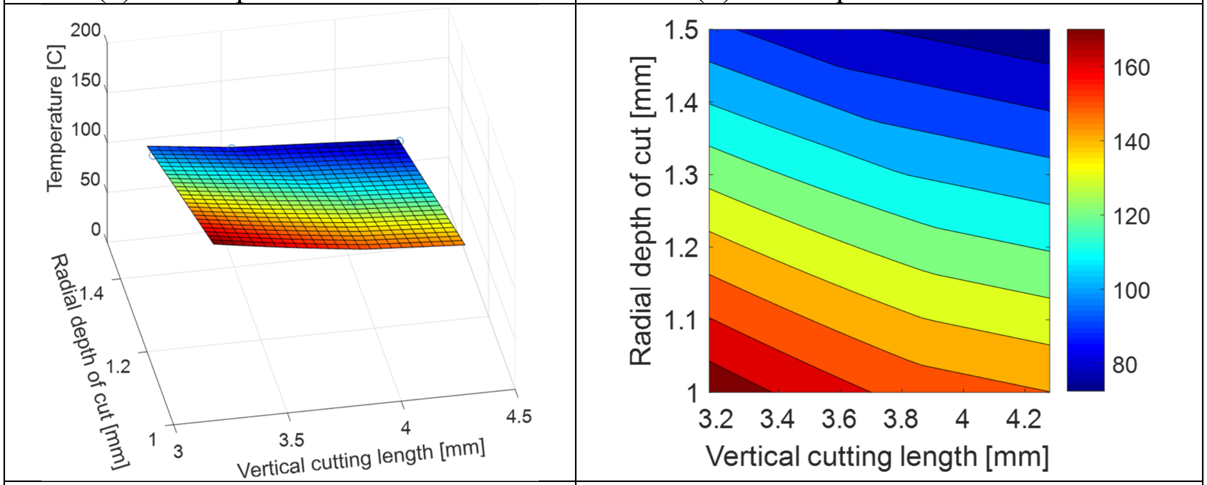

(**c**) 3D temperature for tool #3 | (**d**) 2D temperature for tool #3

Figure 3.12 Vertical cutting temperature at a cutting length of 63.3 mm (thermocouples 3-6-8-10)

Figure 3.13 shows the cutting temperature through the thick distance for thermocouple T3-6-10 within the $[0]_8$/Ti6Al4V plaque using the worst cutting conditions (ft of 0.05 mm/tooth, v of 175 m/min) for tool #3 in different events of the cutting process. As a result, the schematic diagram of the events for the cutting process is shown in Figure 3.13. Both curves (before and after cutting) were symmetrically plotted to compare the heating and dissipation gradient for thermocouples T3-6-10. This is with the aim of maintaining both gradients in the same condition. We found that the heat within the CFRP plaque dissipated much faster than the heat within Ti6Al4V plaque since the spacing between lines (yellow and blue line) is bigger at 3.2 mm than at 3.5 mm and 4.2 mm. In the case of both red lines, the solid red line shows the maximum temperature on each thermocouple using the real data while the slashed line shows the interpolated temperature close to the cutter. Therefore, the highest temperature is in the Ti6Al4V and dissipates through the thickness both for the inter temp on cutting and real temp on cutting.

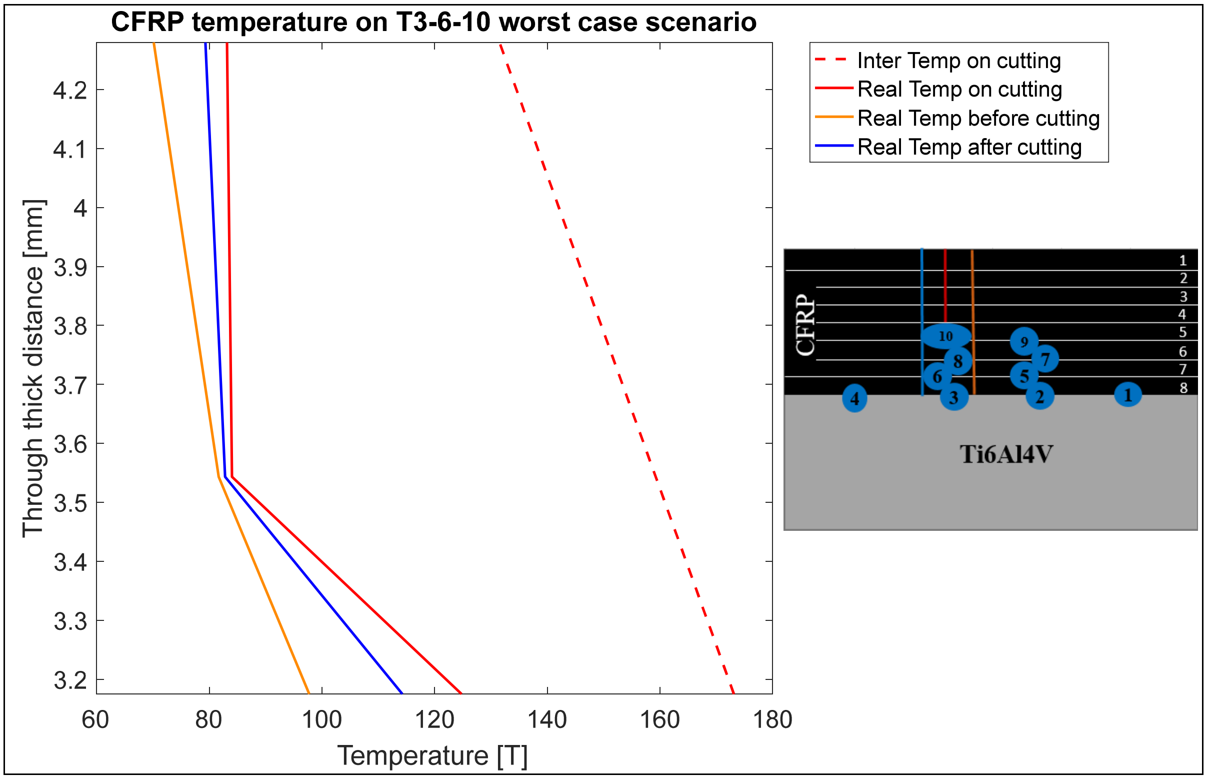

Figure 3.13 Temperature through the thick distance T/C 3-6-10 for the [0]8/Ti6Al4V plaque using tool #3, v of 175m/min, ft of 0.05 mm/tooth and ae of 1mm

In summary, the feed per tooth is the most significant effect on the temperature of the CFRP. Similar results were found by Kerrigan et al. and J. Sheikh-Ahmad et al. (2016; 2018). However, our results are in disagreement with H Wang et al. (2013; 2016; 2016). This is because H Wang followed the same methodology as Yujing et al. (2014) using the semi-artifical thermocouple. Thus, we cannot know if their tool-workpiece thermocouple method was measured the cutter or the workpiece since there is no physical thermocouple on the cutter. As a result, it is not clear how their semi-artificial thermocouple method similar to a sheet of metal was able to measure the temperature in each section of the cutting process. In the case of Takeshi Yashiro (2013), the feed per tooth was constant throughout the experiments and its effect on temperature could not be evaluated. On the other hand, Kerrigan's results (2016) showed that 60% of the energy within the workpiece is due to the feed rate. This was calculated using the cutting forces statistics even though their setup shows a thermal camera. More recently, J. Sheikh-Ahamad et al. (2018), thermal aspects in machining CFRPs: effects of cutter type and cutting parameters, shows that the feed per tooth is the most significant factor. This is because the cutter passes faster through the workpiece. As a result, the heat retention in the workpiece is lower than in a low feed per tooth (ft) in the machining process. Finally and similar to our results obtained with thermocouples, J. Sheikh-Ahmad et al. (2018) reported that the cutting speed is not a significant factor on the temperature variation.

3.1.3 Analysis of temperature on the cutters

In the case of the cutter temperature, the main effect plot shows that the type of tool, radial depth of cut and the feed per tooth are the factors that influence the cutter temperature. The cutting speed does not have any effect, see the top of Figure 3.14. According to the different types of cutters, the tool #3 (PCD material) is the cutter with the highest temperature, followed by the tool #2 (coated carbide TiAlN+ TiAlN) and finally, tool # 1 (uncoated carbide) is the one with the lowest temperature. It is worth mentioning that during the experiments, sparks were observed using tool #1. It is believed that part of the carbide material was fused with the titanium chip, so most of that heat was dissipated through the chip during the experiments. Thus, we could not have an accurate measurement in tool #1.

In the case of the radial depth of cut, the greater the radial depth of cut, the higher the cutter temperature. Thus, the radial depth of cut of 4.3 mm has a higher temperature than the radial depth of cut of 1 mm. Similarly, the feed per tooth has great influences on the cutter temperature. As a result, a low f_t shows a higher temperature than a high feed per tooth. This is because the tool-workpiece interface engages longer, causing more friction and enclosing heat on the surface of the workpiece and the cutting tool. This effect is observed too in the CFRP/Ti6Al4V workpiece. On the other hand, the cutter temperature increases slightly with the cutting speed, although it is not as important as the other factors. In addition, a Pareto Chart of the Standardized effects shows that the radial depth of cut is the most significant factor followed by the type of cut and the feed per tooth, (the bottom of Figure 3.14). Although, there is no interaction of the different factors as opposed to the CFRP/Ti6Al4V plaque.

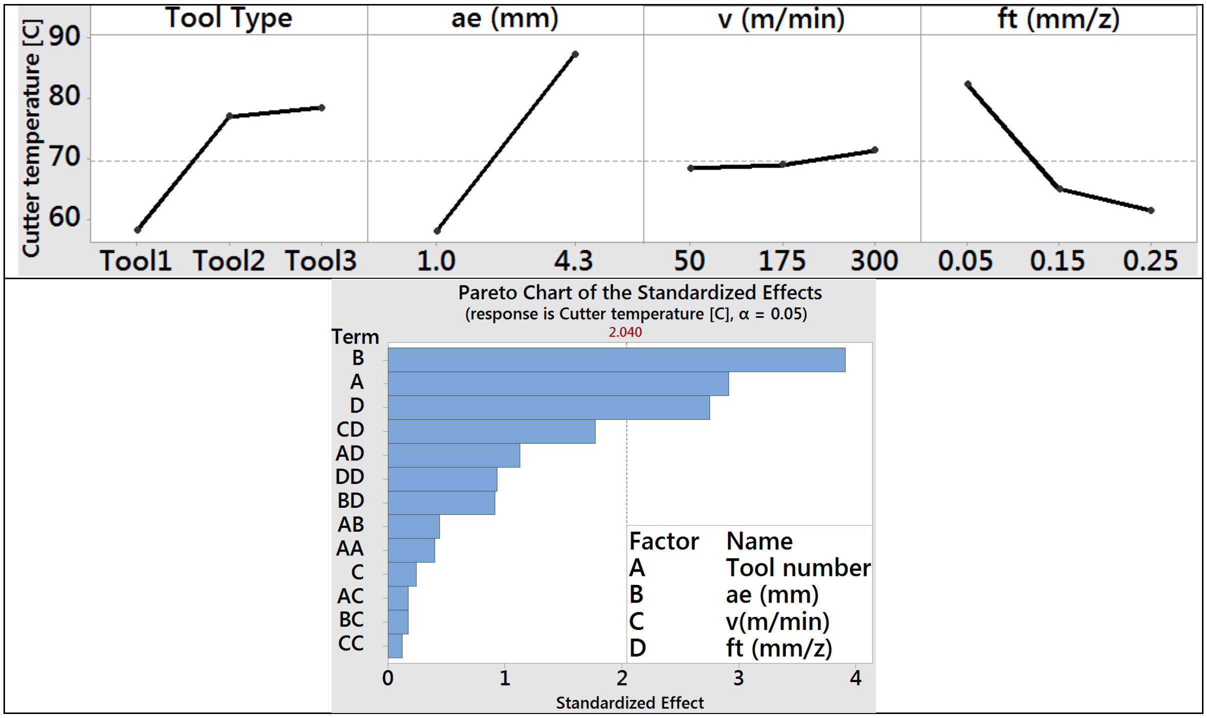

Figure 3.14 Main effect plot for cutter temperature and standardized pareto chart

The left side of Figure 3.15 (data in ANNEX II) shows the contrast between the radial depth of cut, the latter being the least significant factor for a cutting speed of 175 m/min, (the bottom of Figure 3.14). For a radial depth of cut of 4.3 mm, the temperature on the cutter is higher than for a radial depth of cut of 1 mm. This result is constant for all the values of feed per tooth. The highest temperature is observed for a low value of feed per tooth, which represents a similar trend than the workpiece temperature (the right side of Figure 3.2).

The right side of Figure 3.15 (data in ANNEX II) represents the interaction between the first and the second most important factors for a *ft* of 0.05 mm/tooth. This is because in this feed per tooth value is the highest cutter temperature. For a radial depth of cut of 1 mm, the tool #3 has the greatest cutter temperature, followed by the tool # 2 and finally, the tool #1. In the case of tool #1, sparks were observed during the experiments due to the fusion of the carbide material with the Titanium burr. Thus, the heat was expelled through the chip, measuring a lower cutter temperature. On the other hand, for a radial depth of cut *(ae)* of 4.3 mm, tool #2 reaches temperatures close to 140 °C while the tool #1 is below 70°C. It is worth mentioning that the tool #3 temperature is not measured because tool #3 is not designed to perform cuts greater than a radial depth of cut of 1.5 mm as described in Chapter 2.

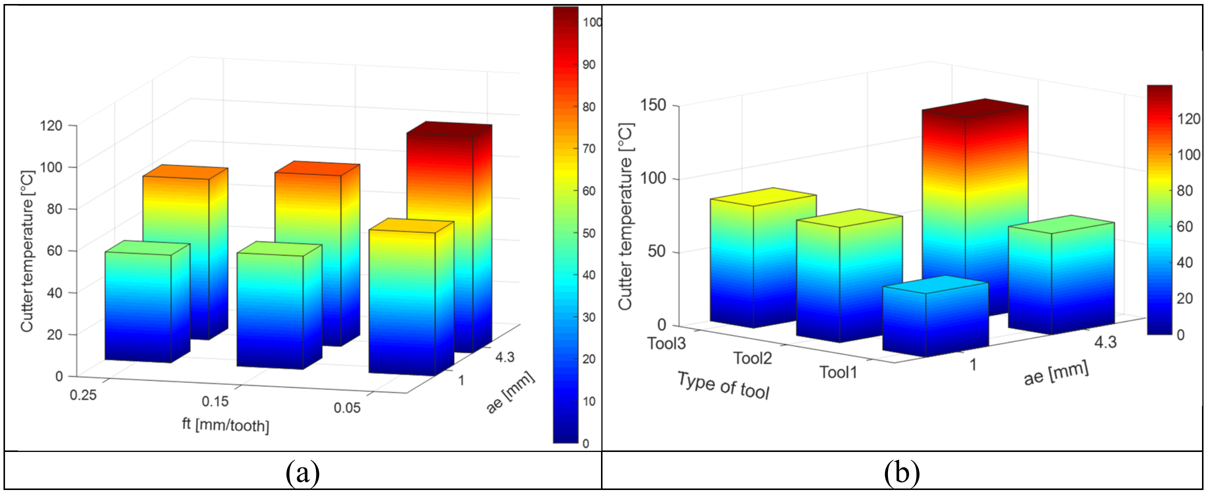

(a) (b)

Figure 3.15 3D Graph cutter temperature (a) feed per tooth vs radial depth of cut for a v of 175m/min (b) Type of tool vs radial depth of cut for a ft of 0.05 mm/tooth

In conclusion, many researchers tried to measure the cutter temperature using different techniques, although only a few of them obtained relevant results. In the case of Yashiro et al. (2013), the thermal cameras could not see the cutter temperature since the heat saturates the thermography in the cutting point. On the other hand, Yujing et al. (2014) measured the cutter temperature using a semi-artificial thermocouple within the workpiece. Their statistical analysis shows that the cutter temperature has the same cutting speed trend as the workpiece, which is the most significant factor, followed by the feed per tooth, and finally the radial depth of cut. The Yujing's results (2014) do not agree with Kerrigan's results (2016) in that the radial depth of cut is the most significant factor. This result is the same as that obtained in this research. It is worth mentioning that both Kerrigan et al., Donnell et al. (2016) and this research use the telemetry system to measure the cutter temperature. Moreover, J. Sheikh-Ahmad et al. (2018) reported that neither the cutting speed nor the feed per tooth are significant factors, as opposed to Yujing's results (2014). Nevertheless, the radial depth of cut was always kept constant in J. Sheikh-Ahmad's DOE (2018). Therefore, we cannot compare their results with our results. Finally, J. Sheikh-Ahmad et al. (2018) also studied the effects of the physical properties of the cutter (geometry and material) on the temperature of the cutter, chip and the workpiece. However, their results for both cutter and workpiece showed a higher temperature than ours. This is because their CFRP cutting length is 5 times longer than our CFRP/Ti6Al4V plaque cutting length, even when we machined the plate under dry conditions. It is worth mentioning that our study is limited to the measurement of the cutter and workpiece temperature, as opposed to (2018) which also covered the chip temperature.

ClicCours.com

3.2 Analysis of Forces

Another objective of this research is the analysis of the cutting forces during the machining process (average over 30 revolutions). Thus, the scheme of the cutting forces are presented as follow (Figure 3.16.):

- F_x → F_f (Feed force) is the force which opposes to the cutter and the plaque. It is positive according to Figure 3.16 and Figure 2.4.
- F_y → F_n (Normal force) is the force normal to F_f and is a component of the direct trihedron (F_f, F_a, F_n). It is positive according to Figure 3.16 and Figure 2.4.
- F_z → F_a (Axial force) is the force on the cutting length direction of cutting tools (+Z) and is positive according to Figure 3.16 and Figure 2.4.

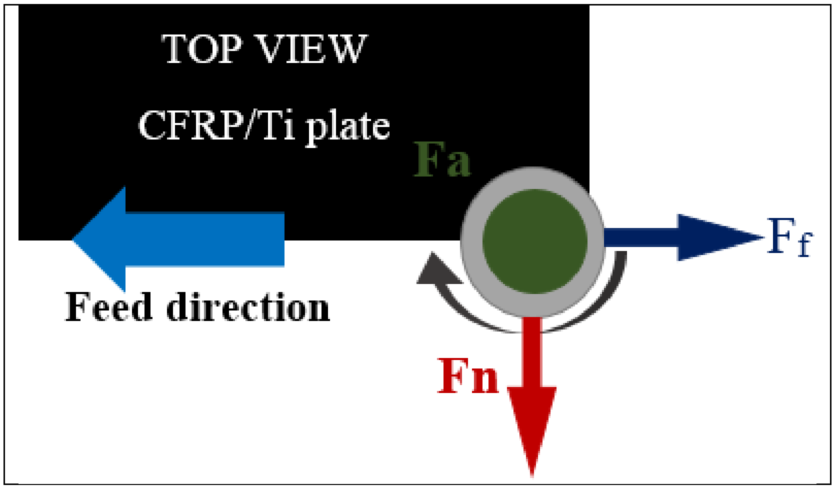

Figure 3.16 Scheme of applied forces on the CFRP/Ti

3.2.1 Feed force

The main effect plot (the top of Figure 3.17) shows that the tool type has less influence on the feed force than on the temperature of the workpiece and cutter. Although, tool #3 shows the less feed force of all the cutters. On the other hand, the radial depth of cut and feed per tooth are the factors that most influence the feed force. Thus, the greater the magnitude of the radial depth of cut or the feed per tooth, the higher the feed force on the cutter. Moreover, the Pareto chart of standardized effects (the bottom of Figure 3.17) shows that the feed per tooth is the factor with the most influence on the feed force, followed by the radial depth of cut *(ae),* and finally the interaction between them. It is worth mentioning that the cutting speed has no influence on the feed force like the other factors.

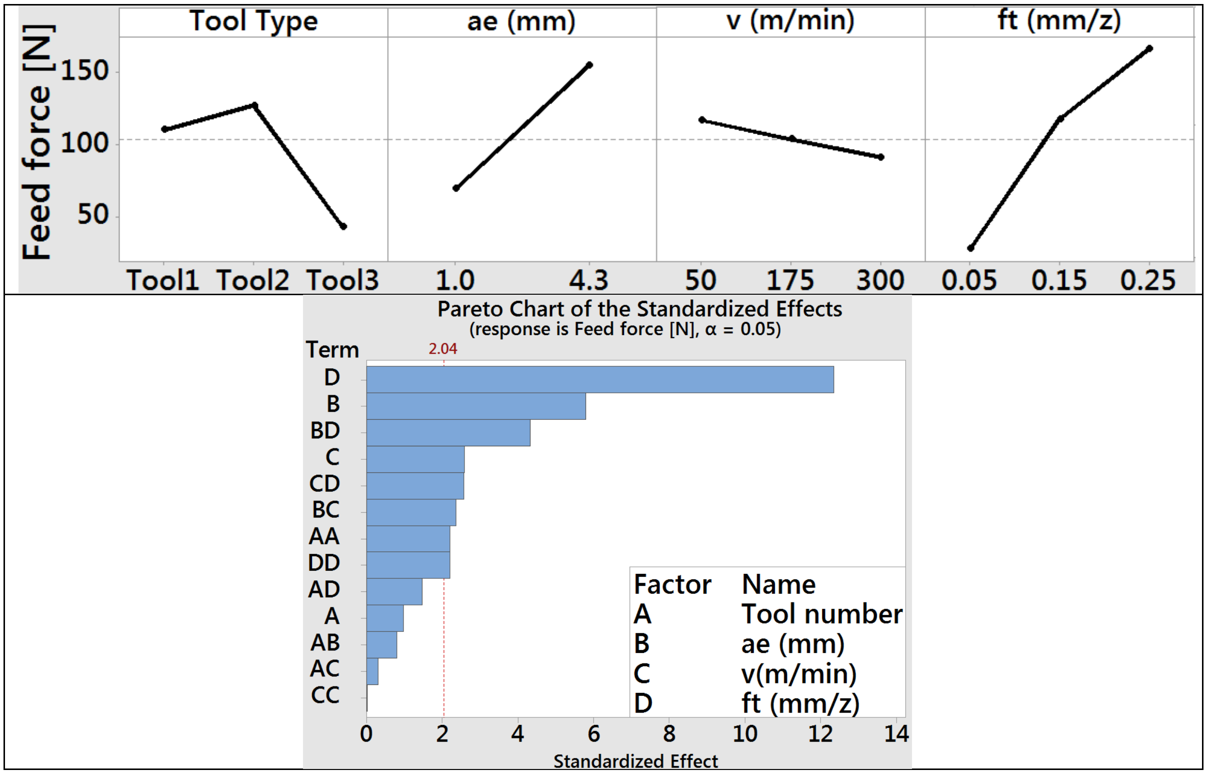

Figure 3.17 Main effect plot for average Feed force result and standardized pareto chart

Figure 3.18 shows the interaction among the different cutting parameters such as the feed per tooth *(ft)*, the cutting speed *(v)* and the radial depth of cut *(ae)* in each cutter. The worst cutting condition of the feed force is for a high feed per tooth of 0.25 mm/tooth, a low cutting speed of 50 m/min and high radial depth of cut of 4.3 mm. The tool # 1 and tool # 2 have a similar behavior although the feed force on the tool #2 is greater than the tool #1 for different cutting speeds. On the other hand, tool #3 has a linear trend and the feed force increases with respect to its feed per tooth for the different cutting speeds. In addition, the feed force on tool #3 is smaller than the feed force on the tools #1 and #2. This might be because the tool # 3 is not

Clicours.COM

stiff enough to cut through the titanium surface, causing tool wear and chipping under harsh cutting conditions.

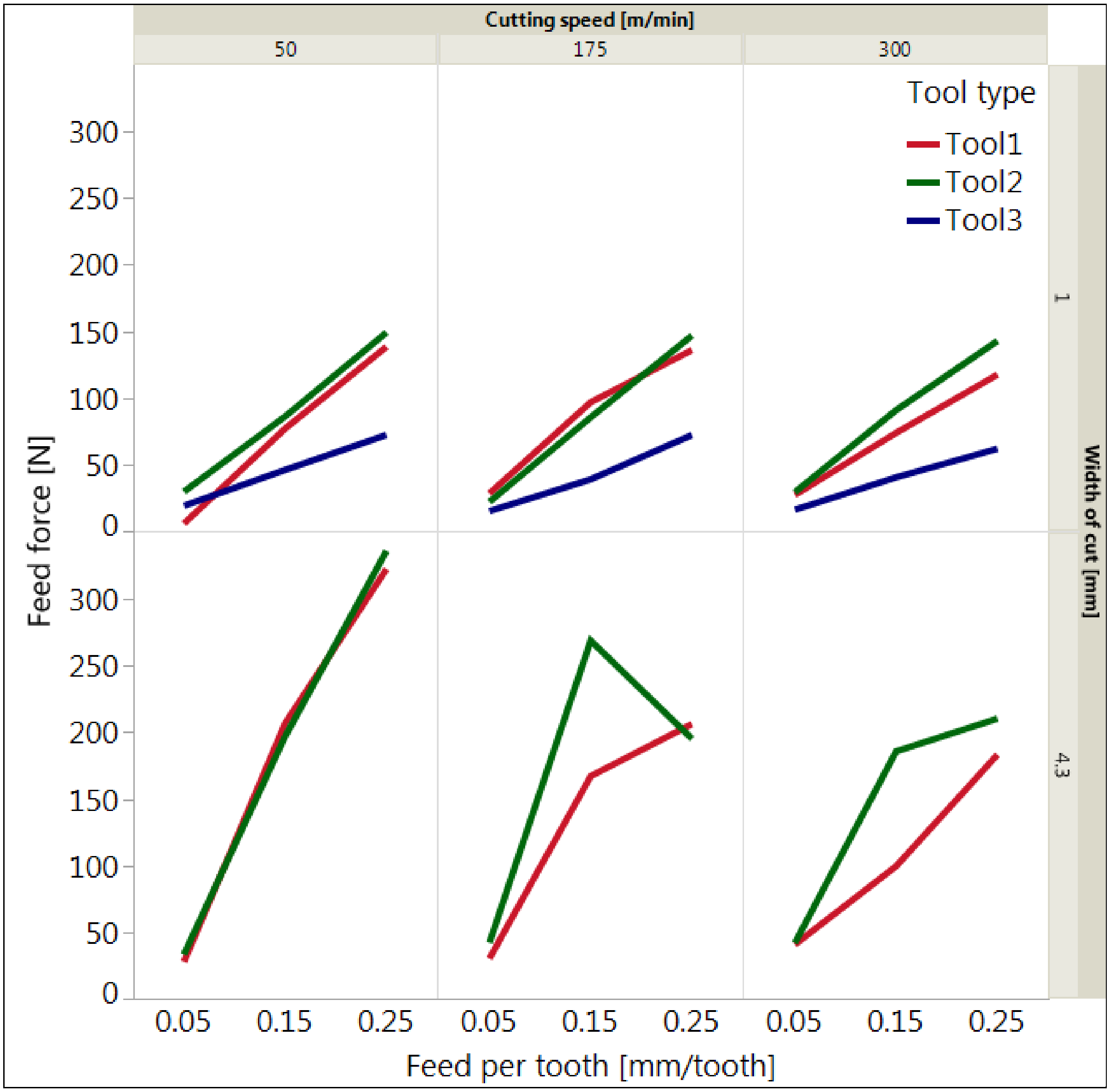

Figure 3.18 Feed force as a function of the feed per tooth according to the different cutting parameters on each cutter

3.2.2 Normal force

The normal force shows a similar trend than the feed force, in which the most significant factors are the feed per tooth and the radial depth of cut. Similarly, the feed per tooth is the most significant factor, followed by the radial depth of cut then by the interaction between the feed per tooth-radial depth of cut and finally, the cutting speed. Figure 3.19 shows the interaction of the different cutting parameters for each cutter. In the case of tool #1, the normal force is lower than the other cutters for the different cutting speeds and 1 mm radial depth of cut, and both tool #2 and #3 have a similar normal force trending. However, the normal force in tool #3 is slightly higher than for tool #2. Thus, tool #3 is prone to chipping, tool wear or tool failure due to the high magnitude of the normal force. Additionally, this tool is not designed to machine titanium since it is brittle.

For a radial depth of cut *(ae)* of 4.3 mm, the normal force is 5 times greater than for the normal force of *(ae)* of 1 mm. In addition, the normal force for tool # 1 is greater than the force for tool #2. It is important to emphasize that the greatest force is seen in a high feed per tooth of 0.25 mm/tooth and a cutting speed of 300 m/min, this is even much greater than any other value of the feed force or the axial force. However, for a cutting speed *(v)* of 175 m/min and 4.3mm radial depth of cut, the trend of the tool #2 is different since the normal force ramps up to 576 N for a feed per tooth of 0.15 mm/tooth, and then decreases to 339 N for a feed per tooth of 0.25 mm/tooth. This might be due to the fact that the chip morphology changes to take off more heat during the cutting process, turning it in a dark-bluish color. Therefore, a second repetition could help to clarify this measure.

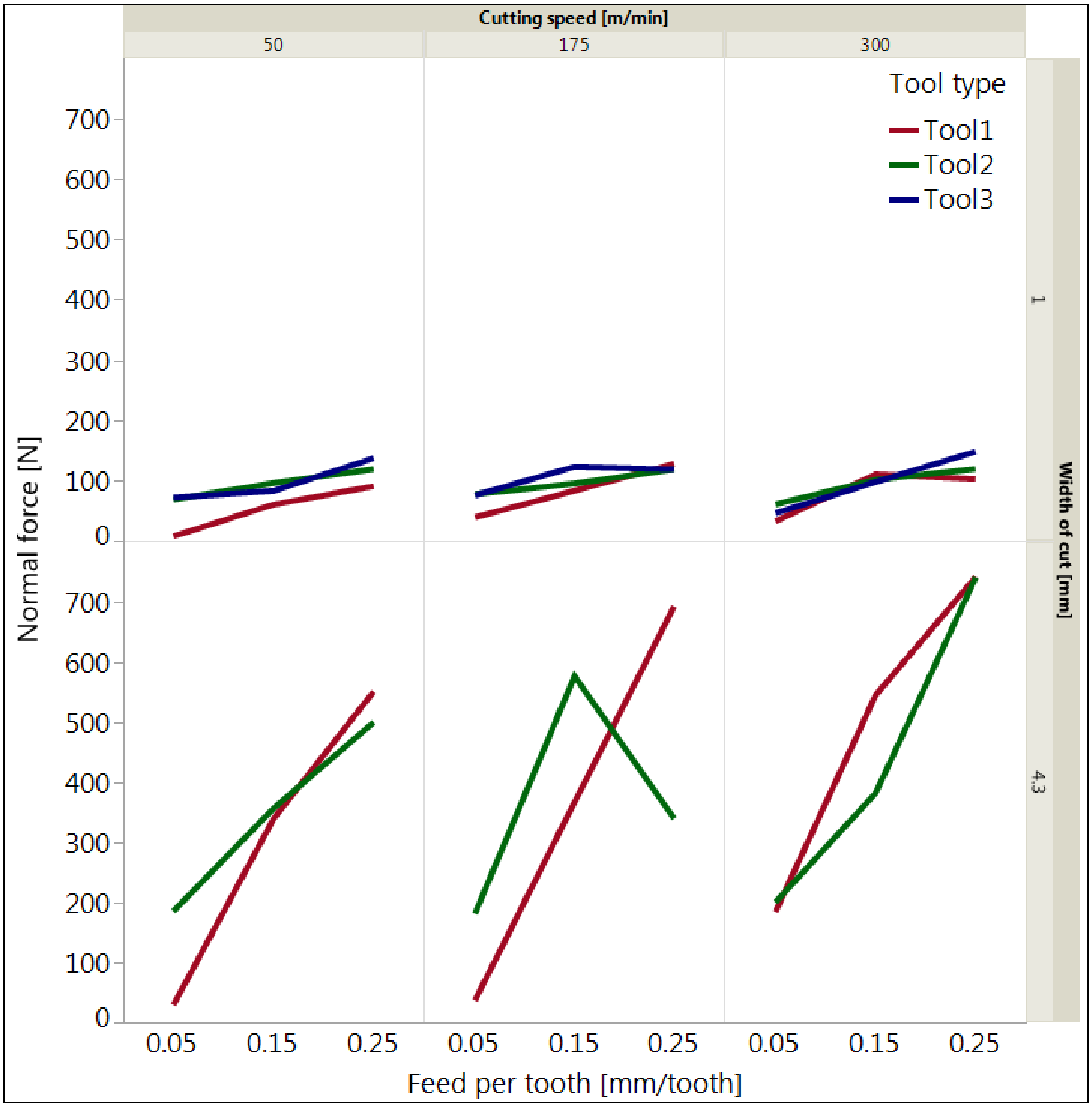

Figure 3.19 Normal force as a function of the feed per tooth according to the different cutting parameters on each cutter

Clicours.COM

3.2.3 Axial force

The main effect plot (the top of Figure 3.20) shows that the tool #2 has the greatest axial force of all tools. This effect can be attributed because tool #2 has wider helix angles, as compared to tool #1 and #3. As a result, there is delamination on the CFRP plies as opposed to tool #3 which has the lowest helix angle. Similarly, the feed per tooth is the most significant factor, followed by the radial depth of cut, and then the interaction between the radial depth of cut-cutting speed and finally, the cutting speed (the bottom of Figure 3.20). This behavior is similar to normal and feed forces.

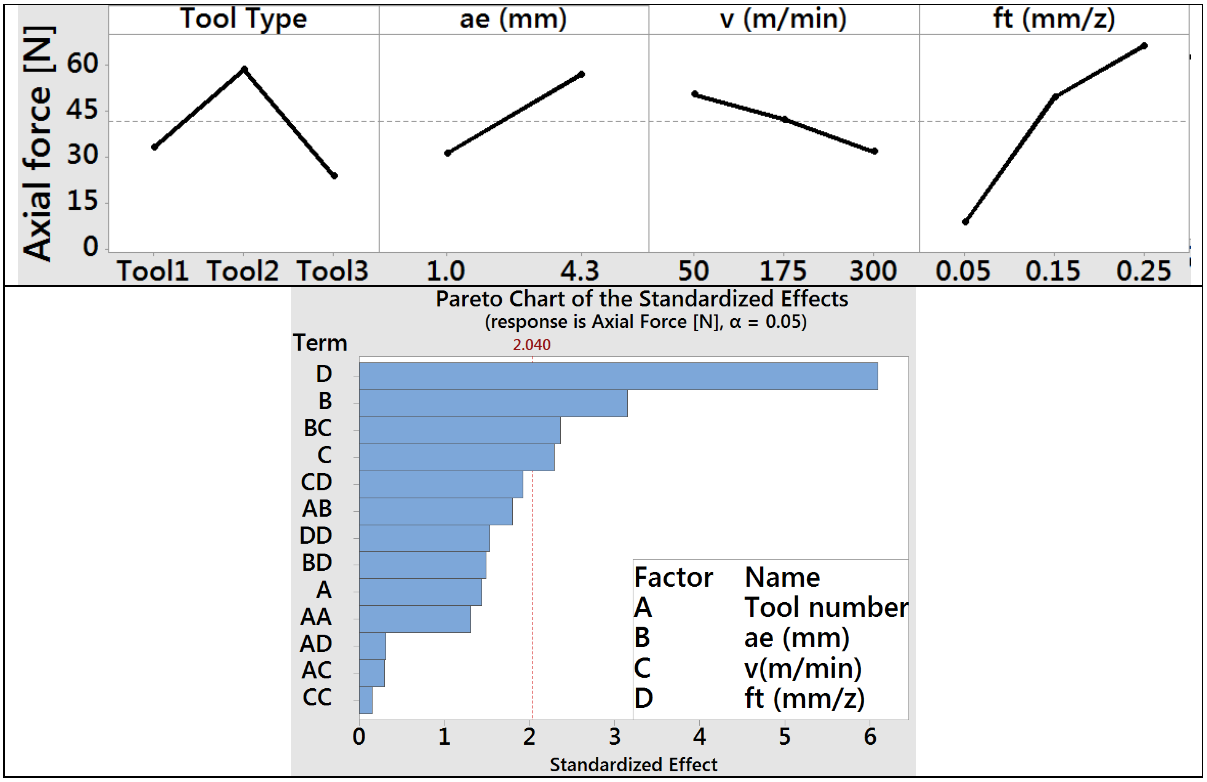

Figure 3.20 Main effect plot for axial force result and standardized pareto chart

Figure 3.21 shows the interaction among the different cutting parameters for each cutter. The tool # 2 shows the highest axial force of all the cutters while the tool #3 the lowest for a radial depth of cut of 1 mm. In addition, the tool #3 remains almost the same for the different values of feed per tooth and cutting speeds. In the case of a *(v)* of 175m/min, the axial force decreases from 0.15 to 0.25 mm/tooth. This may be due to the geometry of 2- flutes tool which provokes the axial force in this direction to be less than that of the other tools. However, the axial force for tool #3 rises linearly with the feed per tooth for a cutting speed *(v)* of 300 m/min. This might happen because the tool #3 is chipped in this cutting parameter.

For a radial depth of cut of 4.3mm, tool #2 has a higher axial force than tool #1. This could be due to its wider helix angle. Even though the axial force is greater for tool #2, it did not suffer any tool wear or chipped. This is due to its protective TiAlN+ TiAlN coating. In addition, both tool #1 and #2 decrease their axial force for a feed per tooth of 0.15 to 0.25 mm/tooth and a cutting speed of 175 and 300 m/min. This might be due to the fact that the chip morphology changes to take off more heat during the cutting process, turning it in a dark-bluish color. Therefore, a second repetition could help to clarify this measure.

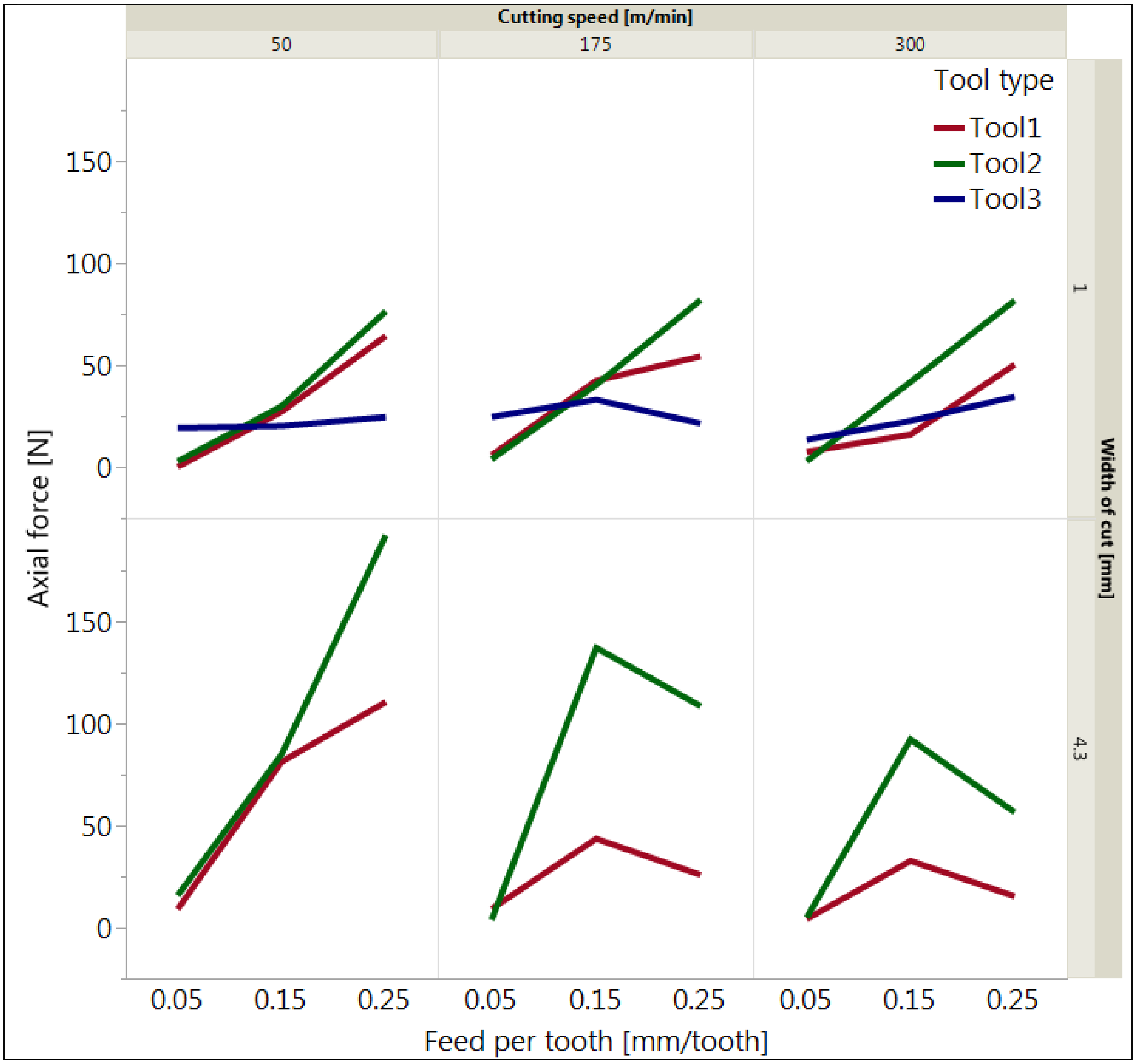

Figure 3.21 Axial force as a function of the feed per tooth according to the different cutting parameters on each cutter

Based on our results, the feed per tooth is the parameter which has more influence on the feed, normal and axial forces for the CFRP/Ti6Al4V plaque. In the case of the cutting forces on titanium, Jinyang et al. and Xu et al. (2016; 2019) remarked that the cutting force *"Fy"* is greater than thrust force *"Fx"* in the orthogonal cutting process of CFRP/Ti6Al4V plaque as we did. However, they machined from CFRP toTi6Al4V or vice-versa and not both materials at the same time. Moreover, their analysis was based on the cutting speed, fiber orientation and depth of cut, excluding the feed per tooth. On the other hand, Yujing et al. (2014) measured the cutting forces in order to find a trend with the cutting temperature within a titanium workpiece. Their results show that the force and temperature vary in a parallel manner and complement each other. In addition, their study was based on getting the most relevant factor of the cutting temperature, excluding the most significant factors in the cutting forces. It is for this reason that we cannot compare our results with the results of their titanium plaques.

Comparing our results with others regarding the CFRP cutting forces, these are similar to the results presented by Haijin et al. and Kerrigan et al. (2016; 2016). In the case of Kerrigan et al. (2016), their results consider the resultant force composed of *Fx*, *Fy* and *Fz*. On the other hand, Haijin's cutting results (2016) shows the resulting cutting force between the *Fx* and *Fy*. Both author's results show that the feed per tooth is the most significant factor. However, this cannot be concluded because the plastic deformation force of titanium is greater than the brittle fracture force of CFRP. As a result, the plastic deformation of the Titanium material in the CFRP/Ti6Al4V plaque is the most influential factor in the cutting force.

3.3 Roughness Analysis

The top of Figure 3.22 shows the main effect plot of the arithmetic mean value (*Ra*) analysis of the $[0]_8$/Ti6Al4V plaque. In addition, the tool #3 has the best performance of all of them and tools #1 and #2 have similar behavior. However, this type of graph does not show the behavior of all the cutters using the same cutting parameters. This is because the tool #3 was only tested for a radial depth of cut *(ae)* of 1 mm and both tool #1 and tool #2 were tested for both radial depths of cut. In the case of the different radial depths of cut, it is seen that a radial depth of cut of 4.3 mm presents a greater roughness than with 1 mm. A similar trend is presented for the feed per tooth and has the most significant effect on the *Ra*. Thus, the higher the feed per tooth, the greater the arithmetic mean value (*Ra*), as opposed to the cutting speed which appears not to be a significant factor. Moreover, the Ti6Al4V plaque presents better surface finish roughness than the $[0]_8$ since it is an isotropic material. The bottom of Figure 3.22 shows that the feed per tooth is the most significant factor, followed by the workpiece surface material, the radial depth of cut, the interaction between the tool type-feed per tooth, etc.

In order to better understand the arithmetic mean value (*Ra*) for the $[0]_8$ and Ti6Al4V material, Figure 3.23 and Figure 3.24 show the performance of each cutter as a function of the radial depth of cut, feed per tooth and cutting speed. In the case of the CFRP, the tool #3 has the best performance in all the cases for a radial depth of cut *(ae)* of 1 mm because it is designed for machining CFRP material. On the other hand, both tool #2 and tool #1 are tools adapted to cut titanium. For a cutting speed *(v)* of 50 and 175m/min and an *ft* varying from 0.15 to 0.25 mm/tooth, the tool #2 shows a better performance than the tool #1. A similar result happens when a radial depth of cut *(ae)* equals 4.3 mm, where the tool #2 has a better surface finish than the tool #1 even though the tool # 1 has a smaller helix angle. This might be due to the fact that tool #1 was melting with the titanium chip, throwing the burr upwards and affecting the CFRP surface. On the contrary, tool # 2 is more resistant to tool wear due to its TiAlN+ TiAlN coating. In addition, the tool #2 experimented a roughness dropping at a cutting speed of 300 m/min and radial depth of cut 4.3 mm. This might be due to the effect of high-speed machining or the dropping of the axial force.

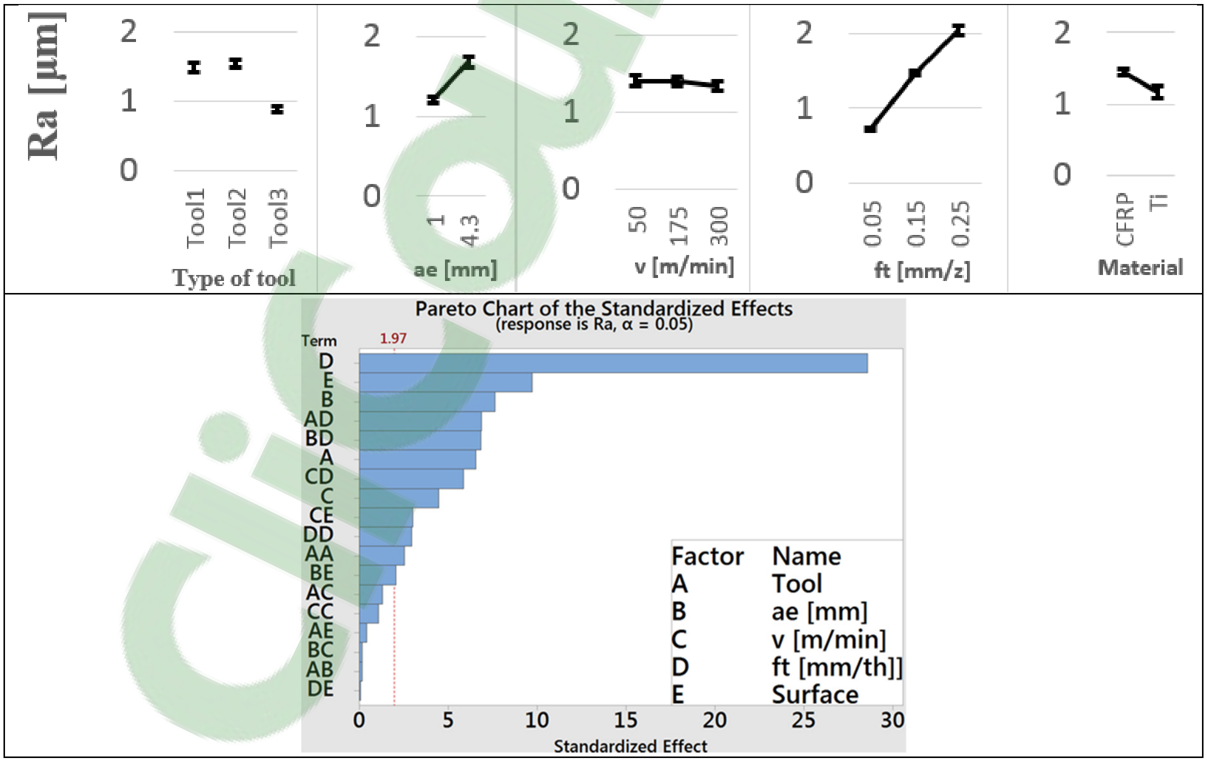

Figure 3.22 Main Effect plot of Ra in function to different parameters giving by ±SEM and Ra Pareto chart of the most significant factor

Clicours.com

In the case of the titanium plaque, Figure 3.24 shows that the best surface finish is given using the tool #3 for *ae* equals to 1 mm even if this cutter is not designed for cutting titanium. In addition, the tool #2 has a better performance than the tool #1 for a high value of feed per tooth since this is specially designed to cut Ti alloys. However, we observe a high *(Ra)* within the range of feed per tooth from 0.15 to 0.25 mm/tooth and cutting speed *(v)* of 175 m/min, as opposed to the tool #1. This is due to a measurement error in tool #1 causing a smaller *Ra*. On the other hand, for a radial depth of cut of 4.3 mm, the tool # 2 and the tool #1 behave similarly for both cutting speeds of 50 and 175 m/min. Additionally, the tool #1 performs well within this cutting range. However, the tool #2 performs much better at high-cutting speeds and at high feed per tooth than the tool #1 due to its coating that prevents tool wear.

Based on our results, the feed per tooth is the most significant factor affecting the arithmetic mean value (*Ra*), which increases with increasing the feed per tooth and slightly decreases with increasing the cutting speed for both the CFRP and Ti6Al4V plaque. As a result, low feed per tooth, high cutting speed and low radial depth of cut are recommended to reduce the surface roughness. In the case of the CFRP material, this result is consistent with the results presented by Chatelain et al. (2012), in which the feed per tooth is the most significant effect. On the other hand, for the Titanium, Yang et al. (2015) suggest low feed per tooth and radial depth of cut and high-cutting speed as we do. Therefore, the same principle can be used to achieve a smoother surface finish during the machining of CFRP/Ti6Al4V plaques.

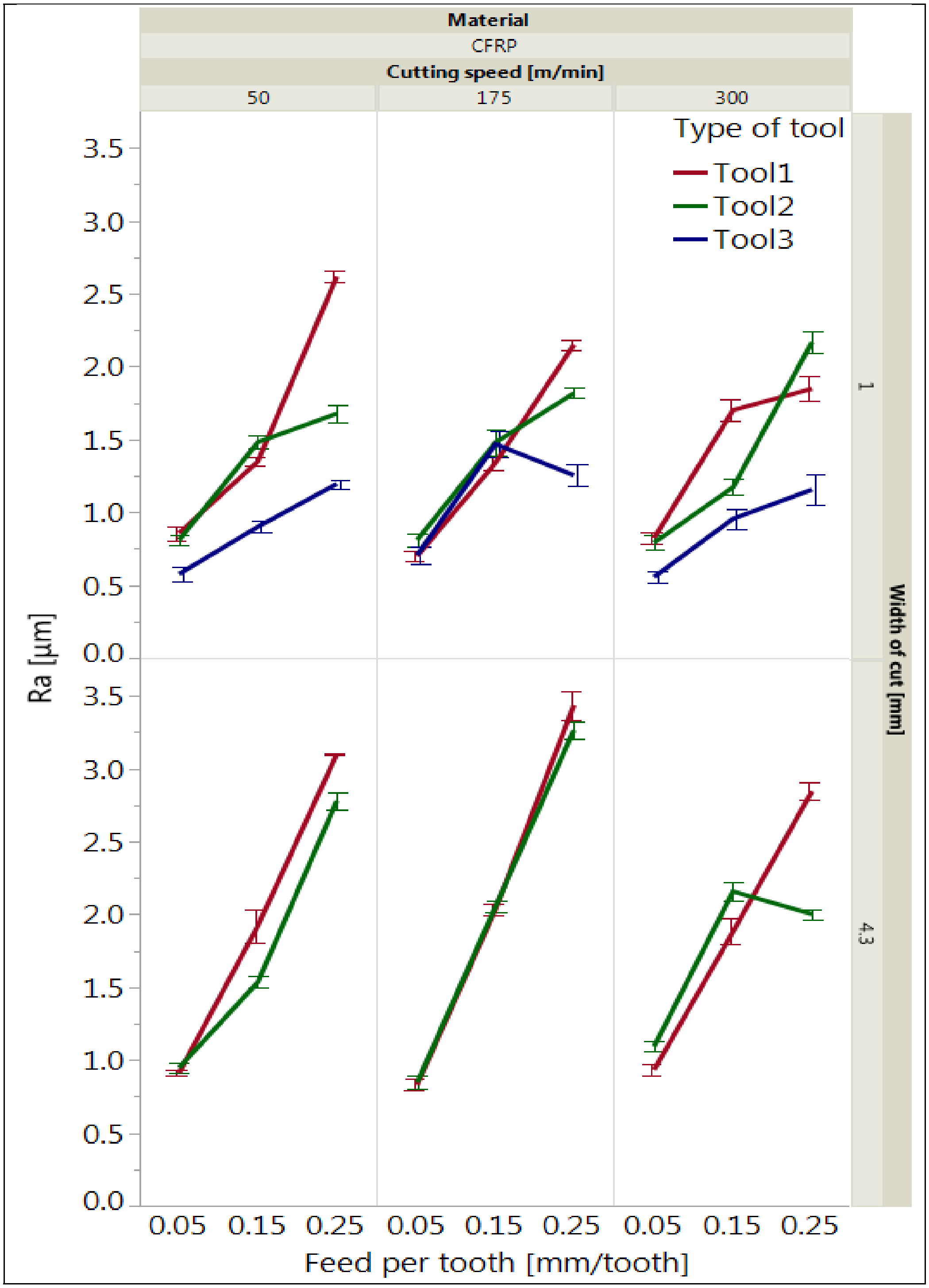

Figure 3.23 Ra on the CFRP plaque in function of different cutting parameters *v*, *ae* and *ft* giving by ±SEM

Clicours.COM

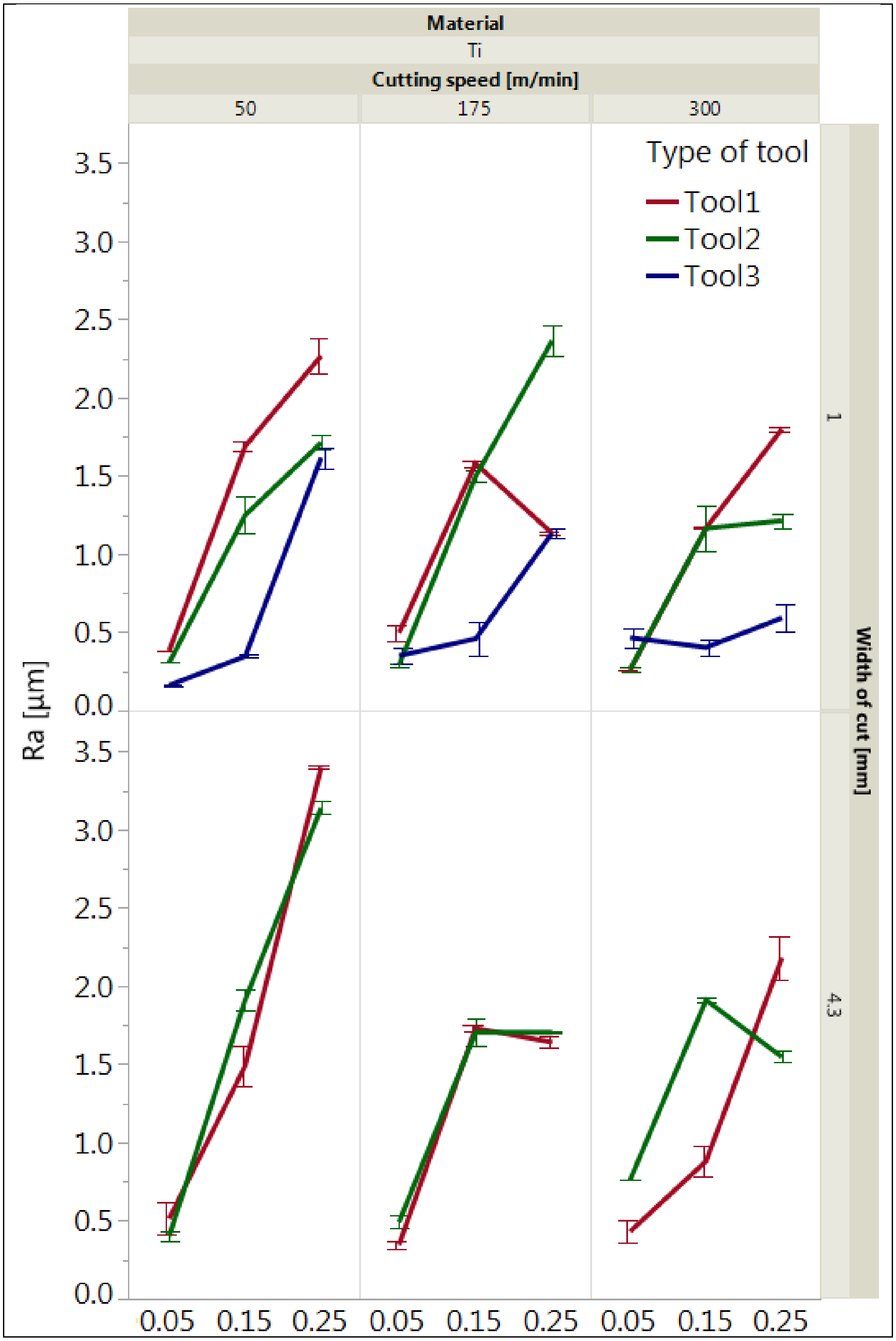

Figure 3.24 Ra on the Ti6Al4V plaque in function of different cutting parameters *v*, *ae* and *ft* giving by ±SEM

3.4 Tool wear

The main effect plot shows that the type of tool, radial depth of cut, cutting speed and the feed per tooth are the factors that influence the tool wear (the top of Figure 3.25). The tool #2 is the cutter with the lowest wear due to its TiAlN+ TiAlN coating protection which aids to resist against the tool wear during the cutting process of titanium alloys even in dry conditions. On the other hand, tool #1 and tool #3 have almost the same tool wear. In the case of the radial depth of cut, the radial depth of 4.3 mm produces higher wear than the radial depth of 1 mm. A similar case is observed with the cutting speed and the feed per tooth where the greater the magnitude, the greater the wear. This is due to the increase of the cutting forces.

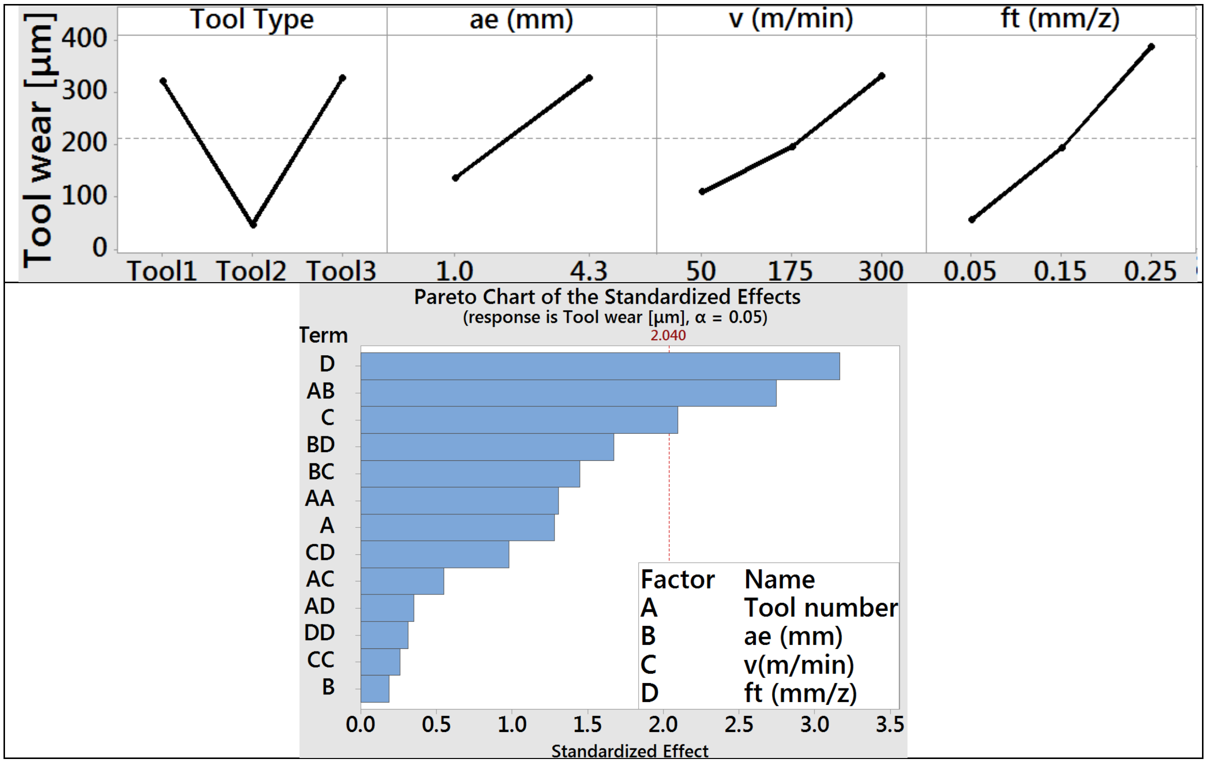

Figure 3.25 Main effect plot for tool wear and standardized pareto chart

In addition, the pareto chart of the standardized effects show that the most significant factor is the feed per tooth, followed by the interaction of tool type-radial depth of cut, and finally the cutting speed (the bottom of Figure 3.25).

By looking at Figure 3.26, both tool #1 and #2 have similar wear and the flank wear (VB) is below 0.3 mm or 300 µm according to the different cutting parameters for a radial depth of cut of 1 mm. Additionally, by looking at Table 3-1, there is no sign of excessive chipping, flaking or fracturing for the different combinations of cutting speed *(v)* and feed per tooth *(ft)*. As a result, both tools can be used within this range of cutting parameters. On the other hand, the tool #3 performs well at low cutting speeds *(v)* of 50 m/min for a feed per tooth *(ft)* varying from 0.5 to 0.25 mm/tooth. However, the wear of the tool #3 ramps up gradually and is very close to the limit of flank wear VB. Moreover, the tool #3 suffers from excessive chipping for a feed per tooth greater than 0.15 mm/tooth in both cases of cutting speed *v* 175 and 300 m/min, see Table 3-1.

In the case of radial depth of cut of 4.3 mm, the too #2 has the best performance at all times and is below to VB. This type of tool is excellent to cut titanium even in dry conditions. On the other hand, the tool #1 starts to have severe chipping after a feed per tooth of 0.15 mm/tooth for both cutting speeds *(v)* of 50 and 175 m/min so it is not recommended for high values of cutting speed *v* of 300 m/min. In addition, there is a peak of tool wear for the tool #1 at a feed per tooth of 0.15 mm/tooth and a cutting speed of 300 m/min. This might be because the vibration in this cutting parameter is higher than at an *ft* of 0.25 mm/tooth provoking more surface roughness too. Moreover, we saw sparks during the machining of the CFRP/Ti6Al4V plaque due to the fusion of the tool with the titanium plaque and due to the absence of lubricant. Table 3-2 shows the progress for the different cutting parameters. It is worth mentioning that Table 3-1 and Table 3-2 show the tooth, which is the most damaged. Additionally, the tool wear of the cutting tools is concentrated on one tooth and it is not distributed around teeth. This may be due because the tests were performed in dry conditions and the retained heat provokes built-up-edge (BUE) on the cutter flukes due to the excess of heat. As a result, the cutting forces were concentrated only on one tooth.

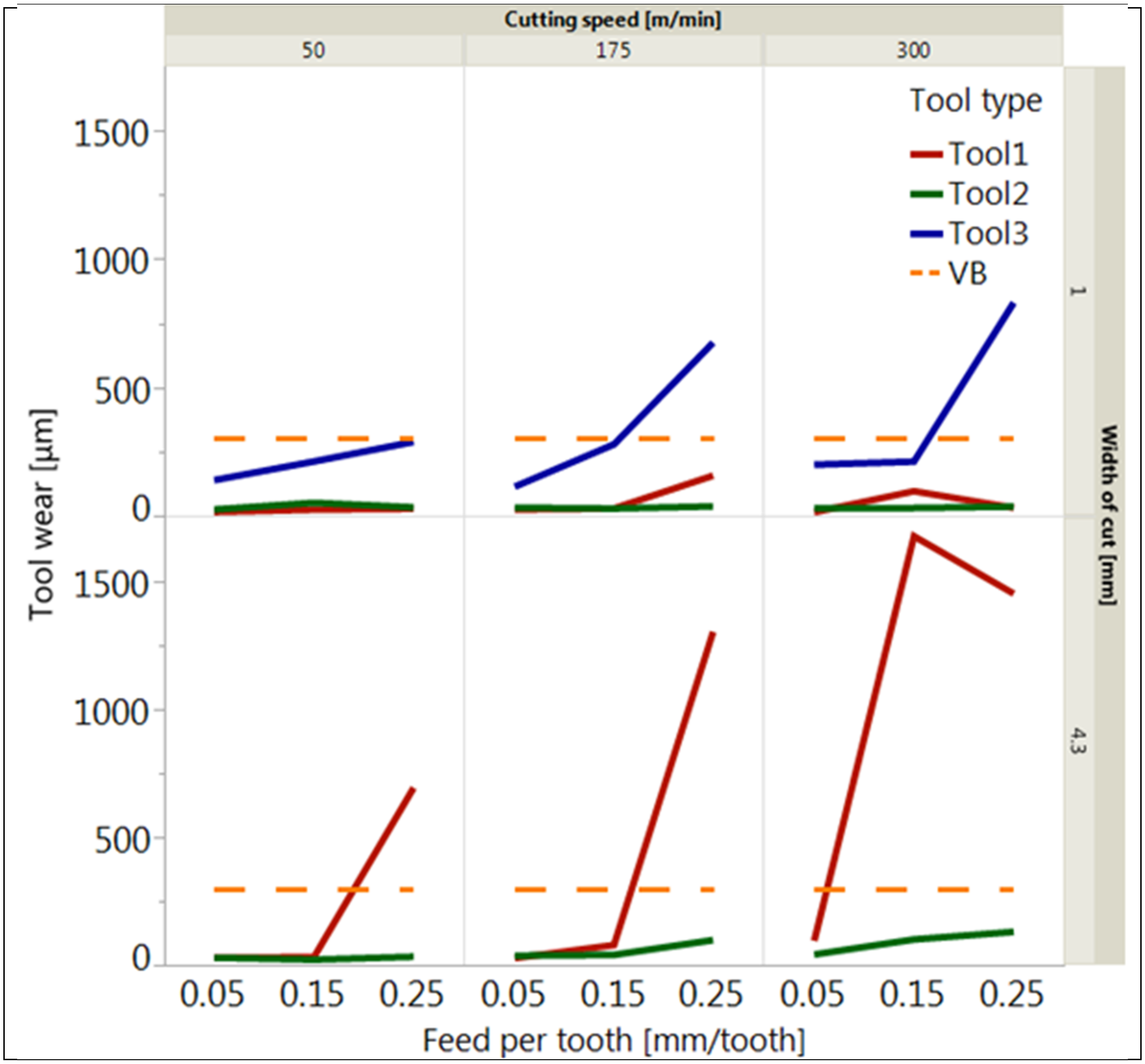

Figure 3.26 Tool wear effect on each cutting tool by using different cutting parameters

Table 3-1 Cutter tool wear progress at different cutting parameters for the ae of 1 mm

v	ft	Tool #1	Tool #2	Tool #3
50 m/min	0.05 mm/th	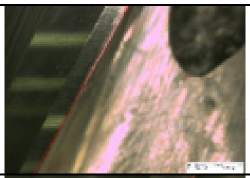	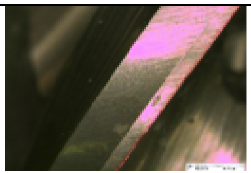	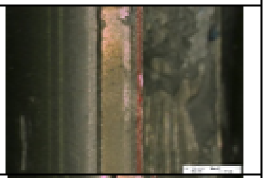
	0.15 mm/th	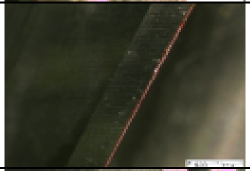	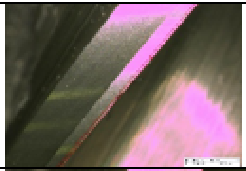	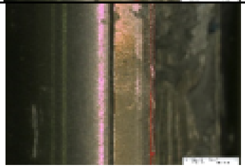
	0.25 mm/th	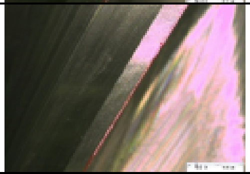	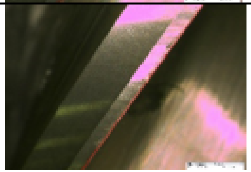	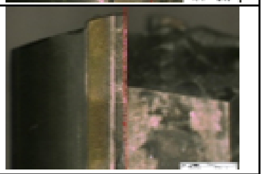
175 m/min	0.05 mm/th	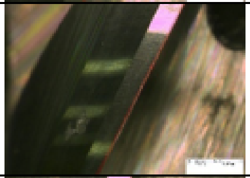	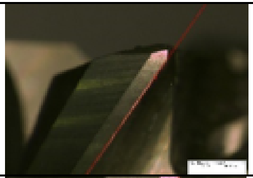	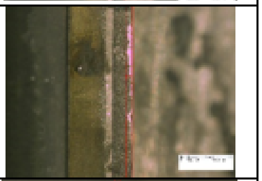
	0.15 mm/th	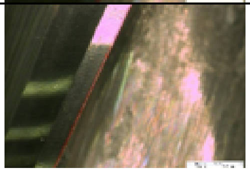	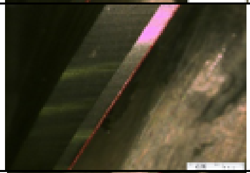	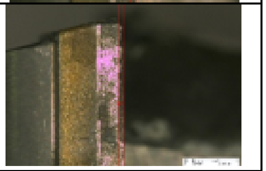
	0.25 mm/th	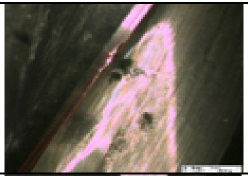	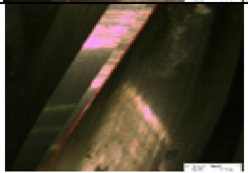	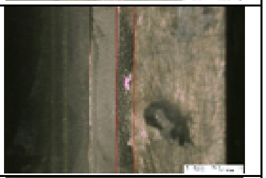
300 m/min	0.05 mm/th	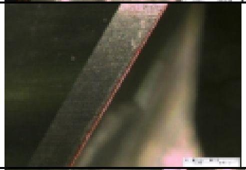	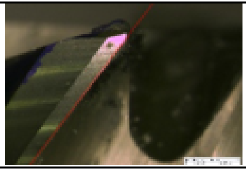	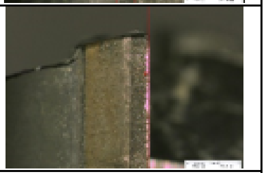
	0.15 mm/th	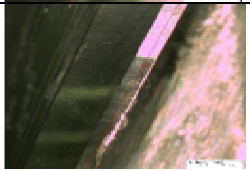	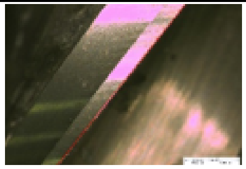	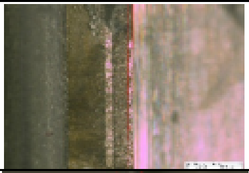
	0.25 mm/th	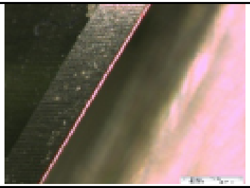	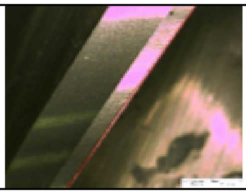	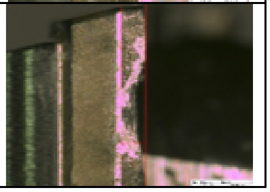

Table 3-2 Cutter tools wear progress at different cutting parameters for the ae of 4.3 mm

v	ft	Tool #1	Tool #2
50 m/min	0.05 mm/th	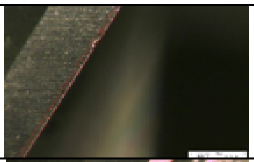	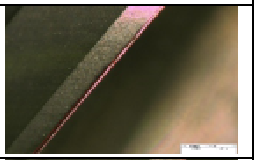
	0.15 mm/th	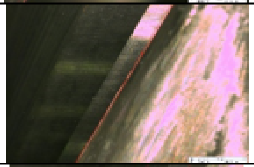	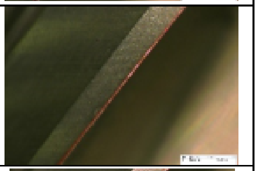
	0.25 mm/th	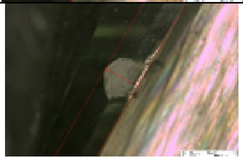	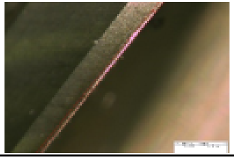
175 m/min	0.05 mm/th	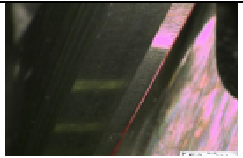	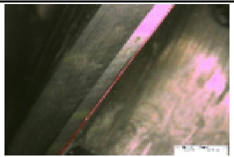
	0.15 mm/th	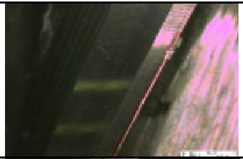	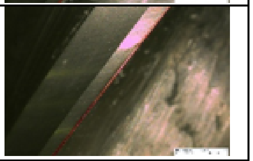
	0.25 mm/th	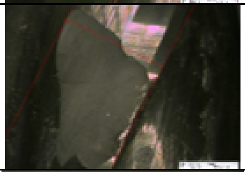	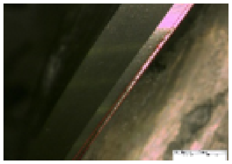
300 m/min	0.05 mm/th	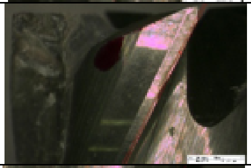	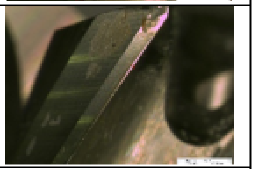
	0.15 mm/th	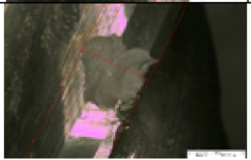	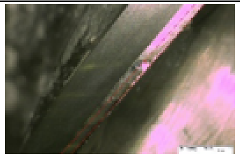
	0.25 mm/th	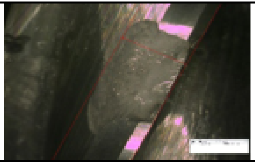	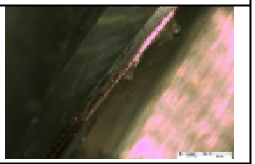

CONCLUSION

We assessed the combinations of different cutting parameters (cutting speed, radial depth of cut and feed per tooth) and tool types using the tool-workpiece thermocouple method to measure the cutting temperature both on the cutter and within the $[0]_8$/Ti6Al4V plaque. In addition, the cutting forces, roughness and tool wear during the edge milling cutting process were evaluated.

We found that, as opposed to what was previously thought a priori, the feed factor is the most significant factor on the cutting temperature for the $[0]_8$ and Ti6Al4V workpiece instead of the cutting speed. Therefore, the temperature of the workpiece increases when decreasing the feed per tooth and decreases when increasing the cutting speed; however, the latter is not as significant as the feed per tooth. In the case of radial depth of cut, this factor is not as significant as in the $[0]_8$/Ti6Al4V temperature as it is in the cutter temperature. In addition, the tool-workpiece thermocouple method showed that even a few tenths of millimeters can change the temperature within the $[0]_8$/Ti6Al4V plaque. This is due to the displacement of the thermocouples within the $[0]_8$ plaque during the curing process. Moreover, due to the size of the $[0]_8$/Ti6Al4V plaque, the workpiece and cutter temperature is within the temperature transition zone. Future work will entail a numerical model using the experimental data in order to predict the temperature within the stack using real workpieces dimensions.

For the cutting forces, the highest force is in the normal direction and this one increases with increasing the feed per tooth, as opposed to the $[0]_8$/Ti6Al4V plaque temperature which decreases with increasing the feed per tooth. Therefore, the temperature and normal force have inversely proportional magnitudes. Additionally, in order to reduce the surface roughness (Ra) resulting from the trimming of $[0]_8$/Ti6Al4V plaque, it is recommended to use a low feed per tooth and radial depth of cut and high-cutting speed in order to compensate the temperature within the CFRP plaque.

clicours.com

RECOMENDATIONS

In order to increase the efficiency of the workpiece machining, we recommend using the tool #2 (TiAlN+ TiAlN). This is because it showed the lowest wear, the most resistant to the cutting forces and good surface finish of the three cutters tested as opposed to tool #1(uncoated tool) and tool #3 (PCD tool). The tool #2 did not fuse with the Ti6Al4V plaque as tool # 1 did or chipped as tool #3 both cutter in harsh cutting conditions. Thus, it is recommended to use a low *ft*, and high *v* and *ae* to increase the efficiency of the workpiece machining, This is with the aim of keeping a good surface roughness and decreases the temperature within the stack. If the machining productivity is not important, the tool #1 can be used at low ft, ae and high v. For PCD cutter, the tool #3 had an excellent surface finish on both the CFRP and Ti6Al4V plaque over the other cutters. However, it suffered from chipping in harsh cutting conditions. As a result, this tool is recommended to use it at low *ft* (0.05 mm/tooth) and *ae* (1 mm) moderate *v* (175 m/min).

Clicours.COM

ANNEX I

Analysis of optimal radial depth of cut

Table-A I- 1 X-ray scanning for Batch A

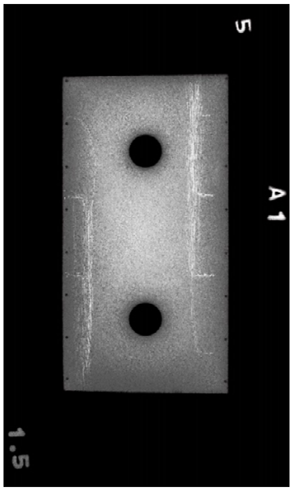	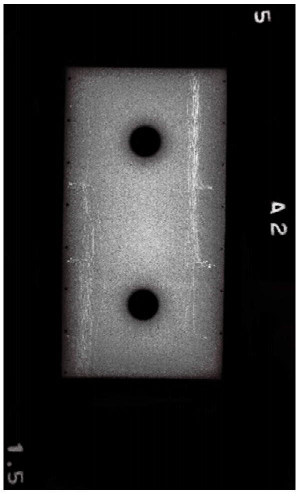	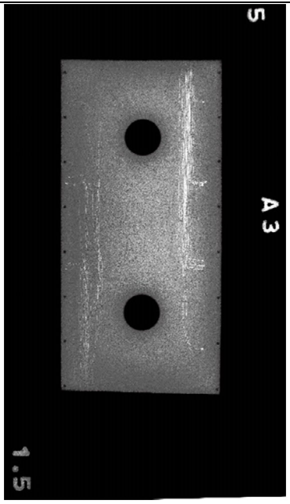
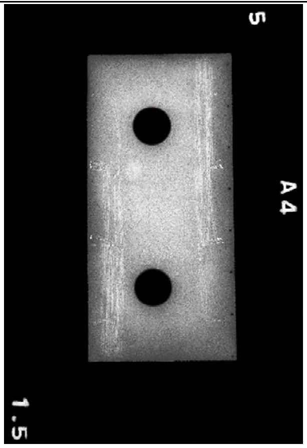	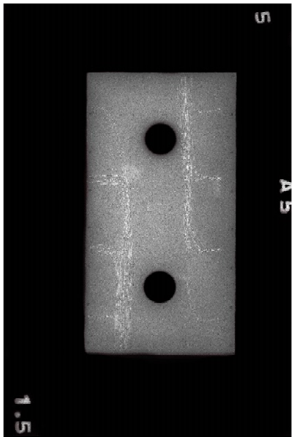	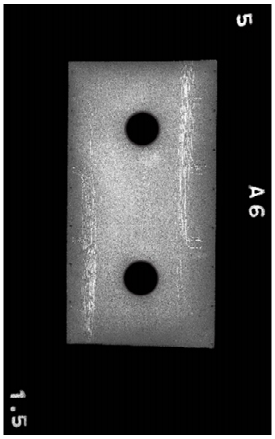
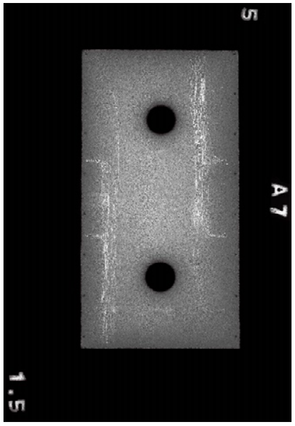	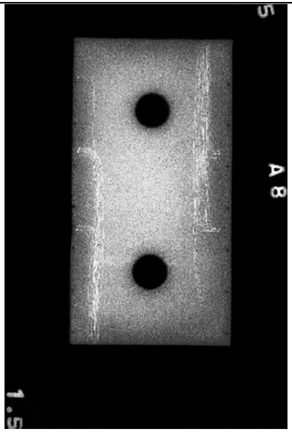	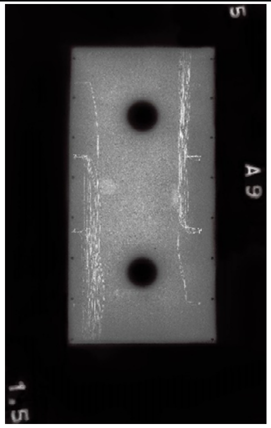

Table-A I- 2 X-ray scanning for Batch B

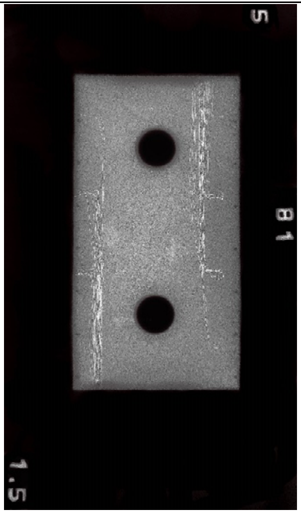	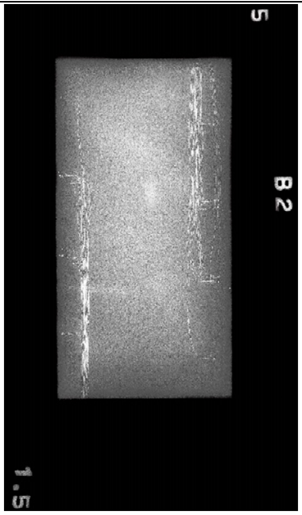	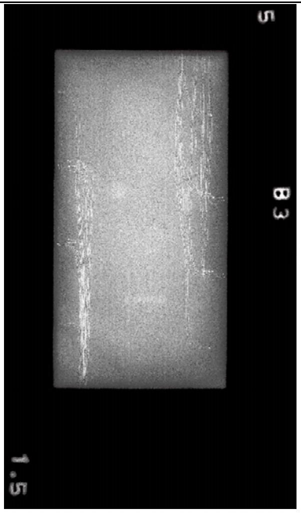
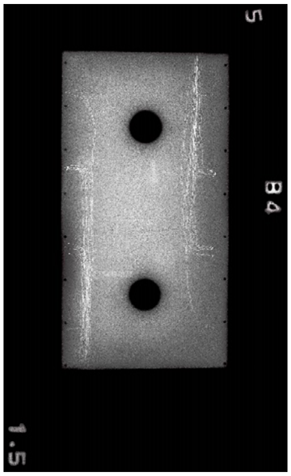	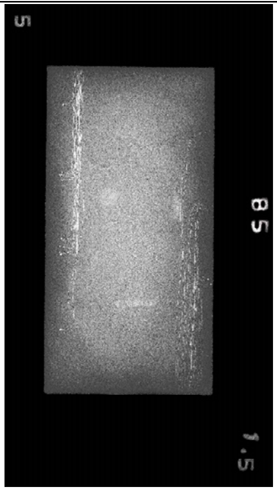	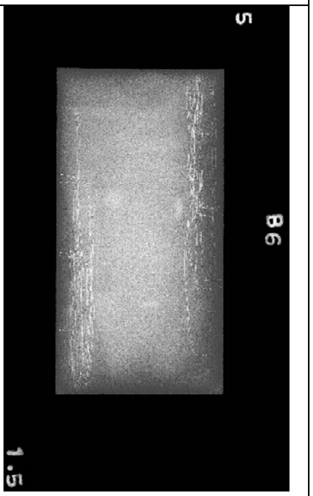
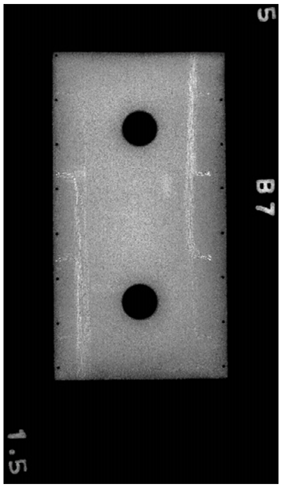	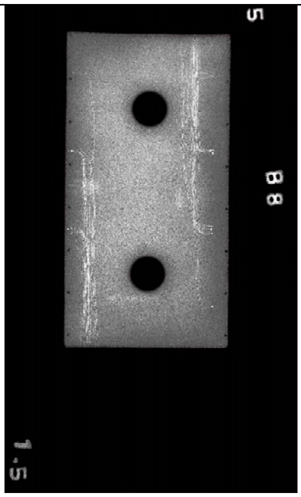	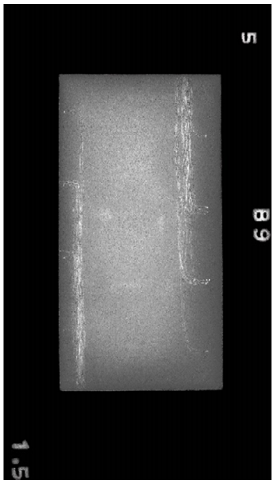

Table-A I- 3 X-ray scanning for Batch C

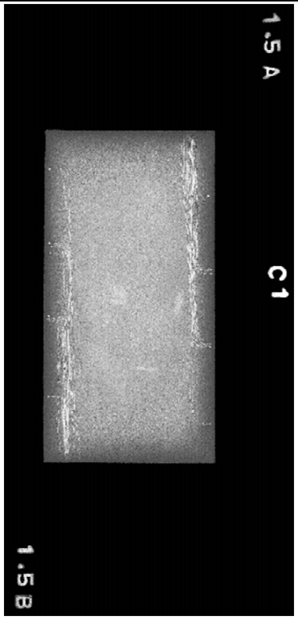	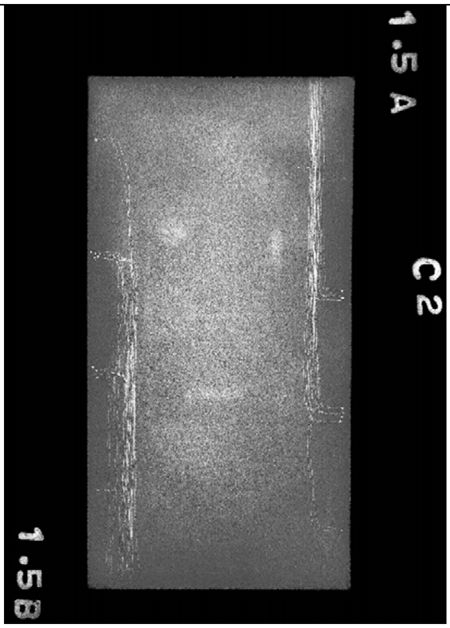	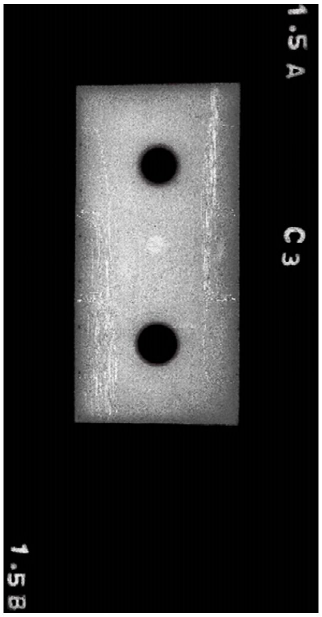
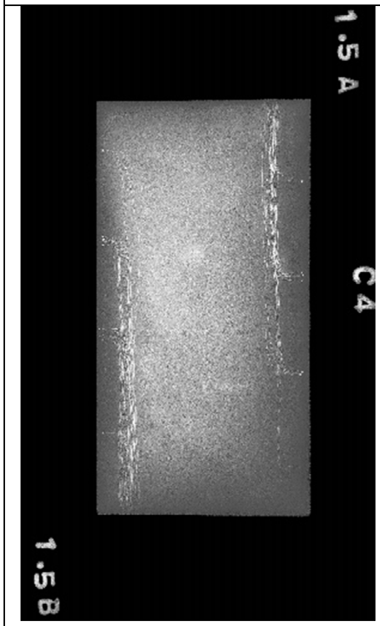	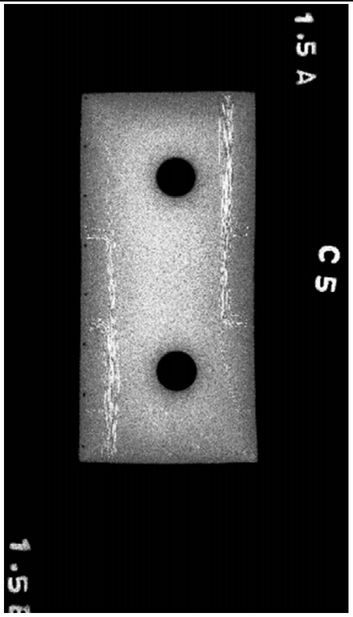	

Analysis of optimal radial depth of cut 1.5 mm

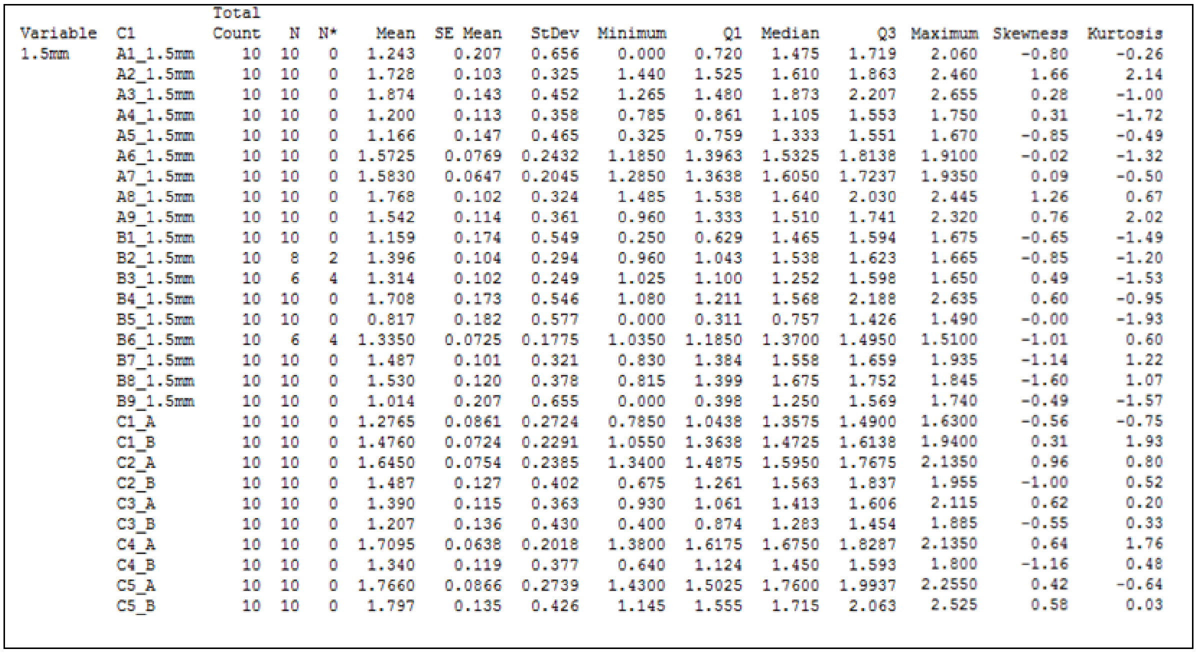

```
                      Total
Variable  C1          Count   N  N*    Mean  SE Mean   StDev  Minimum      Q1  Median      Q3  Maximum  Skewness  Kurtosis
1.5mm     A1_1.5mm       10  10   0   1.243    0.207   0.656    0.000   0.720   1.475   1.719    2.060     -0.80     -0.26
          A2_1.5mm       10  10   0   1.728    0.103   0.325    1.440   1.525   1.610   1.863    2.460      1.66      2.14
          A3_1.5mm       10  10   0   1.874    0.143   0.452    1.265   1.480   1.873   2.207    2.655      0.28     -1.00
          A4_1.5mm       10  10   0   1.200    0.113   0.358    0.785   0.861   1.105   1.553    1.750      0.31     -1.72
          A5_1.5mm       10  10   0   1.166    0.147   0.465    0.325   0.759   1.333   1.551    1.670     -0.85     -0.49
          A6_1.5mm       10  10   0  1.5725   0.0769  0.2432   1.1850  1.3963  1.5325  1.8138   1.9100     -0.02     -1.32
          A7_1.5mm       10  10   0  1.5830   0.0647  0.2045   1.2850  1.3638  1.6050  1.7237   1.9350      0.09     -0.50
          A8_1.5mm       10  10   0   1.768    0.102   0.324    1.485   1.538   1.640   2.030    2.445      1.26      0.67
          A9_1.5mm       10  10   0   1.542    0.114   0.361    0.960   1.333   1.510   1.741    2.320      0.76      2.02
          B1_1.5mm       10  10   0   1.159    0.174   0.549    0.250   0.629   1.465   1.594    1.675     -0.65     -1.49
          B2_1.5mm       10   8   2   1.396    0.104   0.294    0.960   1.043   1.538   1.623    1.665     -0.85     -1.20
          B3_1.5mm       10   6   4   1.314    0.102   0.249    1.025   1.100   1.252   1.598    1.650      0.49     -1.53
          B4_1.5mm       10  10   0   1.708    0.173   0.546    1.080   1.211   1.568   2.188    2.635      0.60     -0.95
          B5_1.5mm       10  10   0   0.817    0.182   0.577    0.000   0.311   0.757   1.426    1.490     -0.00     -1.93
          B6_1.5mm       10   6   4  1.3350   0.0725  0.1775   1.0350  1.1850  1.3700  1.4950   1.5100     -1.01      0.60
          B7_1.5mm       10  10   0   1.487    0.101   0.321    0.830   1.384   1.558   1.659    1.935     -1.14      1.22
          B8_1.5mm       10  10   0   1.530    0.120   0.378    0.815   1.399   1.675   1.752    1.845     -1.60      1.07
          B9_1.5mm       10  10   0   1.014    0.207   0.655    0.000   0.398   1.250   1.569    1.740     -0.49     -1.57
          C1_A           10  10   0  1.2765   0.0861  0.2724   0.7850  1.0438  1.3575  1.4900   1.6300     -0.56     -0.75
          C1_B           10  10   0  1.4760   0.0724  0.2291   1.0550  1.3638  1.4725  1.6138   1.9400      0.31      1.93
          C2_A           10  10   0  1.6450   0.0754  0.2385   1.3400  1.4875  1.5950  1.7675   2.1350      0.96      0.80
          C2_B           10  10   0   1.487    0.127   0.402    0.675   1.261   1.563   1.837    1.955     -1.00      0.52
          C3_A           10  10   0   1.390    0.115   0.363    0.930   1.061   1.413   1.606    2.115      0.62      0.20
          C3_B           10  10   0   1.207    0.136   0.430    0.400   0.874   1.283   1.454    1.885     -0.55      0.33
          C4_A           10  10   0  1.7095   0.0638  0.2018   1.3800  1.6175  1.6750  1.8287   2.1350      0.64      1.76
          C4_B           10  10   0   1.340    0.119   0.377    0.640   1.124   1.450   1.593    1.800     -1.16      0.48
          C5_A           10  10   0  1.7660   0.0866  0.2739   1.4300  1.5025  1.7600  1.9937   2.2550      0.42     -0.64
          C5_B           10  10   0   1.797    0.135   0.426    1.145   1.555   1.715   2.063    2.525      0.58      0.03
```

Figure-A I- 1 Results of statistical analysis of 1.5 mm by plaque

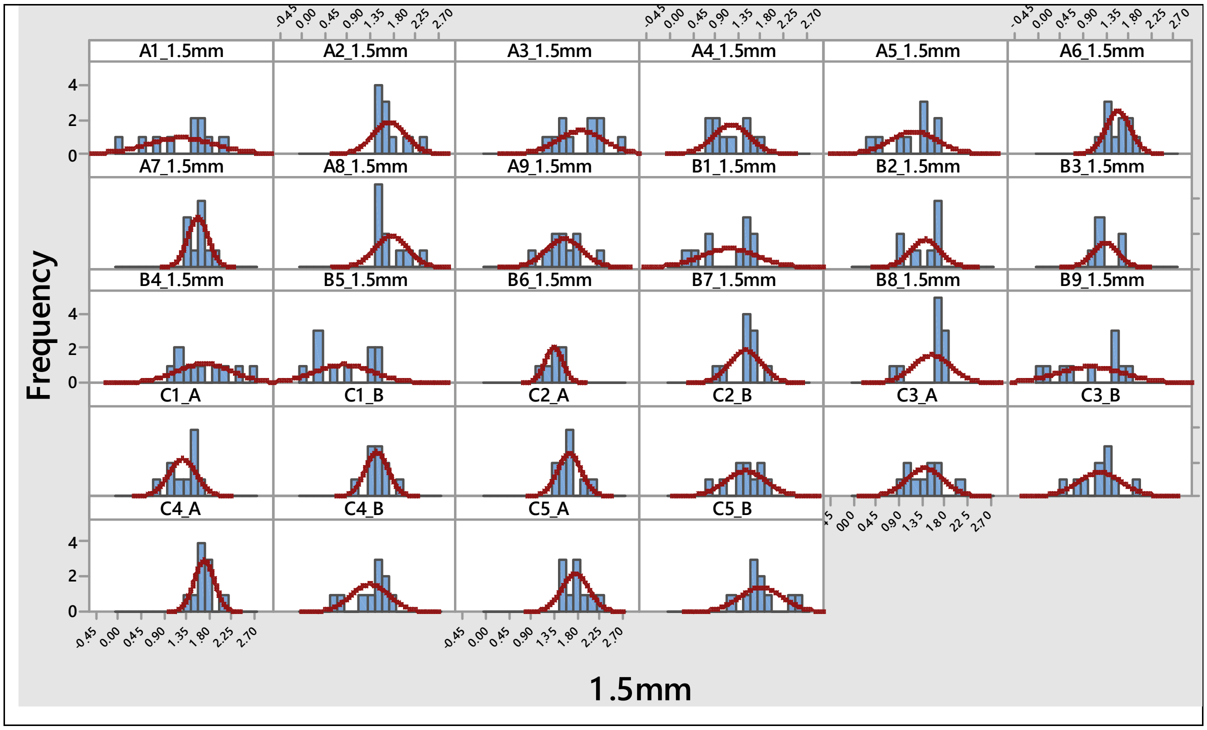

Figure-A I- 2 Graphical normal distribution of 1.5 mm by plaque

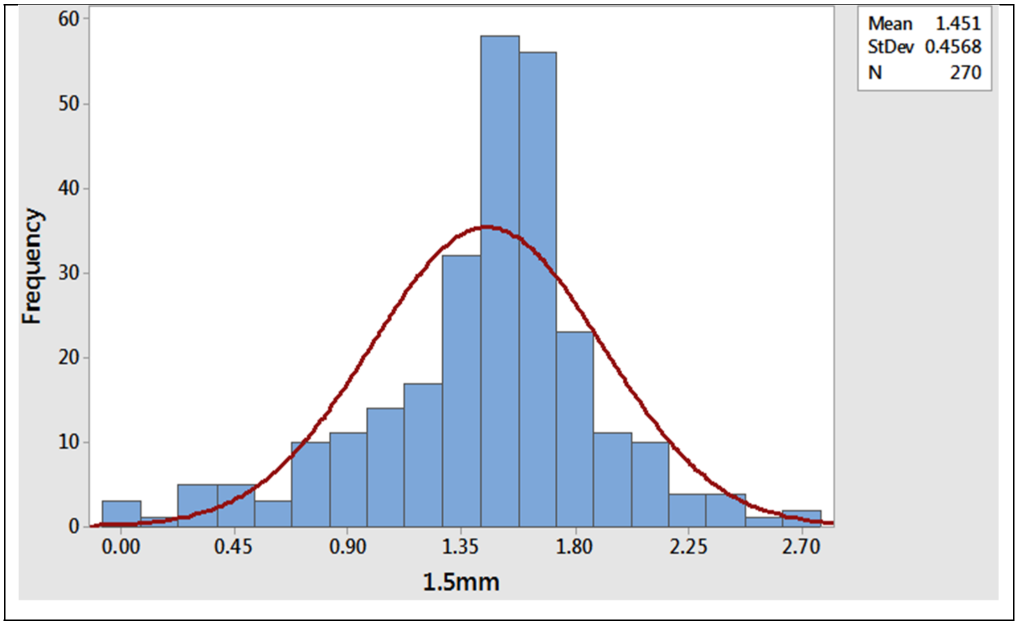

Figure-A I- 3 Graphical normal distribution of 1.5 mm view from the full experimental

Table-A I- 4 Optimal radial depth of cut in the case of 1.5 mm

Proposal distance	**0.7**	**0.8**	**0.9**	**1**	**1.1**	**1.2**	**1.3**
# Lost Thermocouples	20	24	31	40	**51**	**59**	**71**
% Lost Thermocouples	7.41	8.89	11.48	14.81	18.89	21.85	26.30

Analysis of optimal radial depth of cut 5 mm

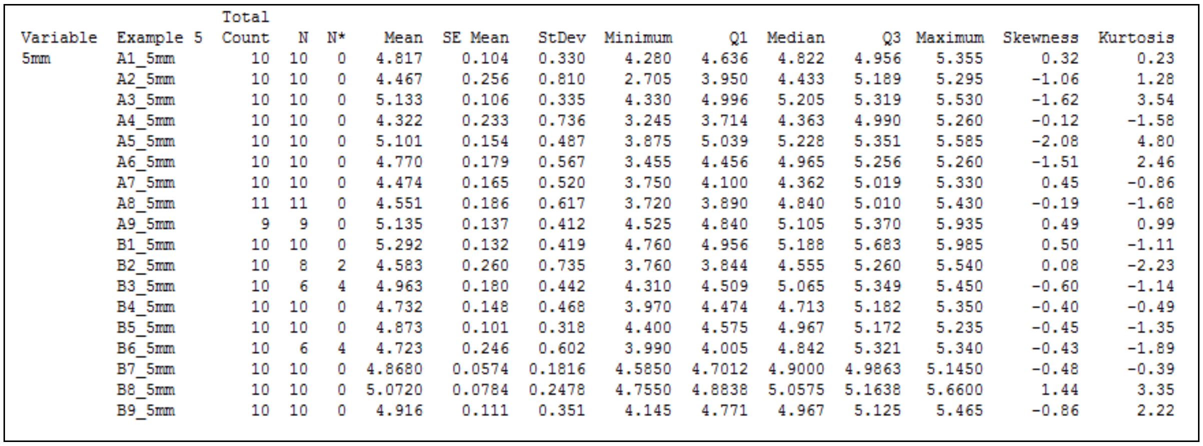

```
                     Total
Variable  Example 5  Count   N  N*    Mean  SE Mean   StDev  Minimum      Q1  Median      Q3  Maximum  Skewness  Kurtosis
5mm       A1_5mm        10  10   0   4.817    0.104   0.330    4.280   4.636   4.822   4.956    5.355      0.32      0.23
          A2_5mm        10  10   0   4.467    0.256   0.810    2.705   3.950   4.433   5.189    5.295     -1.06      1.28
          A3_5mm        10  10   0   5.133    0.106   0.335    4.330   4.996   5.205   5.319    5.530     -1.62      3.54
          A4_5mm        10  10   0   4.322    0.233   0.736    3.245   3.714   4.363   4.990    5.260     -0.12     -1.58
          A5_5mm        10  10   0   5.101    0.154   0.487    3.875   5.039   5.228   5.351    5.585     -2.08      4.80
          A6_5mm        10  10   0   4.770    0.179   0.567    3.455   4.456   4.965   5.256    5.260     -1.51      2.46
          A7_5mm        10  10   0   4.474    0.165   0.520    3.750   4.100   4.362   5.019    5.330      0.45     -0.86
          A8_5mm        11  11   0   4.551    0.186   0.617    3.720   3.890   4.840   5.010    5.430     -0.19     -1.68
          A9_5mm         9   9   0   5.135    0.137   0.412    4.525   4.840   5.105   5.370    5.935      0.49      0.99
          B1_5mm        10  10   0   5.292    0.132   0.419    4.760   4.956   5.188   5.683    5.985      0.50     -1.11
          B2_5mm        10   8   2   4.583    0.260   0.735    3.760   3.844   4.555   5.260    5.540      0.08     -2.23
          B3_5mm        10   6   4   4.963    0.180   0.442    4.310   4.509   5.065   5.349    5.450     -0.60     -1.14
          B4_5mm        10  10   0   4.732    0.148   0.468    3.970   4.474   4.713   5.182    5.350     -0.40     -0.49
          B5_5mm        10  10   0   4.873    0.101   0.318    4.400   4.575   4.967   5.172    5.235     -0.45     -1.35
          B6_5mm        10   6   4   4.723    0.246   0.602    3.990   4.005   4.842   5.321    5.340     -0.43     -1.89
          B7_5mm        10  10   0  4.8680   0.0574  0.1816   4.5850  4.7012  4.9000  4.9863   5.1450     -0.48     -0.39
          B8_5mm        10  10   0  5.0720   0.0784  0.2478   4.7550  4.8838  5.0575  5.1638   5.6600      1.44      3.35
          B9_5mm        10  10   0   4.916    0.111   0.351    4.145   4.771   4.967   5.125    5.465     -0.86      2.22
```

Figure-A I- 4 Results of statistical analysis of 5 mm by plaque

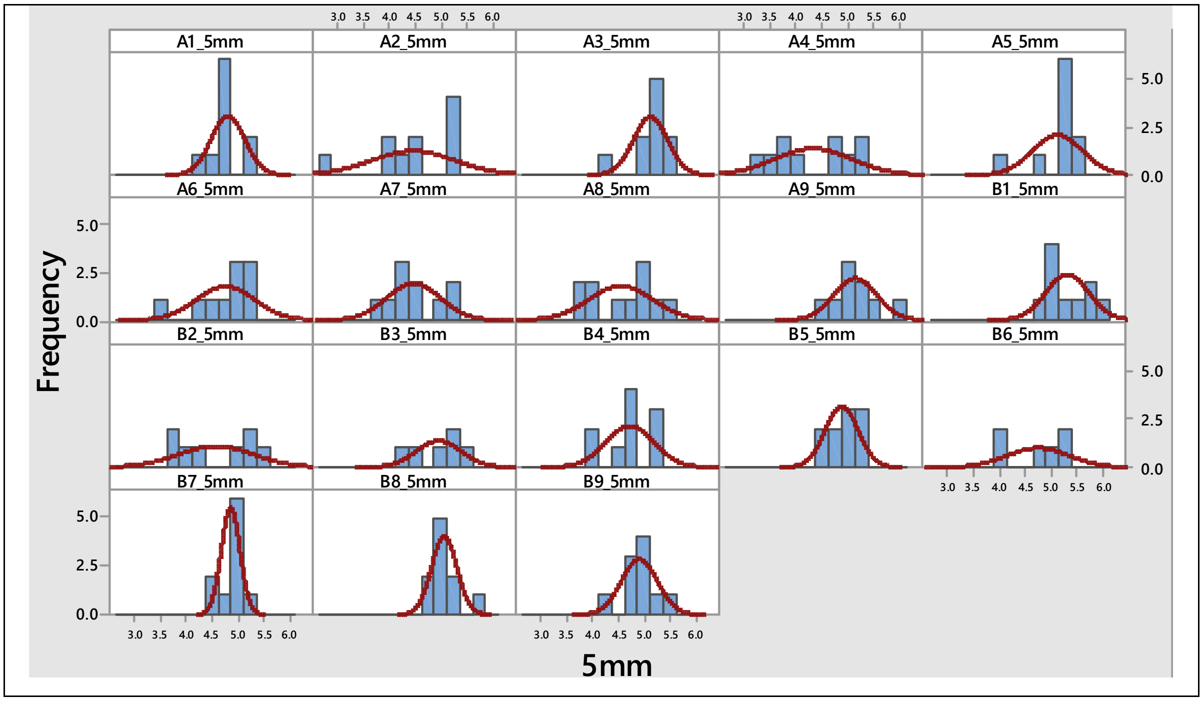

Figure-A I- 5 Graphical normal distribution of 5 mm by plaque

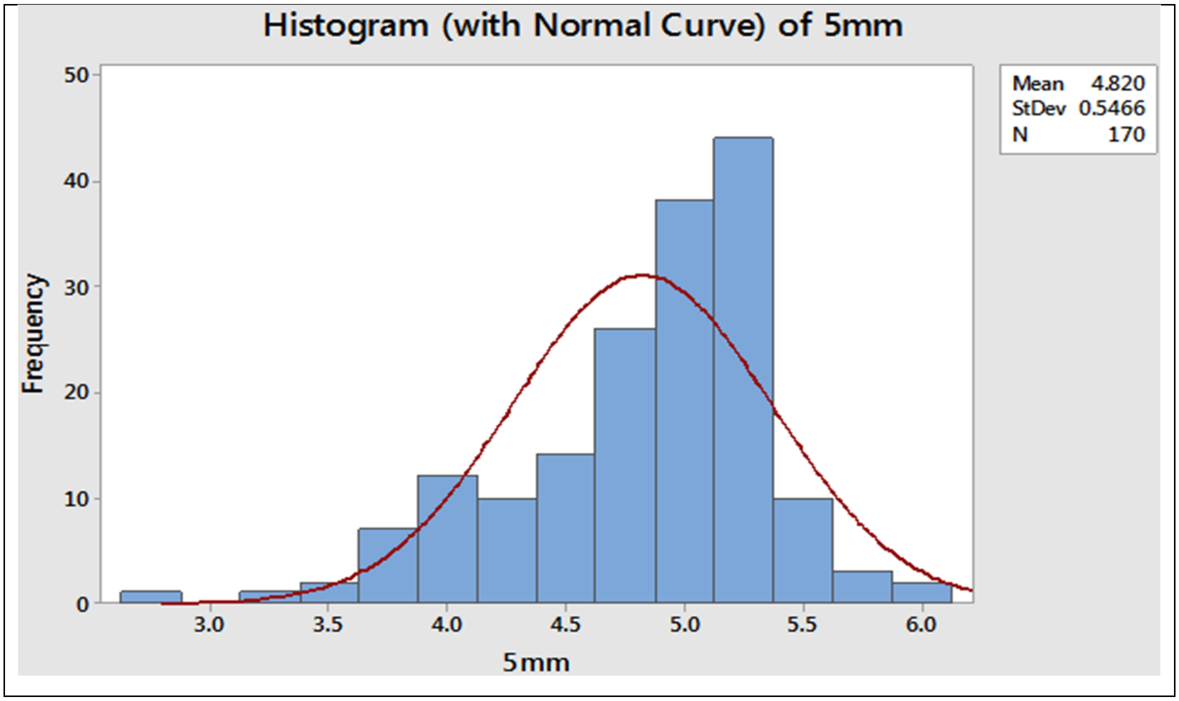

Figure-A I- 6 Graphical normal distribution of 5 mm view from the full experimental

Table-A I- 5 Optimal radial depth of cut in the case of 5 mm

Proposal distance	**3.7**	**3.8**	**3.9**	**4**	**4.1**	**4.2**	**4.3**	**4.4**	**4.5**	**4.6**	**4.7**
# Lost Thermo	4	7	13	20	23	26	28	34	41	46	55
% Lost Thermo	2.35	4.12	7.65	11.76	13.53	15.29	16.47	20.0	24.12	27.06	32.35

clicours.com

ANNEX II

Data

Table-A-II- 1 Data of TC

T4 on the right side of Figure 3.2

T4 ↘	**Feed per tooth**		
	0.05	**0.15**	**0.25**
Tool 1	46.80	44.49	44.20
Tool 2	93.94	49.43	42.65
Tool 3	90.50	57.80	45.85

Table-A-II- 2 Data of Figure 3.3

(feed per tooth of 0.05 mm/tooth vs a radial depth of 1 mm)

Tool ↘	**Thermocouple**				**Distance**			
	T1[C]	**T2 [C]**	**T3[C]**	**T4[C]**	**T1[mm]**	**T2 [mm]**	**T3 [mm]**	**T4 [mm]**
Tool 1	43.15	41.09	46.98	51.03	1.70	1.73	1.76	1.51
Tool 2	87.12	98.21	96.28	106.59	1.52	1.42	1.62	1.48
Tool 3	82.34	88.05	100.95	90.50	1.77	1.55	1.45	1.53

Table-A-II- 3 Data of Figure 3.3

(feed per tooth of 0.05 mm/tooth vs a radial depth of 4.3 mm)

Tool ↘	**Thermocouple**				**Distance**			
	T1[C]	**T2[C]**	**T3[C]**	**T4[C]**	**T1[mm]**	**T2[mm]**	**T3[mm]**	**T4[mm]**
Tool 1	38.23	39.98	41.89	42.57	5.30	5.06	4.98	5.03
Tool 2	73.98	76.07	61.76	85.50	5.27	5.02	5.34	5.21

Clicours.COM

Table-A-II- 4 Data of Figure 3.9

(feed per tooth of 0.05 mm/tooth vs a radial depth of 1 mm)

Tool ↘	**Thermocouple**				**Distance**			
	T2[C]	**T5[C]**	**T7[C]**	**T9[C]**	**T2[mm]**	**T5[mm]**	**T7[mm]**	**T9[mm]**
Tool 1	41.09	38.72	35.99	34.47	1.73	1.81	1.82	1.93
Tool 2	98.21	125.39	92.28	64.59	1.42	0.93	1.15	1.57
Tool 3	88.05	81.36	73.58	67.90	1.55	1.44	1.45	1.68

Table-A-II- 5 Data of Figure 3.9

(feed per tooth of 0.05 mm/tooth vs a radial depth of 1 mm)

Tool ↘	**Thermocouple**				**Distance**			
	T3[C]	**T6 C]**	**T8[C]**	**T10[C]**	**T3[mm]**	**T6[mm]**	**T8[mm]**	**T10[mm]**
Tool 1	46.98	36.14	44.09	39.53	1.76	1.74	1.24	1.70
Tool 2	96.28	64.62	159.30	0	1.62	1.46	0.96	0
Tool 3	100.95	84.21	121.05	74.14	1.45	1.49	1.22	1.49

Table-A-II- 6 Data on the left side of Figure 3.15

Ft ↘	**ae**	
	1	**4.3**
0.05	68.34	103.63
0.15	54.10	81.56
0.25	51.41	76.69

Table-A-II- 7 Data on the rigth side of Figure 3.15

Cutter ↘	**ae**	
	1	**4.3**
Tool 1	43.34	68.91
Tool 2	78.61	138.35
Tool 3	83.066	0.00

Temperature on the CFRP with a ft of 0.05 mm/tooth and ae of 4.3 mm

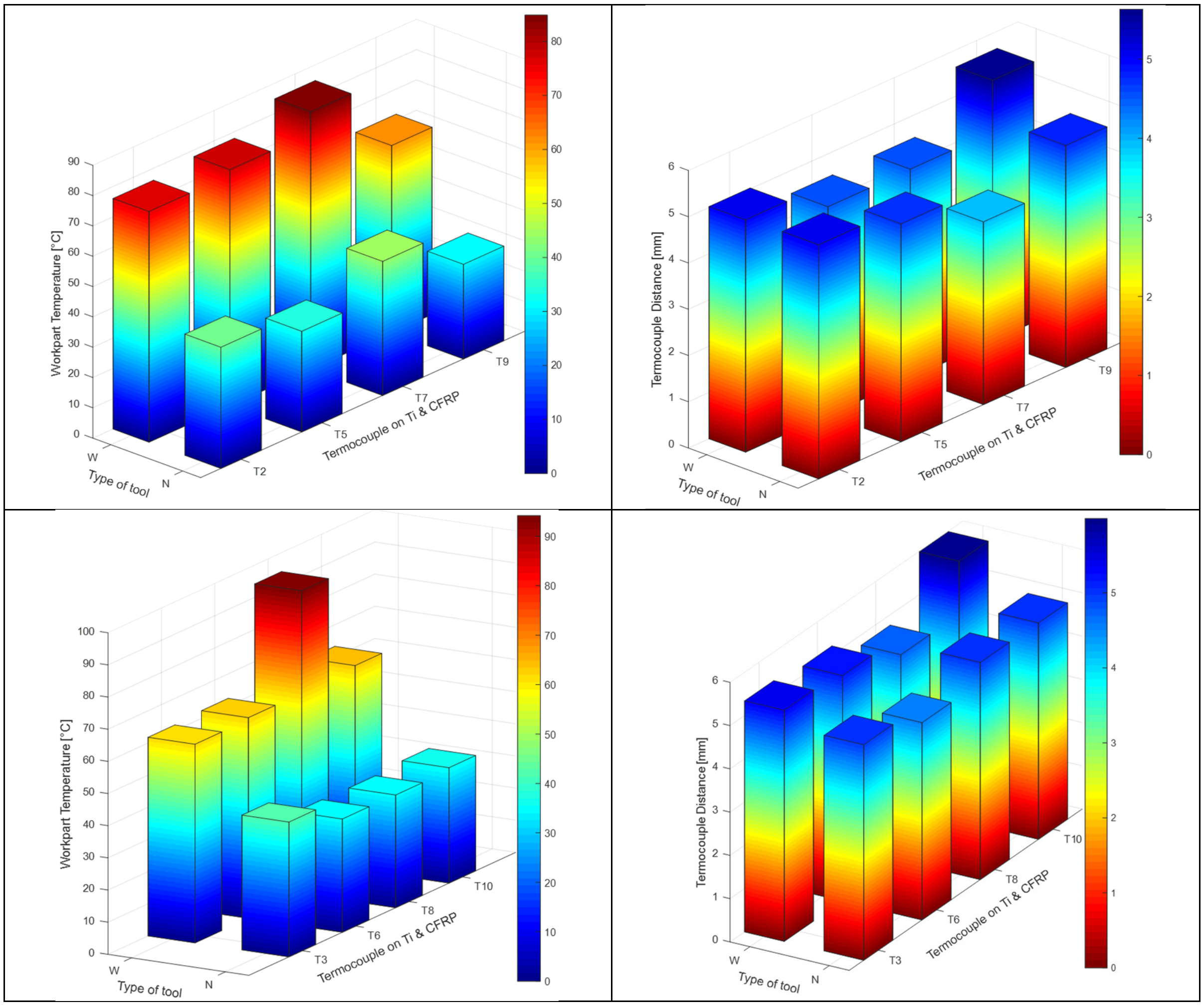

Figure-A II- 1 Temperature on the CFRP with a ft of 0.05 mm/tooth and ae of 4.3mm

BIBLIOGRAPHY

Bérubé, S., Chatelain, J.-F., & Songmene, V. (2012). *Usinage en détourage de laminés composites carbone/époxy* (École de Technologie Supérieure, Montreal, Qc).

Boeing. (2009). Boeing 787 Dreamliner by design. Repéré à https://www.boeing.com/commercial/787/by-design/#/advanced-composite-use

Brinksmeier, E., Fangmann, S., & Rentsch, R. (2011). Drilling of composites and resulting surface integrity. *CIRP Annals - Manufacturing Technology, 60*(1), 57-60. doi: 10.1016/j.cirp.2011.03.077.

Calzada, K., Kapoor, S., DeVor, R., Samuel, J., & Srivastava, A. (2012). Modeling and interpretation of fiber orientation-based failure mechanisms in machining of carbon fiber-reinforced polymer composites. *Journal of Manufacturing Processes, 14*(2), 141-149.

Campbell, F. C. (2010). Structural Composite Materials (New ed. edition (June 30 2010) éd., pp. 612). United State of America: ASM International.

Chatelain, J.-f., & Zaghbani, I. (2012). Effect of Tool Geometry Special Features on Cutting Forces of Multilayered CFRP Laminates. *nternational Journal of Mechanics, 6*(1), 52-59.

Chatelain, J. F., & Zaghbani, I. (2012). A comparison of special helical cutter geometries based on cutting forces for the trimming of CFRP laminates. *International Journal of Mechanics, 6*(1), 52-59.

Chatelain, J. F., Zaghbani, I., & Monier, J. (2012). Effect of Ply Orientation on Roughness for the Trimming Process of CFRP Laminates. *International Journal of Mechanical, Aerospace, Industrial, Mechatronic and Manufacturing Engineering, International Science Index 68, 2012*.

Davim, J. P., Reis, P., & António, C. C. (2004). A study on milling of glass fiber reinforced plastics manufactured by hand-lay up using statistical analysis (ANOVA). *Composite Structures, 64*(3-4), 493-500.

Delahaigue, J., Chatelain, J.-F., & Lebrun, G. (2017). Influence of Cutting Temperature on the Tensile Strength of a Carbon Fiber-Reinforced Polymer. *Fibers, 5*(4), 46.

Ducobu, F., & Rivière-Lorphèvre, E. (2016). Material constitutive model and chip separation criterion influence on the modeling of Ti6Al4V machining with experimental validation in strictly orthogonal cutting condition. *International journal of mechanical sciences, 107*, 136-149. doi: https://doi.org/10.1016/j.ijmecsci.2016.01.008.

El-Hofy, M. H., Soo, S. L., Aspinwall, D. K., Sim, W. M., Pearson, D., & Harden, P. (2011). Factors Affecting Workpiece Surface Integrity in Slotting of CFRP. *Procedia Engineering, 19*, 94-99. doi: http://dx.doi.org/10.1016/j.proeng.2011.11.085.

Ghafarizadeh, S., Lebrun, G., & Chatelain, J.-F. (2016). Experimental investigation of the cutting temperature and surface quality during milling of unidirectional carbon fiber reinforced plastic. *Journal of composite materials, 50*(8), 1059-1071. doi: 10.1177/0021998315587131.

Groover, M. P. (2013). *Fundamentals of modern manufacturing: Materials, Processes, and System*. The United States of America: John Wiley & Sons, Inc. Repéré à www.wiley.com/college/groover.

Hammadi. (2010). Présentation Sandvik. Journée Intercut.

Issac M. Daniel, O. I. (2006). *Engineering mechanics of composite materials* (Second Edition éd.). New York: Oxford University Press.

Jinyang, X., El Mansori, M., & El Mansori, M. (2016). An experimental investigation on orthogonal cutting of hybrid CFRP/Ti stacks. Dans *ESAFORM 2016: 19th International ESAFORM Conference on Material Forming, 27-29 April 2016* (Vol. 1769, pp. 080002 (080007 pp.)). AIP - American Institute of Physics. doi: 10.1063/1.4963477

Kalpakjian, S., & Schmid, S. R. (2014). *Manufacturing engineering and technology* (Seventh edition. éd.). Upper Saddle River: Pearson.

Kerrigan, K., O'Donnell, G. E., & O'Donnell, G. E. (2016). On the Relationship between Cutting Temperature and Workpiece Polymer Degradation During CFRP Edge Trimming. *Procedia CIRP, 55*, 170-175. doi: https://doi.org/10.1016/j.procir.2016.08.041.

Kerrigan, K., Thil, J., Hewison, R., & O'Donnell, G. E. (2012). An integrated telemetric thermocouple sensor for process monitoring of CFRP milling operations. Dans *5th CIRP Conference on High Performance Cutting 2012, HPC 2012, June 4, 2012 - June 7, 2012* (1 éd., Vol. 1, pp. 449-454). Elsevier. doi: 10.1016/j.procir.2012.04.080. Repéré à http://dx.doi.org/10.1016/j.procir.2012.04.080

Khashaba, U. (2013). Drilling of polymer matrix composites: A review. *Journal of composite materials, 47*(15), 1817-1832. doi: 10.1177/0021998312451609.

Krishnaraj, V., Zitoune, R., Collombet, F., & Davim, J. P. (2013). Challenges in Drilling of Multi-Materials. *Materials Science Forum, 763*, 145-168. doi: 10.4028/www.scientific.net/MSF.763.145.

Lance, J., Chatelain, J.-F., & Songmene, V. (2014). *A methodology for thermal damage assessment using temperature data when drilling CFRP/Ti6Al4V stacks*.

Lantrip, J. (2008). News tools needed. *Cutting Tool Engineering, 60*(8), 72-84.

Li, A., Zhao, J., Dong, Y., Wang, D., & Chen, X. (2013). SURFACE INTEGRITY OF HIGH-SPEED FACE MILLEDTi-6Al-4VALLOY WITH PCD TOOLS. *Machining science and technology, 17*(3), 464-482.

Li, L., Chang, H., Wang, M., Zuo, D. W., & He, L. (2004). Temperature measurement in high speed milling Ti6Al4V. *Key Engineering Materials, 259-260*, 804-808.

Lin, Lin, S., Peng, F., Wen, J., Liu, Y., & Yan, R. (2013). An investigation of workpiece temperature variation in end milling considering flank rubbing effect. *International journal of machine tools & manufacture, 73*, 71-86.

Luo, B., Li, Y., Zhang, K., Cheng, H., & Liu, S. (2015). A novel prediction model for thrust force and torque in drilling interface region of CFRP/Ti stacks. *The International Journal of Advanced Manufacturing Technology, 81*(9), 1497-1508. doi: 10.1007/s00170-015-7294-9.

Montoya, J. D., & Chatelain, J. F. (2013). *Étude du perçage orbital d'empilements de matériaux composites carbone-epoxy (CFRP) et titane* (École de Technologie Supérieure (ÉTS)).

Nomura, S., & Haji-Sheikh, A. (2018). *Heat transfer in composite materials*. Lancaster, Pennsylvania, U.S.A.: DEStech Publications, Inc.

Nouari, M., & Ginting, A. (2006). Wear characteristics and performance of multi-layer CVD-coated alloyed carbide tool in dry end milling of titanium alloy. *Surface & coatings technology, 200*(18-19), 5663-5676.

Nurul Amin, A. K. M., Ismail, A. F., & Nor Khairusshima, M. K. (2007). Effectiveness of uncoated WC-Co and PCD inserts in end milling of titanium alloy - Ti-6Al-4V. *Journal of materials processing technology, 192-193*(1-7), 147-158. doi: 10.1016/j.jmatprotec.2007.04.095.

Palanisamy, S., Rashid, R. A. R., Brandt, M., Sun, S., & Dargusch, M. S. (2014). Comparison of Endmill Tool Coating Performance during Machining of Ti6Al4V Alloy. *Advanced Materials Research, 974*, 126-131. doi: 10.4028/www.scientific.net/AMR.974.126.

Pan, W., Ding, S., & Mo, J. (2014). The prediction of cutting force in end milling titanium alloy (Ti6Al4V) with polycrystalline diamond tools. *Proceedings of the Institution of Mechanical Engineers, 231*(1), 3-14.

Pan, W., Kamaruddin, A., Ding, S., & Mo, J. (2014). Experimental investigation of end milling of titanium alloys with polycrystalline diamond tools. *Proceedings of the Institution of Mechanical Engineers, Part B: Journal of Engineering Manufacture, 228*(8), 832-844. doi: doi:10.1177/0954405413514399.

Park, K.-H., Beal, A., Kim, D., Kwon, P., & Lantrip, J. (2013). A Comparative Study of Carbide Tools in Drilling of CFRP and CFRP-Ti Stacks. *Journal of manufacturing science and engineering, 136*(1), 014501-014501-014509. doi: 10.1115/1.4025008.

Pramanik, A., & Littlefair, G. (2015). Machining of Titanium Alloy(Ti-6Al-4V)—Theory to Application. *Machining science and technology, 19*(1), 1-49.

Ramulu, M. (1997). Machining and surface integrity of fibre-reinforced plastic composites. *Sadhana, 22*(3), 449-472.

Samani, M. K., Chen, G. C. K., Ding, X. Z., & Zeng, X. T. (2010). Thermal Conductivity of CrAlN and TiAlN Coatings Deposited by Lateral Rotating Cathode Arc. *Key Engineering Materials, 447-448*, 705-709. doi: 10.4028/www.scientific.net/KEM.447-448.705.

Santiuste, C., Diaz Alvarez, J., Soldani, X., & Miguelez, H. (2014). Modelling thermal effects in machining of carbon fiber reinforced polymer composites. *Journal of reinforced plastics and composites, 33*(8), 758-766.

SenthilKumar, M., Prabukarthi, A., & Krishnaraj, V. (2013). Study on Tool Wear and Chip Formation During Drilling Carbon Fiber Reinforced Polymer (CFRP)/Titanium Alloy (Ti6Al4V) Stacks. *Procedia Engineering, 64*, 582-592. doi: http://dx.doi.org/10.1016/j.proeng.2013.09.133.

Shaw, M. C. (2004). *Metal cutting principles* (2 edition (June 30 2004) éd.). Oxford University Press.

Sheikh-Ahmad, J., Almaskari, F., & Hafeez, F. (2018). *Thermal aspects in machining CFRPs: effect of cutter type and cutting parameters*. doi: 10.1007/s00170-018-2881-1

Sheikh-Ahmad, J., & Cheragui, N. U. a. H. (2012). Machining Damage in Edge Trimming of CFRP. *Materials and Manufacturing Processes, 27*(7), 802-808. doi: 10.1080/10426914.2011.648253.

Sheikh-Ahmad, J. Y. (2009). Machining of polymer composites. *Springer Verlag*.

Sun, J., & Guo, Y. B. (2009). A comprehensive experimental study on surface integrity by end milling Ti–6Al–4V. *Journal of materials processing technology, 209*(8), 4036-4042.

Sun, Y., Sun, J., & Li, J. (2017). Modeling and experimental study of temperature distributions in end milling Ti6Al4V with solid carbide tool. *Proceedings of the Institution of Mechanical Engineers, Part B: Journal of Engineering Manufacture, 231*(2), 217-227. doi: 10.1177/0954405415577553.

Wang, D. H., Ramulu, & Arola, D. (1995). Orthogonal cutting mechanisms of graphite/epoxy composite. Part II: multi-directional laminate. *International journal of machine tools & manufacture, 35*(12), 1639-1648.

Wang, H., Sun, J., Li, J., Lu, L., & Li, N. (2016). Evaluation of cutting force and cutting temperature in milling carbon fiber-reinforced polymer composites. *International Journal of Advanced Manufacturing Technology, 82*(9-12), 1517-1525. doi: 10.1007/s00170-015-7479-2.

Wang, H., Sun, J., Zhang, D., Guo, K., & Li, J. (2016). The effect of cutting temperature in milling of carbon fiber reinforced polymer composites. *Composites Part A: Applied Science and Manufacturing, 91*, 380-387. doi: 10.1016/j.compositesa.2016.10.025.

Wang, Y. G., Yan, X. P., Chen, X. G., Sun, C. Y., & Liu, G. (2011). *Cutting Performance of Carbon Fiber Reinforced Plastics Using PCD Tool* (Vol. 215). doi: 10.4028/www.scientific.net/AMR.215.14

Wu, H., & Zhang, S. (2015). Effects of cutting conditions on the milling process of titanium alloy Ti6Al4V. *The International Journal of Advanced Manufacturing Technology, 77*(9-12), 2235-2240.

Wu, H. B., & Zhang, S. J. (2014). 3D FEM simulation of milling process for titanium alloy Ti6Al4V. *The International Journal of Advanced Manufacturing Technology, 71*(5-8), 1319-1326.

Xu, J., & El Mansori, M. (2015). Finite element analysis when orthogonal cutting of hybrid composite CFRP/Ti. *IOP Conference Series: Materials Science and Engineering, 87*(1), 012059.

Xu, J., & El Mansori, M. (2016). Numerical studies of frictional responses when cutting hybrid CFRP/Ti composite. *The International Journal of Advanced Manufacturing Technology, 87*(1-4), 657-675.

Xu, J., El Mansori, M., Chen, M., & Ren, F. (2019). Orthogonal cutting mechanisms of CFRP/Ti6Al4V stacks. *The International Journal of Advanced Manufacturing Technology*. doi: 10.1007/s00170-019-03734-x.

clicours.com

Xu, J., Mkaddem, A., & El Mansori, M. (2016). Recent advances in drilling hybrid FRP/Ti composite: A state-of-the-art review. *Composite Structures, 135*, 316-338.

Yang, D., & Liu, Z. (2015). Surface topography analysis and cutting parameters optimization for peripheral milling titanium alloy Ti–6Al–4V. *International journal of refractory & hard metals, 51*, 192-200.

Yashiro, T., Ogawa, T., & Sasahara, H. (2013). Temperature measurement of cutting tool and machined surface layer in milling of CFRP. *International Journal of Machine Tools and Manufacture, 70*, 63-69.

Yujing, S., Jie, S., Jianfeng, L., & Qingchun, X. (2014). An experimental investigation of the influence of cutting parameters on cutting temperature in milling Ti6Al4V by applying semi-artificial thermocouple. *International Journal of Advanced Manufacturing Technology, 70*(5-8), 765-773. doi: 10.1007/s00170-013-5294-1.

Clicours.COM